MODULATION TRANSFER FUNCTION ANALYSIS OF THE MODERATE RESOLUTION IMAGING SPECTRORADIOMETER (MODIS) ON THE TERRA SATELLITE

by

Francisco Rojas

A Dissertation Submitted to the Faculty of the

DEPARTMENT OF ELECTRICAL AND COMPUTER ENGINEERING

In Partial Fulfillment of the Requirements
For the Degree of

DOCTOR OF PHILOSOPHY

In the Graduate College

THE UNIVERSITY OF ARIZONA

2002

UMI Number: 3073306

UMI Microform 3073306

ProQuest Information and Learning Company
300 North Zeeb Road
P.O. Box 1346
Ann Arbor, MI 48106-1346

THE UNIVERSITY OF ARIZONA ®
GRADUATE COLLEGE

As members of the Final Examination Committee, we certify that we have read the dissertation prepared by **FRANCISCO ROJAS**

entitled **MODULATION TRANSFER FUNCTION ANALYSIS OF THE MODERATE RESOLUTION IMAGING SPECTRORADIOMETER (MODIS-AM) ON THE TERRA SATELLITE**

and recommend that it be accepted as fulfilling the dissertation requirement for the Degree of **DOCTOR OF PHILOSOPHY**

ROBERT SCHOWENGERDT, PH.D.	Date 11/7/02
MICHAEL M. MARCELLIN, PH.D.	Date 11/7/02
JOHN A. REAGAN, PH.D.	Date 11/7/02
ALFREDO HUETE, PH.D.	Date 11/7/02
KURT THOME, PH.D.	Date 11/7/02

Final approval and acceptance of this dissertation is contingent upon the candidate's submission of the final copy of the dissertation to the Graduate College.

I hereby certify that I have read this dissertation prepared under my direction and recommend that it be accepted as fulfilling the dissertation requirement.

Dissertation Director **ROBERT SCHOWENGERDT, PH.D.** Date 11/21/02

STATEMENT BY AUTHOR

This dissertation has been submitted in partial fulfillment of requirements for an advanced degree at The University of Arizona and is deposited in the University Library to be made available to borrowers under rules of the Library.

Brief quotations from this dissertation are allowable without special permission, provided that accurate acknowledgment of source is made. Requests for permission for extended quotation from or reproduction of this manuscript in whole or in part may be granted by the head of the major department or the Dean of the Graduate College when in his or her judgment the proposed use of the material is in the interests of scholarship. In all other instances, however, permission must be obtained from the author.

SIGNED: Francisco Rojas

ACKNOWLEDGEMENTS

This research was sponsored by NASA grant number NAG5-6339. I am grateful for the cooperation by the MODIS Characterization Science Team (MCST) and the MODIS Land Science Support Team (LSST) in supplying pre-launch datasets and advice on MODIS. Dr. Gerry Godden, now deceased, for productive discussions on the more esoteric details of the MODIS system. Jim Storey, Raytheon ITSS, on the parametric modeling of MODIS and his direction in using the MODIS geolocation data. The Optical Sciences Remote Sensing Center for support on MODIS. Susan Moran and Ross Bryant, USDA-ARS, on sharing the ETM+ data of Maricopa, and Simon Hook, Jet Propulsion Laboratory (JPL), for making us aware of the different reprocessing versions used with ASTER. Dr. R. F. Jurgens, and Dr. Martin Slade III from the Planetary Radar group at JPL for continued support and encouragement throughout my academic career. Alfred Paiz, of JPL, and Dr. Yvonne Freeman, former JPL, on providing the initial push and encouragement to continue on the academic ladder.

The Digital Image Analysis Laboratory (DIAL) students for their assistance and support. Dr. R. A. Schowengerdt, my advisor, for support and guidance. The ECE department, the signal and systems professors and the administrative staff for providing a pleasant academic working environment.

DEDICATION

The work is dedicated to my family, Briana L. Rojas (daughter), Eleno E. Rojas (father), Teresa M. Rojas (mother), Juan Rojas (brother), Maricela Rojas (sister), and finally, my wife Maricela A. Rojas.

TABLE OF CONTENTS

TABLE OF CONTENTS - Continued

TABLE OF CONTENTS - Continued

LIST OF FIGURES

LIST OF FIGURES – Continued

LIST OF TABLES

LIST OF ACRONYMS

- AAC — All American Canal
- AOA-14 — Spatial alignment acquisition, during MODIS assembly Optical Bench Assembly (2^{nd} build results)
- ATBD — Advanced Theoretical Basis Document
- Channel — One detector element
- DAAC — Data Active Archive Center
- EIFOV — Effective Instantaneous Field of View
- ESF — Edge Spread Function
- EVI — Enhanced Vegetation Index
- FFR — Far Field Response
- FPV — Focal Plane Viewer, spatial dataset visualization software
- FWHM — Full Width Half Maximum
- HDF — Hierarchical Data Format
- IFOV — Instantaneous Field of View
- LSF — Line Spread Function
- LWIR — Longwave Infrared
- MCST — MODIS Characterization Science Team
- MFI03_k — Test procedure, Alignment of S/MWIR and LWIR using blackbody
- MFI03_q — Test procedure, Alignment of VIS and NIR using SIS lamps
- MODIS — Moderate Resolution Imaging Spectroradiometer
- MTF — Modulation Transfer Function
- NDVI — Normalized Vegetation Index
- NIR — Near Infrared
- OBA — Optical Bench Assembly
- PSR — Point Spread Response
- PSF — Point Spread function
- RMSE — Root Mean Square Error
- SDS — Scientific Datasets
- SIS — Spherical Integrating Source
- SRCA — SpectroRadiometric Calibration Assembly
- S/MWIR — Shortwave midwave Infrared
- VIS — Visible focal plane

ABSTRACT

The Modulation Transfer Function (MTF) is a standard measure of imaging systems performance. This work addresses determination of the MTF for the Moderate Resolution Imaging Spectroradiometer (MODIS) Earth remote sensing system on NASA's TERRA satellite. Reliable characterization of the MODIS MTF requires using as many sources of information as possible for evaluation. In this research a model, pre-launch and on-orbit measurements are used to develop a consistent characterization of the MTF. The on-orbit characterization is implemented using two approaches. The first is cross-track temporal monitoring using data derived from the SpectroRadiometric Calibration Assembly (SRCA). The second is using a two-image approach in which the reference is Landsat-7 Enhanced Thematic Mapper (ETM+) and Advanced Spaceborne Thermal Emission and Reflection Radiometer (ASTER). This characterization of the MTF is used to evaluate the effect on science products, the Normalized Difference Vegetation Index (NDVI) and the Enhanced Vegetation Index (EVI), and includes partial MTF correction (MTFc) as a way to improve the accuracy. This work has produced the following significant results:

- A model for the pre-launch MODIS MTF.
- Automatic image registration using the geolocation data.
- Cross-track on-orbit MTF are comparable to the pre-launch MTF for bands 1, 2, 6 and 29.
- In-track on-orbit MTF indicate that it is lower for bands 1 and 2 (in most cases), and comparable for bands 6 and 29, in reference to the pre-launch MTF.

1 INTRODUCTION

This dissertation is a study of the Spatial Response (SR) for imaging spectroradiometers, specifically the MODIS via the MTF, and its effect on science products derived from the sensor data. The MTF is the magnitude of the Fourier transform of the Point Spread Function (PSF). For orbital imaging spectroradiometers, most of which are sampled scanning systems, the theoretical continuous PSF is not an appropriate quantity, so we refer to the sampled version as the SR.

In previous studies, the system SR has been measured, via the MTF, for other orbital sensors [1-5]. Some of the studies have included restoration techniques, but none have explicitly followed the analysis in an end-to-end fashion [6, 7]. End-to-end analysis consists of determining how the sensor is performing from the engineering point of view, whether a calibration for the SR is warranted and an accuracy measurement of the science being produced.

The sensor on-board a satellite platform is treated as the system [8, 9]. The system SR includes any applicable factors that blur the image, such as the discretization of the continuous scene (sampling), the detector response, the optical components, the electronic filters, the motion blurring, the electrical and optical cross-talk and the ground processing [6, 10]. Atmospheric effects are not considered part of the system response. An atmospheric MTF would be constantly changing, and the sensor SR is stable over a much larger temporal scale than the atmosphere. In this chapter a justification for the study of the SR, followed by a discussion of its effects on science products are presented.

1.1 EVALUATION OF THE SPATIAL RESPONSE

Evaluation of the MODIS SR is important because it is the system averaging function. This averaging function may be thought of as a blur, which causes a contrast degradation in the imagery. In MODIS, the SR is a function of the following major components: the electronics, the scan mirror integration time and the overall optical system.

The SR may change between the time when the instrument is being tested in a laboratory setting to the time when it is actually acquiring images on-orbit. The changes may be caused by one or more of the following factors: change in electrical detector response, change in the focus due to movement of the focal plane or optical components, or change in optical response due to contamination of the optical components by inappropriate outgassing or settling of dust or vapor on lens elements. These types of undesired changes occur over the life of the instrument and result in a larger spatial averaging function, i.e. SR.

The MTF, which is the magnitude of the Fourier transform of the PSF, is a traditional measure of image quality. The MTF can be used to determine the size and shape of the SR. Any changes in MTF will signify a change in the SR. Therefore, it is important to measure the pre-launch and on-orbit MTF. The pre-launch MTF serves as the reference to the on-orbit MTF.

Once the SR is characterized, improvement of the imagery is feasible by separating the MTF into the fundamental components, i.e. response of the optics, electronic and scan mirror integration. A partial correction for the response of the

components creates an image with higher contrast and sharper boundaries between land, water and clouds, and can therefore lead to improved scientific results.

1.2 SCIENCE PRODUCT DEPENDENCE ON THE SPATIAL RESPONSE

The major MODIS scientific disciplines, ocean, land and atmosphere are all affected by the SR. The affected land discipline science products include, for example, Vegetation Indices (VI). The study Earth's vegetation using VIs requires "...a precise radiometric measure of spatial and temporal patterns ..." [25]. The SR is a limiting factor in obtaining accurate measurements, since averaging takes place over several pixels. In MODIS, clouds or water bodies several kilometers away may influence the measured VIs.

Likewise, the SR also affects ocean and cloud studies. The MODIS geometric response, which excludes the optical component, for the ocean bands is 2km. Currently, since the ocean radiance products are just above the noise equivalent radiance level, any observations have to be away from land and clouds by several kilometers. Land and cloud mask products are created for this purpose [26]. Spatial accuracy in these products is required according to the Ocean Science Team (OST) because only 10% of the radiance signal is due to Water-Leaving-Radiance, which is the quantity they are interested in [27]. An accurate description of the SR is important since Normalized Water-Leaving Radiance is used in other algorithms to estimate chlorophyll concentration.

Another product that is essential to MODIS processing is the cloud mask. The cloud mask is produced by an algorithm, which determines the presence of clouds. The

cloud mask value is assigned to each pixel in the 250m and 1km resolutions. The algorithm is implemented via a series of tests, which indicate the effect of a cloud on a pixel. Spatial and radiometric accuracy is needed for the success of this product.

1.3 DISSERTATION ORGANIZATION

The remaining chapters are organized in the following manner: Chapter 2 is the literature review, Chapter 3 introduces the research approach, Chapter 4 is the pre-launch study, Chapter 5 is the on-orbit analysis, and finally, chapter 6 is a study of the effect of the spatial response on science products.

Chapter 2 introduces the MODIS sensor, data products, pre-launch and on-orbit data formats and geolocation background for MODIS, ASTER and ETM+ used for MTF evaluation. Two MODISs exist, the one used in this study is referred to as MODIS-TERRA (on the Terra satellite and launched December 18, 1999) and using a descending orbit. It crosses the equator at 10:30 am. The other MODIS is referred to as MODIS-AQUA (on the Aqua satellite and launched May 4, 2002) and uses an ascending orbit. It crosses the equator at 1:30pm. This configuration serves to maximize cloud free observations of the Earth's surface and exploit synergism with other Earth Observing Systems (EOS) sensors.

The MODIS data are stored in NASA's new Hierarchical Data Format (HDF). The HDF format is briefly described in this chapter to orient the reader to basic concepts. The HDF format is not limited to imaging data, but can also contain vector, geolocation and calibration data. In addition, attributes are available to describe each item besides the regular metadata. Each sensor HDF product is unique and requires upfront research to

understand. A summary of the geolocation product and accuracy is presented for MODIS, ASTER and Landsat ETM+.

Chapter 3 is a discussion of the traditional methodologies for estimating MTFs and includes simplifying assumptions and relationships to linearize the MTF estimation problem and introduce the approaches used in estimating the MODIS MTF.

Chapter 4 summarizes the pre-launch band-to-band registration, develops the MTF system model and uses radial integration of the spatial response, based on pre-launch data, to obtain upper estimates for the adjacency effect.

The term "adjacency effect" refers to the radiance due to photons entering a sensor's Instantaneous Field Of View (IFOV) from a combination of undesired sources and physical interactions outside the IFOV [11-13]. The net effect from this phenomena is contrast degradation and, in some cases, blurring of sharp boundaries. The severity of the effect depends on a combination of sources including sensor resolution, atmospheric scattering, surface-leaving radiance reflected or emitted from adjacent areas onto the target pixel and the physical shape of the sensor's SR. The scope of the adjacency effect definition, in this study, is limited to the sensor's SR, which includes radiance contributions from points that are several pixels away from the target pixel.

Chapter 5 describes the on-orbit analysis for MODIS. The measurements are based on the spatial mode acquisitions of the SRCA, an internal calibration instrument, and on-orbit dual sensor imagery using ETM+ and ASTER as references for MODIS. The SRCA spatial mode data are used for cross-track MTF temporal monitoring and has

the advantage that the characteristics of the source are known and calibrated. This makes these data better suited than imagery for temporal monitoring.

Estimating the on-orbit MTF using a multi-sensor multi-resolution approach is a non-trivial task. The chapter describes a novel geolocation based image registration procedure for registering ETM+ or ASTER to MODIS at different resolution combinations; all the images are geocoded. In a geocoded[1] image, each pixel is referenced to the Earth using a projection, but the image is not necessarily resampled.

The coordinate systems are different for each instrument, and the procedure requires them to be mapped to a common reference. After the registration process, a normalization stretch algorithm is used for radiometric registration, which is required for MTF estimation. On-orbit in-track and cross-track MTF results are presented.

Chapter 6 describes the effect of the adjacency effect, on science products NDVI and EVI. The adjacency effect on NDVI and EVI is presented by simulation using measurements derived from pre-launch laboratory data. Afterwards, a correction filter is applied to MODIS bands 1 and 2 at-sensor-radiances, which are then converted to reflectance to create an NDVI image. The results show qualitative and quantitative improvement.

---

[1] In this definition, it is not necessary to reproject to a map orientation as defined in [10].
[2] Defined as the spatial dimension equivalent to where the MTF is 0.5 [11].

2 LITERATURE REVIEW

2.1 SENSOR SPATIAL RESPONSE CHARACTERIZATION

A study of Landsat-4 and Landsat-5 Thematic Mapper (TM) has shown that the Effective Instantaneous Field Of View ($EIFOV^2$) derived from a nadir presample (before pixel sampling) analysis is larger than the nominally accepted values [5]. Landsat-5's nominal resolution is 30 x 30m for bands 1-5 and 7 and 120 x 120m for band 6. The study found the nadir presample EIFOV to be 33m (in-track) by 36m (cross-track) for bands 1-5 and 7 and 124m (in-track) by 141m (cross-track) for band 6. The EIFOV on-orbit MTF analysis has been shown to be larger than the nominal resolution, with an EIFOV between 40-50m for bands 3 and 4 [15, 16].

On Landsat-7, the follow-on to Landsat-5, the ETM+ EIFOV is between 33 – 37m instead of the nominal 30 x 30m resolution. On-orbit MTF degradation can result in a larger SR over time. As of this writing, the Landsat-7 bands appear to be within the required specifications except for bands 4 and 8 [17].

The Centre National d'Etudes Spatiales (CNES)'s SPOT 4 HRVIR sensor went through a rigorous two-month evaluation of the image quality performance. One of the comprehensive image evaluation studies was MTF and two approaches were used. One of the approaches included evaluating two satellite images, and the second approach was planned using SPOT 4 and an airborne acquisition. In the first approach, a SPOT 4 scene dated March 27, 1998 and a SPOT 1 scene April 3, 1998 were used. The second approach included an acquisition with a spotlight pointing upward to serve as a point target [18].

The CNES agency has also evaluated the MTF of the VEGETATION instrument using in-track, cross-track and 45° response profiles. The work was compared with pre-launch measurements to monitor the sensor on-orbit response [19].

In addition to the MTF calibration of SPOT and ETM+, Hyperion on the EO-1 platform is also going through extensive MTF analysis. The analysis for this sensor started with pre-launch laboratory characterization [20]. The EO-1 platform is flying in formation and lagging by less than a minute with the Landsat 7 platform. During pre-launch MTF characterization, laboratory setups included knife-edge and slit measurements to evaluate the 1-D MTF profiles. The results show that the MTF ranges between 0.26 and 0.3 (assumed to be at Nyquist frequency, although not specified in reference [20]). In addition to the pre-launch measurements, on-orbit measurements have been planned [21]. Preliminary results have been presented using the Ross Ice Shelf and Mid-Bay bridge near Desding, Florida and show a σ equal to 4.5% [22]. These MTF studies, pre-sample and on-orbit, show that EIFOV is larger than the nominally accepted values.

The EIFOV is generally good enough to describe a sensor's SR when the detector (channel) is the limiting MTF component for orbital sensors. In MODIS, the scan-mirror integration time is a non-negligible component, therefore it is not adequate to only use the EIFOV to describe MODIS's SR. The resultant shape of the SR, section 4.5, affects the radiance measurements at every pixel. Neglecting the optics, the geometric response is triangular in shape with a cross-track length of 500m and in-track width of 250m (bands 1 and 2). Using the theoretical geometric response, 25% of the signal is derived

from the adjacent pixels [23, 24]. This is due to the convolution of scene with the geometric response. When blurring due to the optical components is introduced, the geometric response increases both in-track and cross-track.

2.2 MODIS TECHNICAL SPECIFICATION

The MODIS was built by Raytheon (formerly Hughes) Santa Barbara Remote Sensing (SBRS) center. MODIS is a passive spectroradiometer that provides complete global coverage in 36 spectral bands every 2 days from a polar orbit. This MTF study is conducted on MODIS-TERRA. Another MODIS, launched May 4, 2002, is referred to as MODIS-AQUA due to the 1:30pm equatorial crossing time. As part of NASA's Earth's Observing Systems mission, MODIS is one of five sensors on the Terra platform. Terra was launched December 18, 1999. The MODIS imagery is at three spatial resolutions: 250m (2 bands with 40 channels each), 500m (5 bands with 20 channels each), and 1km (29 bands with10 channels each). A channel is a single detector element.

The 36 MODIS bands are configured in 4 focal planes (Figure 1): VIS, NIR, S/MWIR and LWIR. The bands used in this MTF analysis are bands 1, 2, 6 and 29 (Table 1 and 2). The selection of these bands is based on the spectral matches between MODIS and ETM+ or ASTER, and MTFs are computed for three of the four focal planes using the spectrally matching bands.

Some general characteristics are

- Spatial Resolution: 250m, 500m and 1km
- Orbit: 705km altitude, polar orbit
- Scan rate: 20.3 rpm (cross-track)
- Swath: 2330km (cross-track) x 10 km (in-track/scan at nadir)
- Quantization: 12 bits
- Focal length: 0.381m (nominal)
- Spectral Range: 0.405-14.385μm
- Expected Lifetime: 6 years
- Power: 162.5 W (single orbit)
- Data Rate: 10.6 Mbps (daytime peak)
- Spectral bands: 36
- Spectral coverage: 0.4μm – 14.3μm

2.2.1 MODIS product formats

The MODIS data products are produced from the level 1A product. Level 1A contains uncorrected imagery and telemetry in its raw form. From this low level engineering data, higher-level products are produced.

Table 1. Nominal parameters for MODIS bands used in this study. (Adopted from MODIS website)

Primary use	Band	Bandwidth[3]	Spectral Radiance[4]	Required SNR[5]	Required NE[Δ]T(k)[6]
Land/Clouds/	1	620-670	21.8	128	N/A
Aerosols Boundaries	2	841-876	24.7	201	N/A
Land/Clouds/	6	1628-1652	7.3	275	N/A
Aerosols Properties					
Cloud Properties	29	8.400-8.700	9.58(300k)	N/A	0.05

2.2.2 Level 1A

The level 1A product includes all the Digital Numbers (DNs) for all 36 bands and all engineering and ancillary data. The DNs are the raw uncalibrated recorded values for each pixel. The VIS, NIR, and SWIR focal planes operate only during the day, while the LWIR focal plane operates continuously. The file sizes are on the order of 528Mb for one granule, which is 5 minutes worth of data. During nighttime acquisitions, the file sizes are reduced to 178Mb since only thermal bands are active. This product includes quality indicators for missing channels, bad pixels, different instrument operating modes and all detector views. The detector views include the Earth view, the SRCA, the Deep Space View, the Solar Diffuser, and the black body (Figure 2) [23]. Once the data arrives at the

[3] Bands 1, 2, and 6 in nm, and 29 in μm
[4] W-m^2-μm-sr
[5] Signal-to-noise-ratio
[6] NE(Δ)T = Noise-equivalent temperature difference

Data Active Archive Center (DAAC), it is processed into several level 1B products and the Geolocation level 1A product, referred to as MOD-03.

Table 2. Basic parameters for the MODIS geometric SR.

GIFOV (m)	Sample time (microseconds)	Integration time (microseconds)	Ratio Integration/sample time
250	83.333	73.333	0.88
500	166.667	156.667	0.94
1000	333.333	323.333	0.97

2.2.3 Level 1B

The level 1B product is at-sensor radiance in W-m^2-μm-sr. The 1A product contains all the ancillary MODIS data in one file. The 1B product consists of three files, corresponding to the three resolutions. In addition, the higher resolution bands are aggregated into the lower resolution product. For example, the 500m product contains the 250m bands aggregated to 500m, and the 1km product contains the 250m and 500m aggregated to 1km. The 1B product is not resampled, which mean that data are in the original geometry as observed by the sensor.

This data product includes geolocation information. However, the MODIS Characterization Science Team (MCST) has stated that the geolocation data file is copied directly from the level 1A data and should not be used for precise measurements. Any geolocation corrections are applied to the MOD-03 product are not reflected in the level 1B files.

2.2.4 Geolocation

The geolocation product, MOD-03, is derived from level 1A and includes ephemeris corrections. The geolocation references image pixels to an Earth reference frame. It includes the sensor and sun viewing geometry. The accuracy specification is given as 0.2km, but in reference to the land control point algorithm, the accuracy approaches 50m [28]. The geolocation data are defined for the 1km pixel. Reference [23] includes information on interpolating the 1km data to 500 and 250m resolutions, and offsets are required in the in-track and cross-track directions.

2.3 Introduction to Pre-Launch Laboratory Data

The extensive pre-launch tests performed by SBRS and NASA on MODIS-AM are described here, as relevant to the SR. The testing consists of spatial mode internal calibration measurements using the SRCA, registration tests at two levels of assembly, and an acquisition to view the MODIS SR. Some of the acquisitions were successful and others were not.

2.3.1 SRCA spatial mode data

The SRCA can be operated in three modes: radiometric, spectral and spatial. The spectral mode uses an integrating sphere, a grating and a filter wheel to create the desired signal. In radiometric mode, the filters and the grating are removed. This mode is used to determine calibrated radiance response. In spatial mode, the SRCA is used to estimate the band-to-band registration. An undesirable limitation with the SRCA is that it does not

fully illuminate the primary mirror. References [29] and [30] have shown that the SRCA is still useful for on-orbit calibration, however.

Two reticles are used in spatial mode to provide an edge. One reticle, 5 x 12km as projected to the ground, is used to create an edge in cross-track illumination. The edge is scanned across the detector arrays and creates an over sampled Edge Spread Function (ESF). The other reticle is used to estimate the in-track band registration. This reticle is not rectangular and is not optimal for MTF analysis. As a result, the in-track measurements are undersampled. The reticles depend on a phasing approach to obtain sufficient data points to measure the edge response. The oversampled cross-track reticle obtains sufficient data points for reliable cross-track MTF component analysis.

The SRCA data consist of pre-launch and on-orbit measurements (only on-orbit measurements are discussed). The pre-launch dataset was acquired in thermal vacuum to simulate on-orbit conditions [27, 28]. The on-orbit data have been acquired periodically at intervals of 2-3 months. To find these tests, a search of the MCST weekly reports is performed using the MCST website[7]. See appendix A. Once a probable time is found for the acquisition, an hours worth of level 1A data are retrieved. The spatial mode acquisitions follow the order in Table 3. The acquisition is repeated three times each at lamp power setting of 30w, 20w and 10w, since the bands have different SNR requirements. The samples are taken every 200m, and the pixel size for bands 1 and 2 is 250m. The phase difference between the sample and the pixel size is 50m. Therefore, the

[7] The MCST website is at http://mcstweb.gsfc.nasa.gov/

sampling rate increases to 1 sample per 50m instead of one sample per 200m. This is a 5x oversampling.

2.3.2 Spatial registration using the pre-launch laboratory measurements

Some of the measurements are used for channel registration at different assembly levels. Another measurement includes a special acquisition to view the out-of-field response by saturating the focal planes with a 1x1km reticle.

Table 3. Summary of the SRCA spatial mode calibration acquisition.

Step number	Procedure
1	Blackbody source warm-up for 15 minutes
2	At the 13th minute, the 3x10 w lamps are turned on.
3	A 3 minute wait for lamp stabilization
4	Acquire 36+2 scans at 0.0 phase delay
5	Acquire 36+2 scans at 0.2 phase delay
6	Acquire 36+2 scans at 0.4 phase delay
7	Acquire 36+2 scans at 0.6 phase delay
8	Acquire 36+2 scans at 0.8 phase delay
9	Acquire 36+2 scans at 1.0 phase delay
10	Repeat for 20w configuration
11	Repeat for 10w configuration

2.3.2.1 MFI-03 datasets

The MFI-03 datasets are integration level tests and were used to estimate channel alignment and focal plane registration [33]. They were performed at the optical bench

assembly integration level [34]. The optical bench assembly level is the phase when MODIS is being built, but the aft-optics are not integrated.

The channel registration is inferred by computing the centroid and the Full Width Half Maximum (FWHM) for each channel via Line Spread Function (LSF) measurements in the in-track and cross-track directions. The measurements were taken using an external source, the Internal Alignment Collimator (IAC). The IAC is a precision instrument for LSF measurements, and unlike the SRCA, fully illuminates the MODIS primary mirror [35].

The MFI-03 tests consist of two parts, MFI-03_q and MFI-03_k. In both cases, the MODIS primary scan mirror was locked in a nadir position. The MFI-03_q measurement is taken with the SIS lamps and is valid over the VIS and NIR focal plane. The MFI-03_k measurement uses a black body at an elevated temperature as a source and is valid over the S/MWIR and LWIR focal planes. These tests are integration level tests and are presented with the AOA-14 test, a system level test. The three are compared to determine whether biases existed during testing procedures.

2.3.2.2 AOA-14 dataset

The AOA-14 dataset is similar to the MFI-03 test with several differences: the AOA-14 test is a system level test, the IAC is the source, and the scan mirror was rotating at its normal velocity, and MODIS was in thermal vacuum [36]. The AOA-14 is a MODIS science mode of operation test, corresponding to the on-orbit mode of operation.

2.3.2.3 PSR dataset

The PSR dataset is a special acquisition to see if the MODIS Far Field Response[8] (FFR) could be detected [37]. The response is based outside the nominal IFOV of MODIS. A 1x1km reticle was scanned across the focal plane, and each band recorded the response as the source was scanned. By viewing all the data, an image of the response across the focal plane is created, section 4.3.

2.4 DATA FORMAT

HDF is a general format that is capable of encompassing several different data types within one or multiple files. Each HDF file may be accessed in a variety of ways. NASA has adopted a new standard for their EOS products, HDF-EOS, which is an extension to HDF to accommodate satellite imagery. A brief introduction to HDF and HDF-EOS is presented below and some software tools are referenced in appendix B.

2.4.1 HDF

The National Center for Supercomputing Applications (NCSA) at University of Illinois at Urbana-Champaign created the HDF product specification. There are presently two HDF versions 4.1.X and HDF 5.X, which, as of this writing, are incompatible [38, 39]. Special conversion software between the two versions exists, but it has many limitations.

The HDF format is similar to a book. Using the book analogy, it contains a table of contents with chapters, indexes, footnotes, etc. The user may not access any of the

[8] The FFR describes the energy in the SR beyond 2km from the pixel center. It is not the same as the traditional optical FFR, which refers to Fraunhofer diffraction.

HDF information directly, as there is no unique way to know where any of the information is actually located, but the user is allowed to query the HDF file using HDF libraries. The HDF libraries return the information pertaining to the data products that the user wishes to request. Inside the HDF format, data may be compressed, indexed, vectorized, etc. The HDF file may consist of one very large file or it may be composed of several individual files. The MODIS and ASTER HDF products consist of one file per product, while the ETM+ HDF files consists of several files.

Using the book analogy, the HDF file contains chapters. The chapters are Scientific Data Sets (SDS), Vector Data Sets (Vdatas), Vector groups (Vgroups), raster images and other types of formats. For the MODIS 1A and 1B products, the data falls under SDS. This is satellite imagery, floating point and scaled integer data. The attributes for each dataset provide the correct conversion factors to convert the scaled integers, etc. to meaningful geophysical units.

Accessing HDF is a non-trivial task. A brief explanation to accessing HDF is described in pseudo code, Table 4. Step 8, in Table 4, is useful because it describes the units for the data along with limitations, such as the maximum and minimum expected values. All the calls interface with the HDF libraries [38].

2.4.2 HDF-EOS

HDF-EOS follows the same access procedures as regular HDF, but contains three new interfaces. They are the Swath Data Set (SWS), Grid and Point interfaces. These new interfaces are similar to the SDS.

The EOS extension is more applicable to referencing an image or several points by specifying points in some coordinate system such at latitude, longitude, or UTM coordinates. The point interface is designed to support geolocation data that is not organized in any spatial or temporal order. The swath interface is designed to address temporally ordered data. The grid interface supports data that has been projected to some type of well-defined explicit coordinate system [39].

Table 4. Pseudo code for extracting data from an HDF file.

HDF pseudo code
1. Open HDF file
2. Obtain the HDF Table of Contents.
a. Global metadata
b. SDS
3. Tag the appropriate SDS
a. Obtain the SDS tag for the selected dataset
4. Query the selected SDS
a. Returns the amount of data in terms of bands, lines, samples, sample width, type of data, etc.
5. Allocate memory for the selected SDS
6. Set up the array indexing
a. Initial index values
b. Stride count in each direction, band, line, sample
c. Final index values
7. Read the SDS
8. Read the attributes
a. Tag the attributes
b. Extract the information using an ascii array
9. Release the tagged SDS and close the HDF interface

2.5 GEOLOCATION SUMMARY

The satellite imagery used for the MTF analysis is geolocated. The geolocation details and reference coordinate system vary from sensor to sensor. The geolocation

aspect plays an important role in this study because it serves as the basis for a new image registration technique, registration via geolocation.

2.5.1 MODIS geolocation product

The MODIS geolocation data is called MOD-03. The MOD-03 product is based on 1km geodetic latitude, longitude grid. Each 1km pixel has the following geolocation information associated with it (Table 5). The 1km geolocation is interpolated to 250m for the image registration of bands 1 and 2 as illustrated in [23]. The interpolation scheme includes offsets and scaling factors.

Table 5. 1km geolocation data from MOD-03.

Geolocation parameters
Latitude
Longitude
Land/Water Mask
Zenith
Solar Azimuth
Solar Elevation
Sensor Azimuth
Sensor Elevation
Range to Satellite

Another major part of the geolocation is scan data, quantized to one value per scan, and each datum pertains to each mirror side. A granule, 5 minutes worth of MODIS data, contains approximately 203 scans. These data include the following: the scan number, a flag indicating whether the moon is visible in space view port flag, the mirror side used for the scan, type of scan, etc.

and 4 are used for the MODIS MTF analysis. Therefore, only the geolocation for ETM+ at the 30m resolution is relevant here.

ETM+ 1G geolocation is defined for two formats. One is "map" which refers to a north-up configuration. The other orientation is "path", which means the top of the image is in the direction of the orbit. There is a difference of approximately 9^{o}, the inclination angle of the polar orbit, between the map and path formats. The geolocation information is different for both orientations. The path orientation requires a rotation and a shift as indicated by a transformation matrix to get to a UTM system. The map orientation is in UTM coordinates, and the origin for map orientation is the upper left corner. The UTM reference for both ETM+ and MODIS is a geodetic system.

2.5.4 ASTER geolocation

The ASTER geolocation is specified by a 10x10 latitude and longitude grid, which is geocentric. The geocentric reference frame must be converted to a geodetic reference frame for reference to MODIS. The ASTER level 1B at-sensor radiance is resampled/corrected to a path orientation. The 10x10 geolocation grid is not on rectangular basis, but rotated. At this level in the ASTER data corrections for the platform orientation and telescope pointing are included. In order to use the ASTER data in the image registration via the geolocation technique, the 10x10 grid is resampled to 15m for bands 2 and 3, which spectrally match MODIS bands 1 and 2. The grid is also resampled for ASTER bands 4 and 11, which match MODIS 6 and 29 at the appropriate resolution. The ASTER geolocation requirement is ±431m in-track and ± 437m cross-track, but the accuracy estimated goal is 47m in-track and 54m cross-track [41].

ASTER and ETM+ data are registered to MODIS data for MTF analysis as described in Chapter 5. ASTER offers the advantage of almost simultaneous viewing with MODIS, thus atmospheric effects are minimized. ETM+ leads MODIS by 30 minutes; so this configuration is more susceptible to atmospheric changes.

Figure 1. Block layout of focal planes. Bands 1 and 2 have 40 channels (detectors), and bands 3-7 have 20 channels.

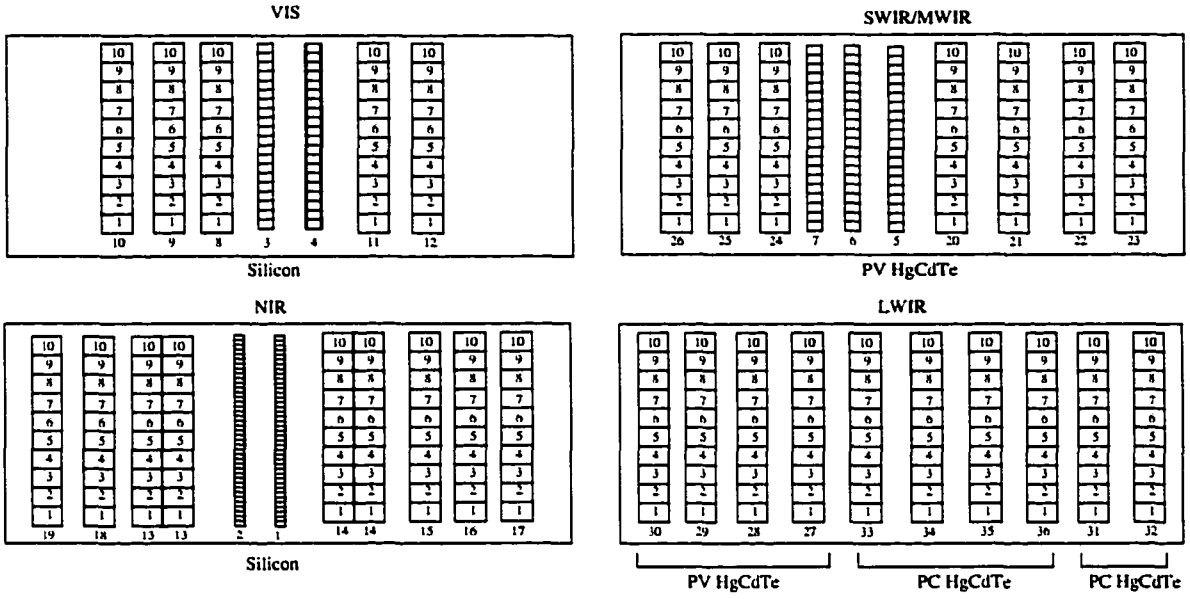

Figure 2. MODIS acquisition cycle (Adopted from [23]).

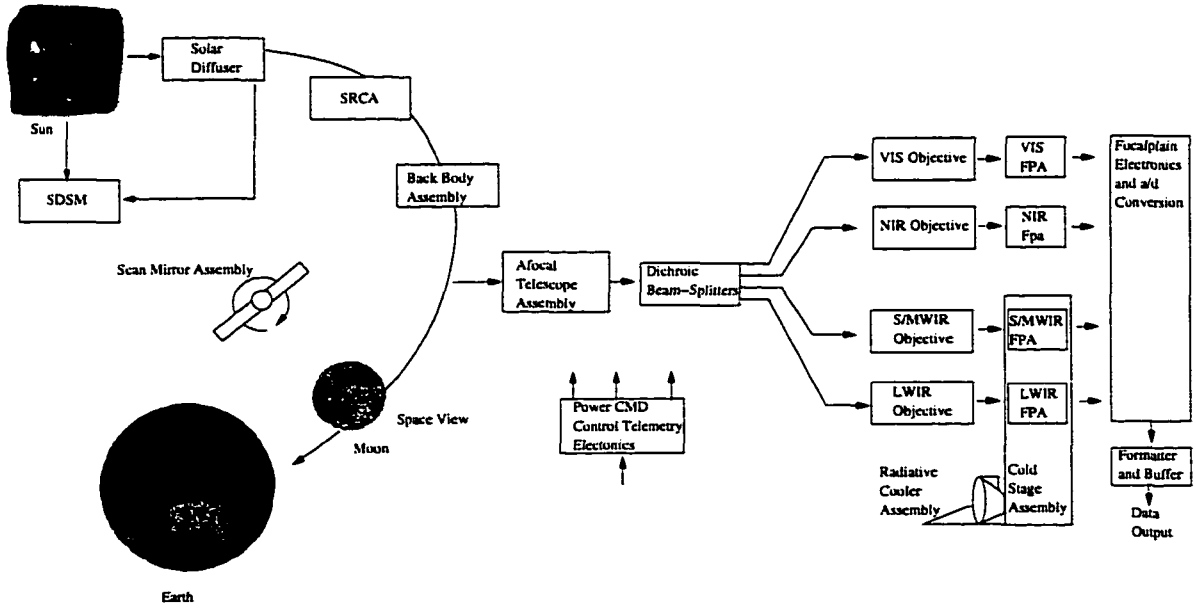

3 RESEARCH APPROACH

3.1 MTF RELATIONSHIPS: ESF, LSF AND SEPARABILITY

By definition, the MTF is the magnitude of the Fourier transform of the PSF. The PSF is often referred to as the impulse response of an imaging system.

$$MTF(u,v) = \left| F(PSF(x,y)) \right| \tag{1}$$

Separability, when applicable, simplifies the analysis to 1-D for the u and v directions. Using this assumption, the combined PSF(x,y) is the product of the in-track and cross-track components [10], $PSF_1(x)$ and $PSF_2(y)$, which correspond to the LSFs in the two directions respectively.

$$PSF(x,y) = PSF_1(x)PSF_2(y) = LSF_1(x)LSF_2(y) \tag{2}$$

Separability does not apply to every system, but in Earth observing sensors the in-track satellite velocity is negligible compared to the cross-track velocity for whiskbroom scanners. The separability assumption neglects non-separable artifacts such as optical scattering in the sensor.

MTF estimation is typically implemented via the following 1-D analysis using the ESF and the LSF, which is the derivative of the ESF.

$$ESF(x) = \int_{-\infty}^{x} LSF(\tau)d\tau \tag{3}$$

LSF targets are used during pre-launch system integration since they are easy to fabricate in a controlled laboratory setting (Figure 3). The LSF slit width should be no more than 0.2 of a detector for it to be negligible in analysis. If the LSF approach is not feasible, usually because of insufficient signal, an ESF target is implemented. The ESF is measured with a wide rectangular reticle in MODIS tests (Figure 4). The reticle width should be at least 5 times the pixel size. Both sides of the aperture can be used to obtain ESF measurements.

3.2 TARGET TAXONOMY FOR POINT, LINE AND EDGE TARGETS

In practice, finding near ideal targets in real scenes is not a trivial task. The best targets may be natural or artificial, depending on the resolution. Ideal targets (point, line and edge) should be high contrast with a homogeneous background [42]. A difficult criteria to satisfy using physical targets and orbital sensors is the Nyquist sampling rate. In a novel MTF measurement study, a powerful spotlight was used to create a point source for the SPOT 4 satellite, but the sampling problem cropped up in the MTF analysis [18]. The point source technique has to overcome inadequate sampling and have high contrast to provide enough signal. In another novel approach, an array of point sources was used to overcome the sampling problem for Landsat 4 TM [4]. The setup consisted of a 4x4 grid in White Sands New Mexico with the array spacing at 7.5m. This technique allowed exploitation of the scene-phasing by oversampling the 30m PSF and produced acceptable results. Practical limitations of this technique are that the target and background uniformity over large areas are difficult to maintain for repeated quality

observations [43]. When point sources of sufficient quality cannot be found, a line source target may be an appropriate substitute.

A target is considered a line source if the target and background are uniform and the line width is 0.2 of a pixel or less. The definition of uniformity implies spatial, spectral, temporal and radiometric uniformity under ideal conditions. The contrast between the target and background must be high so that the sensor may detect the sub-pixel target with sufficient signal strength. In addition to these requirements, the sampling rate should be high enough to oversample the SR.

The angle between the target and sensor should be almost parallel or perpendicular, but not exactly parallel or perpendicular, so that a number of "phased" samples are obtained across the target [2]. In Figure 5, the All American Canal (AAC) serves as a line source for MTF estimation. This target is difficult to analyze since the angle of the canal in reference to the scan orientation is not close to the in-track or cross-track directions.

Generally coastlines, buildings and roads may serve as targets, but they are dependent on the scale in relation to the sensor's nominal resolution. If the resolution is on the order of several meters, many buildings, roads and bridges will satisfy the requirements; but for lower resolution sensors, targets of opportunity are more difficult to find. For example finding a 20km long, straight road with a uniform background for a 1km resolution sensor is not a trivial task. The road should be approximately 0.2km wide such that it has significant contrast, in reference to the background, to be reliably

observed by the sensor. When suitable LSF targets are not found, edge targets are the next candidates. Examples are coastline or lake boundaries (Figure 6).

3.3 MTF APPROACH

Along with the approaches mentioned to estimate the pre-launch MTF, a dual image technique can be used to estimate the on-orbit MTF. The dual image technique is based on equation 4 under ideal conditions, where the same scene is observed by MODIS and the reference sensor. Under ideal conditions, a cancellation of the scene occurs, thus leaving the MTF pertaining to MODIS and the reference, equation 6. The indices u,v are spatial frequency coordinates in units of cycles per pixel, and the terms for equations 4 - 7 are defined in Table 5.

$$\text{estMTF}_{\text{MODIS}}(u,v) = \frac{|\,\text{image}_{\text{MODIS}}(u,v)\,|}{|\,\text{image}_{\text{REFERENCE}}(u,v)\,|} \tag{4}$$

$$= \frac{|\,\text{scene}(u,v)\,|\,\text{MTF}_{\text{MODIS}}(u,v)}{|\,\text{scene}(u,v)\,|\,\text{MTF}_{\text{REFERENCE}}(u,v)} \tag{5}$$

$$= \frac{\text{MTF}_{\text{MODIS}}(u,v)}{\text{MTF}_{\text{REFERENCE}}(u,v)} \tag{6}$$

$$\cong \text{MTF}_{\text{MODIS}}(u,v) \tag{7}$$

Table 7. Explanation of terms for equations 5-7.

Variable	Definition
$MTF_{MODIS}(u,v)$	The true MODIS system MTF
$estMTF_{MODIS}(u,v)$	The estimated system MTF for MODIS
$MTF_{REFERENCE}(u,v)$	Higher resolution sensor's reference MTF
scene(u,v)	The observed scene spectrum
image(u,v)	The observed image spectrum by MODIS and the reference sensor.

The numerator in equation 5 contains the term $image_{MODIS}$, the "ideal" MODIS image, which is the scene frequency spectrum multiplied by the MTF_{MODIS} (equivalent to the scene being convolved with the MODIS SR). MTF_{MODIS} includes the channel response, the electronic response, the optical response and any second order effects present in MODIS [44]. In the denominator, the higher resolution sensor's term, $image_{REFERENCE}$, which is equal to the scene is multiplied by the term $MTF_{REFERENCE}$. Cancellation of term |scene| leads to equation 6. The term $MTF_{REFERENCE}$ term is nearly 1 compared to MTF_{MODIS} at frequencies of interest and therefore is negligible. This results in an estimate for the MTF equation 7. Since the "real" MODIS imagery is not ideal, further processing is required to estimate an MTF. The non-ideal aspects include discretization of the continuous image (sampling), system noise, low frequency amplitudes in the scene (leading to high noise in the ratio of equation 5, and any other degrading effects [6]. Obviously, the radiometric spectral responses of the reference and test (MODIS, in this

case) system should be as similar as possible. The spectral matches for the three EOS sensors used in the analysis are listed in Table 8.

Table 8. Matching spectral bands for MODIS, ETM+, and ASTER.

Sensor	Bands (resolution in meters)				
MODIS	1 (250)	2 (250)	6 (500)	4 (500)	29 (1000)
ASTER	2 (15)	3 (15)	4 (30)	1 (15)	11 (90)
ETM+	3 (30)	4 (30)	5 (30)	2 (30)	

3.3.1 Pre-launch channel validation and out-of-band response

The characterization of the MODIS MTF is best achieved by examining the pre-launch and on-orbit data. The pre-launch test data are combined with a model to derive an MTF estimate. In addition to estimating the pre-launch MTF, three related studies have been performed: a review of the channel registration for each band, analysis of cross-talk anomalies and estimates of the SR based on laboratory data. The channel registration determines whether the channel offsets for each band are negligible for the MTF analysis. Pre-launch channel registration alignment is analyzed by comparing the two datasets MFI-03 and the AOA-14 described in Chapter 2. A software package, the Focal Plane Viewer (FPV), was developed as a visualization tool for these data. FPV shows the channel locations relative to the focal plane grid during which measurements are taken with respect to the grid. The FPV also uses Point Spread Response (PSR)[9] data to show anomalies and cross-talk problems [37].

[9] These data were referred to as PSR at the MODIS reflective bands workshop. In an effort to reduce confusion this name is retained here.

The analysis of cross-talk anomalies and the PSR data are used to obtain upper estimates for the tails of the SR (the area outside the EIFOV) and determine whether the measurements are consistent with design specifications. The measurements are used to study the MODIS SR effect on the NDVI and EVI and discussed in section 3.3.3. The PSR data has some problems, as described later, but it is a unique acquisition.

After the channel registration offsets and the tails of the SR are computed, the pre-launch MTF model is introduced. The model is based on theoretical design specs and pre-launch MTF validation data. The validation data comes from the IAC. The goal is to use the model as the reference to determine whether the on-orbit measurements validate the model or whether a correction is needed in the case that the on-orbit measurements show a bias. The model is also used to develop an MTF correction filter based on the pre-launch system MTF and an ideal MTF response.

3.3.2 On-orbit MTF analysis

The second major part of the study is on-orbit MTF estimation. The on-orbit analysis is separated into three major complementary areas: image registration, MTF estimation, and temporal stability. The MTF estimation technique used for MODIS consists of a two-image analysis in which the reference is ETM+ or ASTER. The MODIS bands 1, 2, 6 and 29 are used in the analysis for three of the four FPs, NIR, S/MWIR and LWIR (Table 8). The ETM+ and ASTER scenes are registered to MODIS using geolocation data, explained in section 2.5, in a semi-automatic process. The MODIS 1B data are not resampled, scan shifts occur in the imagery, and registration process is able to reproduce the shifts. After the images are registered, any global (consistent across the

entire image) cross-track and in-track offsets are removed; the offsets are relative geolocation errors between the two sensors.

The registered images are processed using an MTF estimation algorithm [44]. The algorithm was validated and optimized using three cases at 250m resolution: estimation of the transfer function under ideal conditions (case I), estimation of the transfer function under aliased conditions (case II) and estimation of the transfer function using MODIS 1B data and referencing the estimate to case II (case III). This validation shows how the algorithm may behave under the aforementioned conditions, especially since the MODIS imagery is undersampled.

As part of the on-orbit validation, the SRCA spatial mode data are used to monitor temporal changes in cross-track MTF. The variation is less in MTF response using the SRCA, than in the dual image method, because the source is the National Institute of Standards and Technology (NIST) lamps; the lamp output is precisely controlled and the SRCA is contained within MODIS. Temporal changes in MTF response using the SRCA are not apparent. The SRCA data cover a span of one year using five acquisitions. Two limitations in using the SRCA data are that only cross-track MTF estimates are obtained, and the SRCA does not illuminate the full primary mirror as do the Earth view acquisitions.

A shortcoming in the analysis is the in-track on-orbit MTF estimates are not as indicative as the cross-track measurements. This may be due to the undersampling and lack of filtering in the in-track direction. Two methods to improve the sampling rate are introduced. One uses a model convolved with the geometric spatial response. Phases

from the convolved model are extracted and correlated with the scenes to improve the sampling rate. The second method is a multi-date approached based on geolocation. The desired sampling grid is created in which one image is held as the reference and the other dates are used to fill in the grid. This second technique improves the sampling rate, but suffers from temporal changes, which are based on the sensor repeat cycle.

Some of the desired features for interleaving are cloud free scenes with minimal atmospheric interference, localized radiometric matching, correction solar angle changes and atmospheric correction. In addition, localized temporal radiometric values should be highly correlated within the different scenes.

3.3.3 MTF effect on science products

Using the out-of-band estimates, section 3.3.1, simulations show that the MODIS SR affects the accuracy of the sampled measurements via the NDVI and the EVI products. These two products are used in MODIS global maps in 16 day and monthly cycles. The simulations in the section show that the MODIS SR affects the accuracy of the science products.

Therefore, one way to improve the science results is to apply an MTF correction to the MODIS imagery. The correction filter results in an improvement near high contrast boundaries, but the correction is slight in reference to the total scene. Improvement is limited by inadequate sampling in the MODIS sensor, but a partial correction can still be applied to the data. Currently, the correction filter is based on the pre-launch MTF and is being validated using ETM+ as a reference for the NDVI product. If the on-orbit or

SRCA cross-track MTF measurements do not match the pre-launch MTF, an adjustment can be made to the correction filter.

Figure 3. Example of an LSF reticle to scan across the NIR focal plane. (40 channels in center bands).

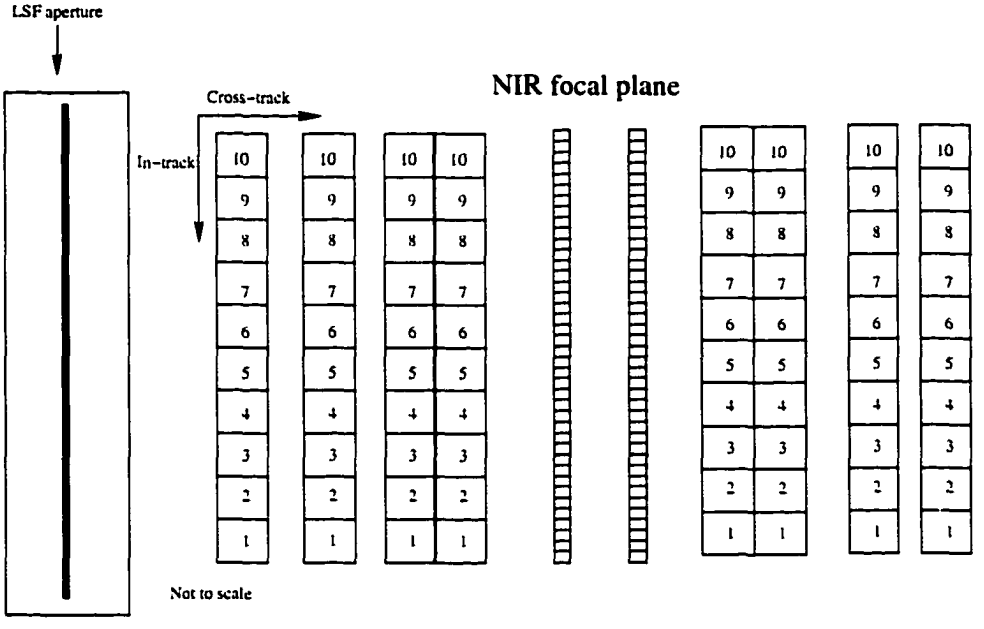

Figure 4. Example of an ESF reticle to scan across the NIR focal plane. (40 channels in center bands).

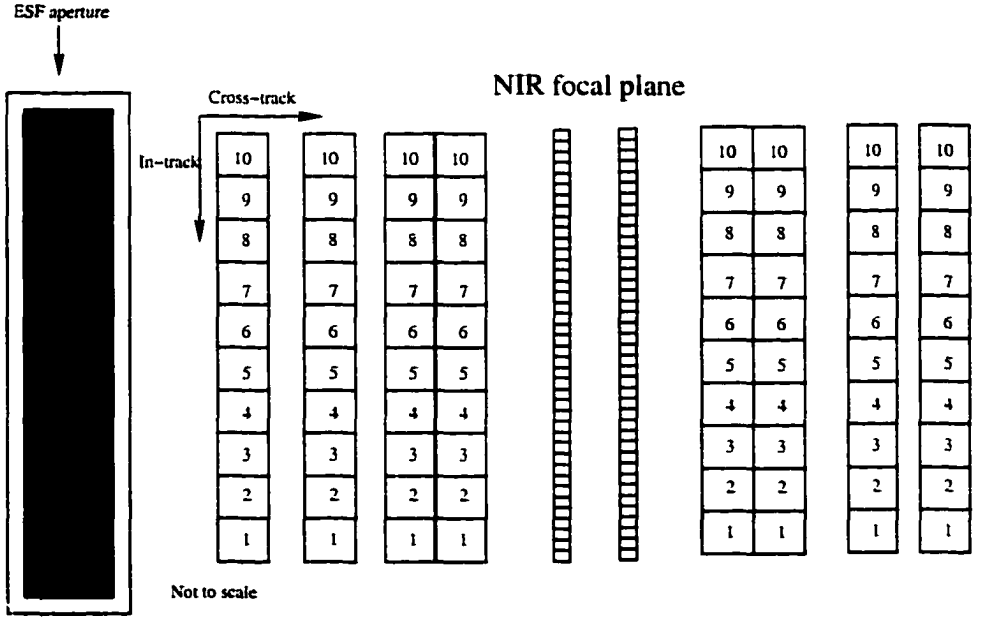

Figure 5. All American Canal near Yuma, AZ as seen by MODIS on June 29, 2000.

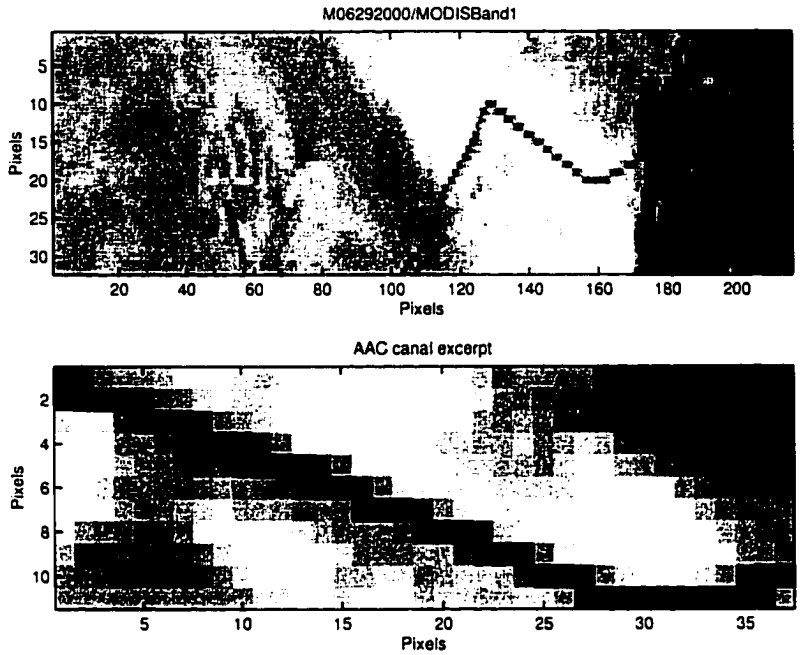

Figure 6. Areas on the Lake Tahoe shoreline may serve as edge targets, but the non-unifomity may cause problems. Acquired on April 16, 2001 by MODIS.

4 PRE-LAUNCH ANALYSIS

4.1 INTRODUCTION

Before a sensor is put on-board a satellite, extensive pre-launch validation is required. Several tests were performed on MODIS-AM to validate the focal plane registration, channel alignment, MTF response and to identify cross-talk problems on all four Focal Planes (FPs) VIS, NIR, S/MWIR and LWIR [45]. The spatial registration results can determine whether the channel misalignment errors are negligible on a band-by-band basis for MTF analysis, or if the registration errors must be taken into account. The pre-launch registration data are derived using LSF measurements and are in ground units of meters.

Another dataset used is the PSR data, section 2.3.2.3, acquired using a different configuration. The configuration consists of a 1x1km aperture, which is scanned cross-track at the channel 5 of a 1km band using a 1km sampling rate. These data are overlaid on the spatial registration measurements to observe combined electronic and optical cross-talk. The out-of-field response contribution on the illuminated channel is computed using radial summing (ensquared energy), a simplified version of encircled energy, for this coarsely sampled data [46-48]. The computed out-of-field response values are used in section 6.2 to see how the MODIS SR effects the science products.

The final part of the chapter is the derivation of the pre-launch MTF system model. The model serves as the basis for the on-orbit MTF estimation and correction. It consists of three major MTF contributors, the optics, the scan mirror integration, and the

channel response. The scan mirror integration and the channel response are taken from theoretical design specs, and the optical component parameters are estimated using laboratory MTF data.

This chapter is organized in the following manner: the spatial data and the FPV software, observations using the PSR data, ensquared energy results and the pre-launch MTF model. The spatial data test results are summarized in Tables 10-12.

4.2 SPATIAL REGISTRATION DATA ANALYSIS

The spatial registration tests were implemented in the cross-track and in-track direction using LSFs (Figure 3). The first two acquisitions were without the aft-optics assembly and are referred to as integration level measurements. These acquisitions are referred to as MFI-03_q and the MFI-03_k, section 2.3.2, the test procedure report name [33]. The MFI-03_q test is valid over the VIS and the NIR focal planes, and the MFI-03_k test is valid over the S/MWIR and the LWIR focal planes. The third acquisition is the AOA-14. The AOA-14 test is valid over all four focal planes and is considered a system level test, in which MODIS had the aft-optics integrated and operated in science mode, the normal operating mode while in orbit [34, 49]. The centroids indicate channel position, and the FWHM values represent the channel width and height.

The MFI-03_q data were taken with the optical bench assembly and the mirror assembly in a locked position using NIST qualified lamps as the source [33]. Even though this dataset was used to analyze the VIS and NIR FPs, the NIST lamp frequency response has a spectral output in the S/MWIR and LWIR region; therefore, the S/MWIR and LWIR FPs responded during the test. The MFI-03_k uses the same configuration as

the MFI-03_q, but the source is a black body [33]. The frequency spectrum of MFI-03_q validates the S/MWIR and LWIR focal planes; however, not all the acquisitions were successful.

The tests are compared to determine if the focal plane channel results are consistent. The comparison is implemented by evaluating the channel alignment for each band across the three acquisitions using the FPV.

4.2.1 The Focal Plane Viewer (FPV) analysis tool

The FPV is a Tcl/Tk software visualization tool developed to compare the three datasets: MFI-03_q, MFI-03_k and AOA-14 [50]. The user can overlay and compare the measurements for the different tests simultaneously on a FP basis. The FPV allows the user to view the intra-band registration to 50m. In order to display each individual channel, two datasets are needed. One is the FWHM data, and the other is the centroid data. The FWHM contain the channel width and height and the centroid data contain the 1st moment. All three datasets MFI-03_q, MFI-03_k and AOA-14 should contain these two measurements. If either of these measurements are missing, then the channels are not displayed and are referred to as missing channels. This tool is available via the DIAL webpage[10] under the MODIS project.

4.2.2 Spatial registration summary

In the following sections, the data results corresponding to a particular FP are shown for comparison. The cross-track direction is referred to as scan, and the in-track

[10] http://www.ece.arizona.edu/~dial

direction is referred to as track. The nomenclature used for the figures are as follows Figure 7),

- track: direction is from channels 10-1 (vertical)
- anti-track: direction is from channels 1-10
- scan: direction as indicated in the figure is from right to left
- anti-scan: direction opposite to the scan[11]

4.2.2.1 Summary of the VIS FP results

In Figure 7 the FP is aligned on the 1km grid, and the FP origin is represented by the cross-hairs in the figure. The alignment results as seen in the figure are very good for the AOA-14. MFI-03_q data was comparable to the AOA-14. The AOA-14 in general show mis-alignment errors within the 10% range of a 1km bands. Bands 3, 4, 8, 9 and 10 of this test are within 50m as estimated using FPV. The MFI-03_q test (not shown but summarized in Table 10) also showed an alignment within the 10% tolerance level, but the MFI-03_k test did not (Figure 7). The results for MFI-03_k are biased compared to the previous two acquisitions, which shows that not all tests were successful.

4.2.2.2 Summary of the NIR FP results

The AOA-14 test shows that band 18 and 19 are mis-registered by 0.15km in the track direction (Figure 8[12]). This dataset has a slight bow-tie type profile across the FP along channel 1. The mis-registration is minimum at the FP origin and greatest at the

---

[11] The NIR FP scan direction is opposite to the other three focal planes' scan direction, but this is neglected for the analysis.

[12] Note in bands 13 and 14 there are two sets of reported measurements overlaid on the channels. The channel count starts from 11-20 and 30 - 40.

edges by 0.2km. The in-track tolerances are within the 10% specification, except at the edges. Bands 1 and 2 are within the 50m misalignment. The MFI-03_q test shows that all the bands in this focal plane are aligned in the track direction (Figure 8). This set of measurements does not exhibit the similar offsets that the AOA-14 test exhibits. Unlike the AOA-14 data for bands 1 and 2, the MFI-03_q data exhibit an offset of 50m. The MFI-03_k test also exhibits a scan offset. The AOA-14 data has a track direction bias. These data exhibit the anti-scan offsets in the FP in the 20% range.

4.2.2.3 Summary of the S/MWIR FP results

In the AOA-14 dataset, the 1km bands are within 10% tolerance. The 0.5km bands are mis-registered by 20% (Figure 9). Bands 6 and 7 have a 0.1km anti-track offset. Band 5 did not respond in this test. The MFI-03 test results are similar to the AOA-14 results with the exception of bands 7, 21, 22 and 23. Bands 24-26 are under 0.1km mis-registered for both datasets. In particular, band 21 and 7 show a noticeable offset in the anti-track and scan direction. The offset is only 0.1km in the AOA-14 data.

4.2.2.4 Summary of the LWIR FP results

The MFI-03_q data shows several problems as indicated by Figure 10. They range from channels not responding, to large band mis-alignments. The FPV shows that bands 24 - 29 have a 0.1km track offset, band 30 has a 0.2km track in channel 1, and channel 10 has a 0.2km scan offset. The channels that did not respond in the test are in bands 27 (channels 9 and 10), 36 (channels 8 and 9) and 32 (channel 1). Some of the same channels did not respond in the AOA-14 and the MFI-03_k, which indicates that

they may have potential problems. The conclusions from the three different tests for this FP are: the responses due to channels 9 and 10 in band 27 are unreliable, and band 30 has a track and scan offset. This band is out of spec and will require an offset correction if used for MTF analysis.

4.2.3 Summary of candidate bands for MTF analysis

The candidate bands for MTF analysis of MODIS are 1, 2, 4, 6 and 29, as shown in Table 8. The offsets and responses as given by the centroid and the FWHM measurements indicate that no correction is needed for MTF analysis. Bands 1 and 2 had a 20% offset error in the MFI_03 integration level test, but the offset was reduced to 10% in the system level test, AOA-14. Band 4 shows misregistration under 10% in two of the tests. Band 6 did respond in the AOA-14 test and the offset error was under 10%. Band 29 has an offset error of 10% in the integration test and 15% in the final system level test.

4.3 PSR Data Analysis

The PSR data were created for MODIS in order to characterize the FFR [37]. The definition used for the FFR is the integrated response at a distance greater than 3km away from a pixel of interest. The PSR data generally spans about ±15km in the scan and ±5km in the track direction, from channel 5 in a 1km band. The PSR test procedure setup used the IAC, a precision instrument for LSF analysis. A 1x1km (ground units) reticle illuminated the FPs. The data acquisition included other channel illumination, but only channel 5 is discussed here.

4.3.1 PSR at a 1 km sampling

Some of the desired features for this type of PSR measurement are sub-pixel sampling, a point source, and a fine quantization scale. The PSR data scale is 12bit quantization. This is an adequate quantization scale, as defined by orbital passive Earth sensors, but sub-pixel sampling is not achieved, since the sampling rate is one sample per km. The source was a 1x1km aperture, clearly not a point source.

The PSR data contain certain peculiarities such as the source saturating channel 5. When the source was on channel 5, approximately a 1 to 2km area was also saturated. In reference [37], the saturated cap was replaced with a normalized PSF from another dataset (Figure 11). The ratio of the saturated DN to the normalized DN over the saturated range is unknown. In addition to the saturation, a noise floor of 10^{-6} was added for DN values below this level.

All PSR figures are on log scale colormaps. The naming convention used for the figures and bands is the following. The prefix "elim" means that the DN floor was substituted. The suffix _psr# refers to PSR data for band #. Figure 12 shows the response for each band as the aperture was scanned across the FP. The respective band response is aligned by sample number (x-axis). The values in Figure 12, elim_psrb8, were read from band 8 as the aperture was scanned across the FP as indicated by the brightest white pixel, channel 5. A spatial anomaly which occurred in the acquisition for this focal plane was the cross-talk in samples 26, 29 and 32-33. The cross-talk near samples 29 and 32 corresponds to bands 11 and 12, respectively.

4.3.2 PSR data summary for VIS focal plane.

In Figure 12 possible systematic cross-talk areas are labeled as "anomaly". As the aperture was scanned, bands 8, 9 and 10 responded in the same region, indicating that cross-talk occurred. Elim_psrb8 has a response in samples 25-34 due to the edges of bands 11 and 12, indicated by the arrows. There should not be a response in this area. There is no obvious interference from other bands in the figure.

4.3.3 PSR data summary for NIR focal plane.

The PSR response in Elim_psrb14 does not exhibit similar anomalies as the aperture is scanned across the FP (Figure 13). At the left edge of the FPs, the response is fairly low for samples 5-12 for Elim_psrb15 and 16. The striping patterns by samples 34 and 35 affect the response and are mentioned in reference [37]. Elim_psrb14 had to be offset 2km in scan, while the other data did not, because the sample numbers where not aligned with the FP. Band correlated cross-talk due to band 18 appears by bands 14-16.

The dataset Elim_psrb13 uses two channels to improve the SNR. MODIS combines the output of both channels to create a higher SNR (Figure 14). Cross-talk from other bands affecting band 13 start from sample 11. The cross-talk is less in Elim_psrb18 and 19.

4.3.4 PSR data summary for S/MWIR focal plane

Elim_psrb24 and 25 exhibit similar response characteristics that contain signs of band correlated cross-talk (Figure 15). The striping features that were mentioned in reference [37] also appear here, but the striping in sample 37 does not appear correlated

to another band. Elim_psr for 20 - 23 show signs of either very high noise offset or band correlated cross-talk. The striping in samples 37 and 38 are consistent across the S/MWIR measurements. The band-to-band cross-talk that was mentioned in reference [51] is also seen.

4.3.5 PSR data summary for LWIR focal plane

The LWIR data in this acquisition are not valid; there is no clear response for the scan across the FP. A definite explanation could not be found, but one plausible explanation is that the MODIS system temperature was higher than the 83k required for normal operation during the acquisition. The response for bands 28-30 are shown in Figure 16. The PSR data for the other bands on this FP are not shown.

4.4 ENSQUARED ENERGY ANALYSIS

Encircled energy is a concept in which integrated energy around the PSF is computed as a function of radial distance [46-48]. It is one way to describe the localization of a given PSF, i.e. is it narrow or wide. The ensquared energy concept, a simplified variant of encircled energy, also computes the energy as a function of distance, but summing is implemented in squares. This concept reflects the discrete FP more realistically. The PSR data is used in computing ensquared energy to obtain upper estimates for the adjacency effect, section 4.4.

Using Figure 17 as a guide for the 1km bands, the 0^{th}km cell corresponds to channel 5 of a 1km pixel. The ensquared energy is computed as a function of distance from cell 0 until the track direction edge (top and bottom) of the FP is reached. Then,

cross-track direction summing continues as shown by the 6th and 7thkm cells. Figures 18 and 19 show profiles of the ensquared energy as a function of distance from the center channel, for bands 8-24. The results of the measurements are summarized in Table 12. The measurements for bands 1-3 are used to examine the adjacency effect and it's affect on science products, NDVI and EVI, using simulations in Chapter 6.

4.5 DERIVATION OF THE SIMPLIFIED MTF MODEL

The SBRS team who designed and built the MODIS included an MTF model, known as the MODIS Model-N. References [30] and [29] discuss the model in greater detail than discussed here. The model consists of the following parameters,

$$MTF_{system} = MTF_{optics} \cdot MTF_{Fab/Align} \cdot MTF_{Det} \cdot MTF_{Int} \cdot MTF_{OptX-talk} \cdot MTF_{DetX-talk} \quad (8)$$

where the MTF_{system} is the complete 2-D system MTF in the u and v directions. The terms are summarized in Table 9. Based on the frequency response in references [30] and [52], the $MTF_{OptX\text{-}talk}$ and the $MTF_{DetX\text{-}talk}$ terms are omitted, because they are not considered to be major MTF contributors. In other words, the MTF frequency response of $MTF_{OptX\text{-}talk}$ and $MTF_{DetX\text{-}talk}$ is high relative to the other components. In the spatial domain, they amount to very little smearing (blurring) in the image. Equation 8 reduces to Equation 9.

$$MTF_{system} \cong MTF_{optics} \cdot MTF_{Fab/Align} \cdot MTF_{Det} \cdot MTF_{Int} \quad (9)$$

Table 9. Summary of terms for the MODIS model-N.

Terms	Meaning	Function/Form
MTF_{optics}	Optical component	Assumed Gaussian
$MTF_{Fab/Align}$	Fabrication and alignment component	Assumed Gaussian
MTF_{Det}	detector component	Assumed sinc
MTF_{Int}	integration component	Assumed sinc
$MTF_{OptX\text{-}talk}$	Optical cross-talk component	Assumed negligible
$MTF_{DetX\text{-}talk}$	detector cross-talk component	Assumed negligible

According to [52], the MTFoptics and MTFFab/Align components are coupled, and there is an uncertainty as to the actual MTF contributions. A Gaussian function is assumed to represent the MTFFab/Align multiplied by the MTFoptics. The resultant MTF equation is

$$MTF_{system}(u,v) \approx MTF_{optics}(u,v) \cdot MTF_{Det}(u,v) \cdot MTF_{Int}(u) \tag{10}$$

The MTF model used for the remainder of the dissertation consists of these three major components: the optics, the scan mirror integration and the finite aperture of the detectors. The term "geometric response" is a generic term, which refers to the SR and excludes the optical component, MTF_{optics}. The geometric response ideally creates a triangular SR whose dimensions are 250m by 500m in the in-track and cross-track direction, respectfully.

Equation 10 is the simplified two-dimensional MTF model in the u and v frequency axis. The term MTF_{Int} only occurs in the cross-track direction and is due to mirror rotation during non-zero integration time. The multiplications are convolutions in the spatial domain. The frequency domain terms are described in equations 11 - 13. The definition for the Gaussian is adopted from [53]. MTF_{Det} and MTF_{Int} are nominal values (Table 13). The unknowns in the simplified MTF model are a and b in the MTF_{optics} term.

$$MTF_{optics}(u,v) = e^{\frac{-(2\pi u)^2 a^2}{2}} \cdot e^{\frac{-(2\pi v)^2 b^2}{2}} \tag{11}$$

$$MTF_{Int}(u) = \mathrm{sinc}(u \cdot Int) \tag{12}$$

$$MTF_{Det}(u,v) = \mathrm{sinc}(u \cdot Detx)\,\mathrm{sinc}(v \cdot Dety) \tag{13}$$

Assuming separability, $MTF_{system}(u,v)$ is separated into the two 1-D components dependent only on u and v as discussed in section 3.1 [10].

$$MTF_{system}(u,v) = MTF_{system}(u) \cdot MTF_{system}(v) \tag{14}$$

During the MODIS laboratory validation tests, the IAC was used to obtain LSF measurements, and derive MTF and FWHM values [30, 36, 54]. These validation tests are important because the MODIS Earth view port was illuminated using an external light source, the IAC, and the primary mirror was rotating at its on-orbit rate. Using the un-published MTF results from reference [54], the optical parameters, a and b, were

estimated by fitting equations 11 - 13 to measured MTF values at 5 spatial frequencies in the u and v directions, 0.0, 0.125, 0.25, 0.375 and 0.5 cycles per pixel. The fitting was done for bands 1, 2, 6 and 29, which are on three focal planes, but only bands 1 and 2 are discussed here (Figures 20 and 21). The fit was implemented using a MATLAB function based on the Nelder-Mead algorithm, an unconstrained nonlinear minimization routine [55].

The combined in-track and cross-track RMS errors between the model and the data are 0.0067 for band 1 and 0.0107 for band 2. The estimate takes into account the integration time, mirror velocity, and doubling due to the reflection angle. The ratio of $a_{band1}\,(b_{band1})^{-1} = 0.795$ and $a_{band2}\,(b_{band2})^{-1} = 0.729$ show that there is consistency in the results, Table 13, between the two bands (Figure 22). The model's spatial response does appear correct in resembling the MODIS SR, and the geometric response is triangular in shape with a cross-track length of 500m, and in-track width of 250m as indicated by the ATBD (Figure 23).

Table 10. Summary of FP spatial alignment.

Band	MFI-03_q	MFI-03_k	AOI-14	Focal Plane
3	offset < 10%	N/A	offset ≈ 10%	VIS
4	offset < 10%	N/A	offset < 10%	VIS
8	offset < 10%	N/A	offset ≈ 10%	VIS
9	offset < 10%	N/A	offset ≈ 10%	VIS
10	offset < 10%	N/A	offset ≈ 10%	VIS
11	offset ≈ 10%	N/A	offset ≈ 10%	VIS
12	offset ≈ 10%	N/A	offset ≈ 10%	VIS
1	offset ≈ 20%	N/A	offset ≈ 10%	NIR
2	offset ≈ 20%	N/A	offset ≈ 10%	NIR
13	offset < 10%	N/A	scan < 10%	NIR
14	offset < 10%	N/A	scan < 10%	NIR
15	offset < 10%	N/A	scan offset ≈ 10%	NIR
16	offset < 10%	N/A	scan offset ≈ 10%	NIR
17	offset < 10%	N/A	scan offset ≈ 20%	NIR
18	offset < 10%	N/A	scan offset ≈ 20%	NIR
19	offset < 10%	N/A	scan offset ≈ 20%	NIR
5	N/A	N/A	No Response	S/MWIR
6	N/A	N/A	offset < 10%	S/MWIR
7	N/A	N/A	offset < 10%	S/MWIR
20	N/A	offset < 10%	offset < 10%	S/MWIR
21	N/A	offset ≈15%	offset ≈ 10%	S/MWIR
22	N/A	offset < 10%	offset ≈ 10%	S/MWIR
23	N/A	offset < 10%	offset ≈ 10%	S/MWIR
24	N/A	offset < 10%	offset < 10%	S/MWIR
25	N/A	offset < 10%	offset < 10%	S/MWIR
26	N/A	offset < 10%	offset < 10%	S/MWIR
27	N/A	channel 9 & 10 no response	channel 9 responded	LWIR
28	N/A	offset ≈ 10%	track offset ≈ 15%	LWIR
29	N/A	offset ≈ 10%	track offset ≈ 15%	LWIR
30	N/A	track offset ≈ 20%	track offset ≈ 20%	LWIR
31	N/A	track offset ≈ 20%	track offset ≈ 15%	LWIR
32	N/A	channel 1 no response	channel 1 no response	LWIR
33	N/A	offset < 10%	offset < 10%	LWIR
34	N/A	Not enough info.	channel 4 no response	LWIR
35	N/A	channel 7 offset ≈ 20%	offset < 10%	LWIR
36	N/A	channel 8 & 9 no response	channel 8 & 9 no response	LWIR

Table 11. Summary of PSR response.

Band	Problem Sample numbers
8	Cross-talk
9	Cross-talk
10	Cross-talk
11	No cross-talk
12	No cross-talk
13	No cross-talk
14	Cross-talk with bands 15 and 16 in Fig. 13.
15	Striping in samples 33 - 35, middle Fig. 13
16	Striping in samples 33 - 35, bottom Fig. 13
17	Striping in samples 33 - 35, bottom Fig. 13
18	No cross-talk.
19	No cross-talk.
20	Data invalid
21	Data invalid
22	Data invalid with striping
23	Cross-talk in samples 11-16.
24	Cross-talk with bands 20 - 23.
25	Cross-talk with bands 20 - 23.
26 - 36	Invalid data

Table 12. Summary of Far Field DN response via ensquared energy.

Band	Accumulated % response
1	0.29361 (measured to 2.5 km)
2	0.30778 (measured to 3 km)
3	0.08920 (measured to 2 km)
4	0.33602 (measured to 2 km)
7	0.26296 (measured to 6 km)
8	0.033237(measured to 3 km)
9	0.021575(measured to 3 km)
10	0.018032(measured to 3 km)
11	0.015200(measured to 3 km)
12	0.013639(measured to 3 km)
13	0.020975(measured to 3 km)
14	0.025785(measured to 3 km)
15	0.016589(measured to 3 km)
16	0.013754(measured to 3 km)
17	0.014928(measured to 3 km)
18	0.015003(measured to 3 km)
19	0.014467(measured to 3 km)
20	Invalid data
22	Invalid data
23	Invalid data
24	Invalid data
25	0.056885(measured to 3 km)
26	Invalid data
27	0.14669(measured to 3 km)
28	Invalid data
29	Invalid data
30	Invalid data
31	0.15062(measured to 3 km)
32	0.17482(measured to 3 km)
33	0.14120(measured to 3 km)
34	0.13524(measured to 3 km)
35-36	Invalid data

Table 13. Nominal and estimated parameters for simplified MTF model for bands 1 and 2.

MTF	Meaning	Value (μrad)
Detx	Detector scan direction	83.333 (nominal)
Int	Integration time	311.92 (nominal)
Dety	Detector track direction	83.333 (nominal)
a_{band1}	Optical estimate scan (band1)[13]	81.677
b_{band1}	Optical estimate track (band1)[2]	102.681
a_{band2}	Optical estimate scan (band2)[2]	66.853
b_{band2}	Optical estimate track (band2)[2]	91.637

[13] These are preliminary values for model development only and by no means are the official blurring parameters.

Figure 7. VIS FP layout based on the AOA-14 test procedure (top) and mfi03_k (bottom).

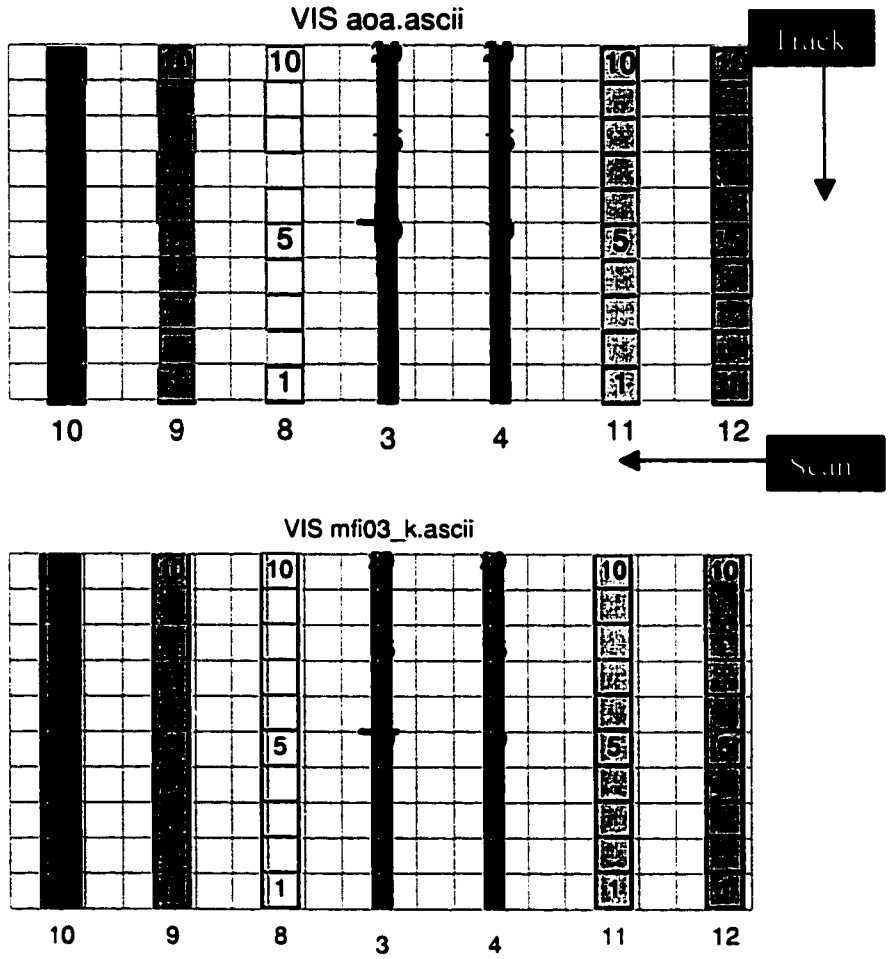

Figure 8. NIR FP layout based on the AOA-14 (top), MFI03_q (middle) and MFI03_k (bottom).

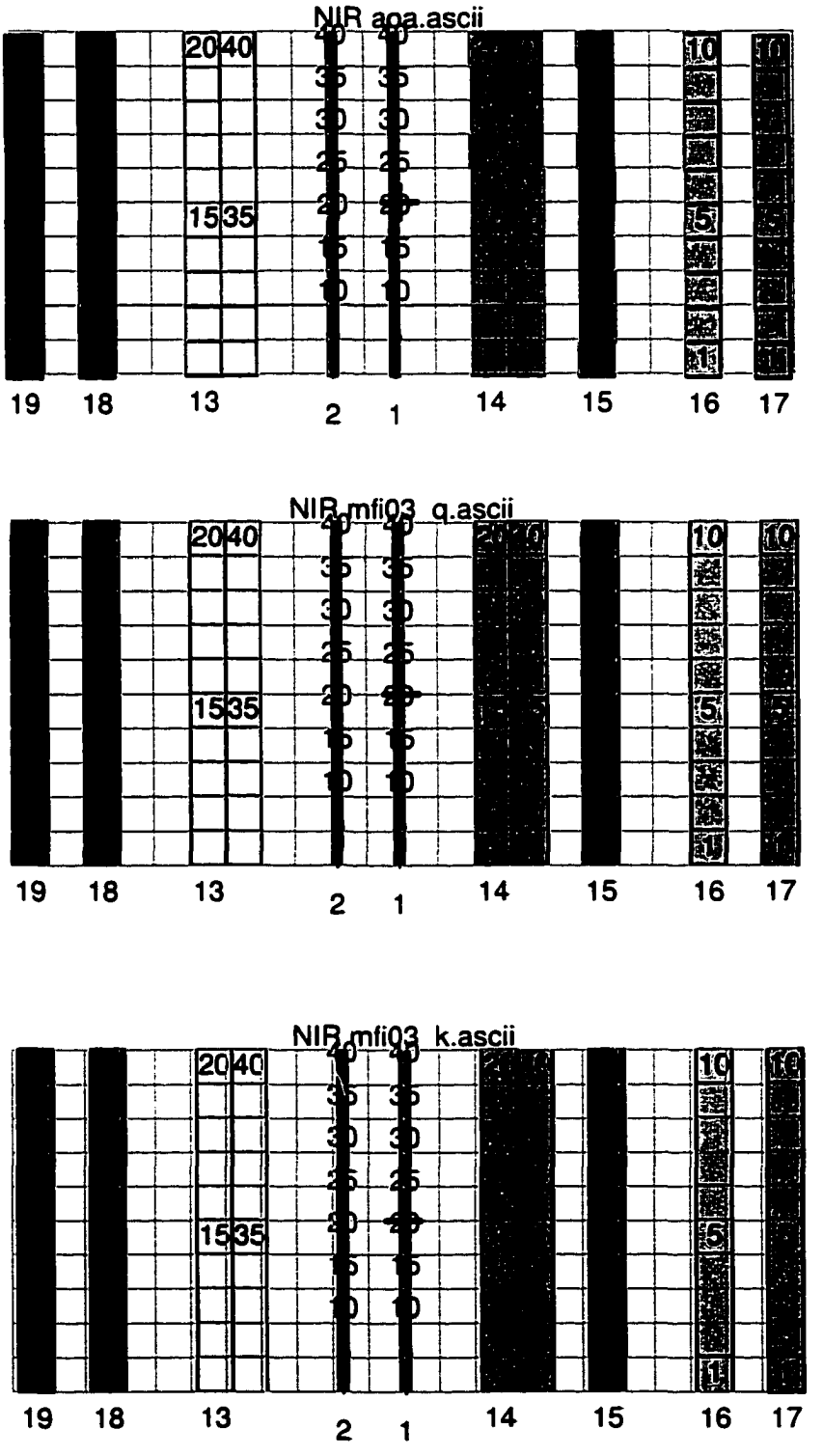

Figure 9. S/MWIR FP layout based on the AOA-14 (top) and MFI03_k (bottom).

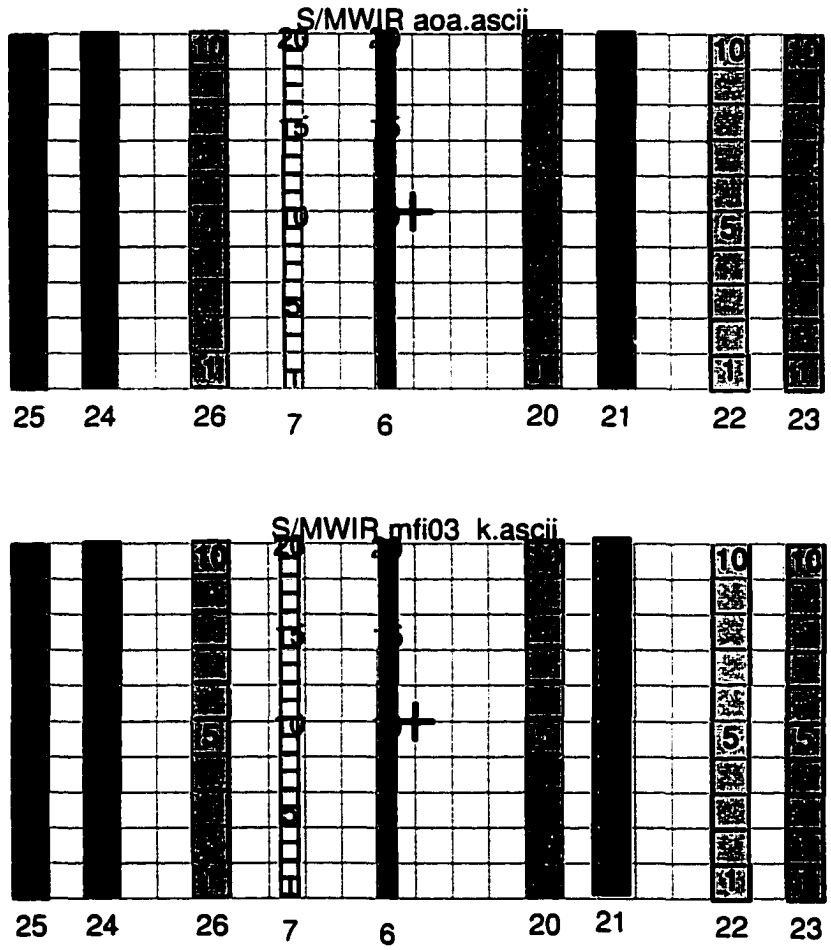

Figure 10. LWIR FP layout based on the MFI-03_q (top), AOA-14 (middle) and MFI03_k (bottom).

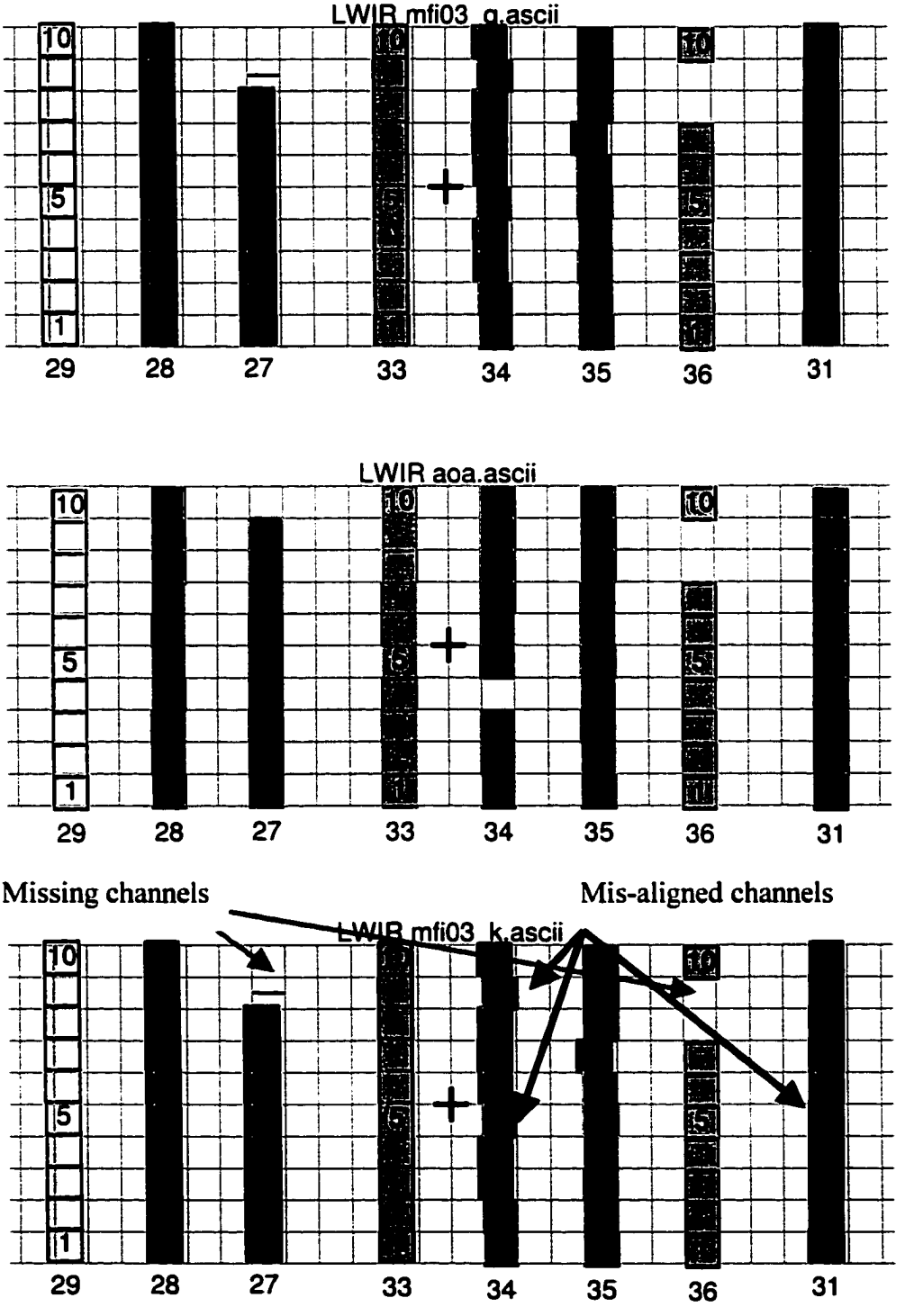

Figure 11. 1-D PSR with normalized cap replacement.

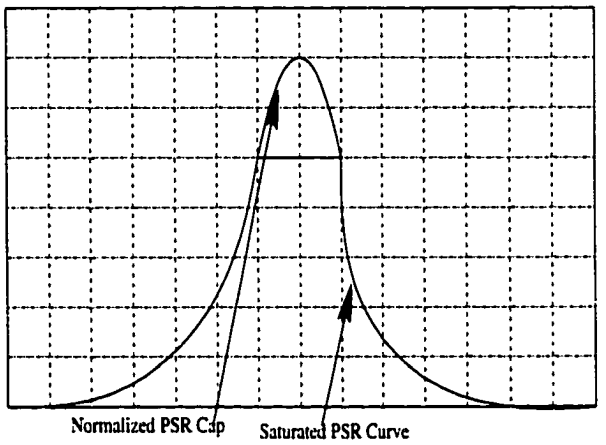

Figure 12. Example PSR for bands 8 - 12. Spatial anomalies are band-correlated crosstalk from bands 4 (not shown), 11 and 12. Sample numbers shown at bottom of each figure.

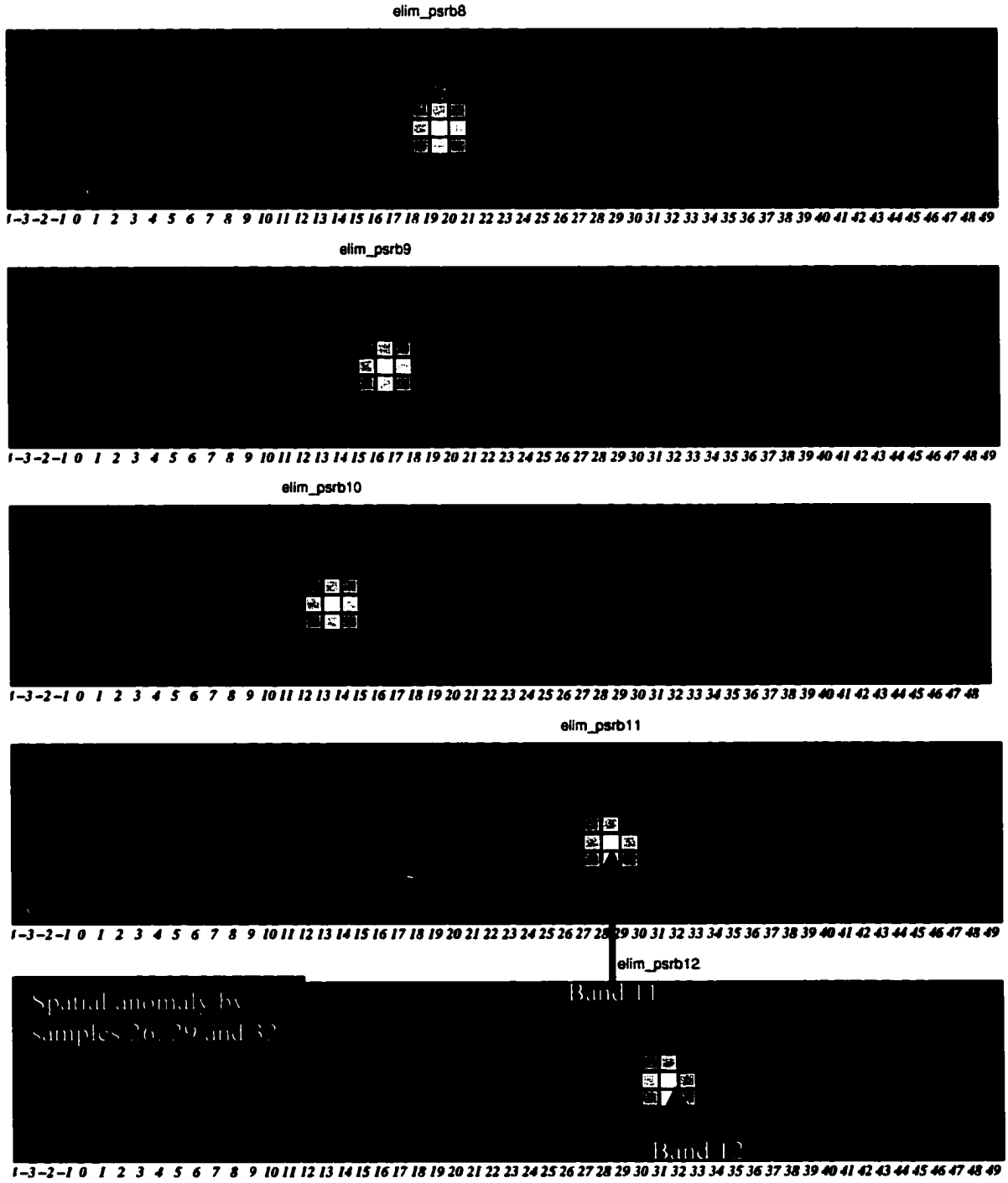

Figure 13. PSR bands 14, 15, 16 and 17. Bright centers correspond to channel 5 of respective band number. Cross-talc next to bands 18 and 19 (not shown here see FP layout figures).

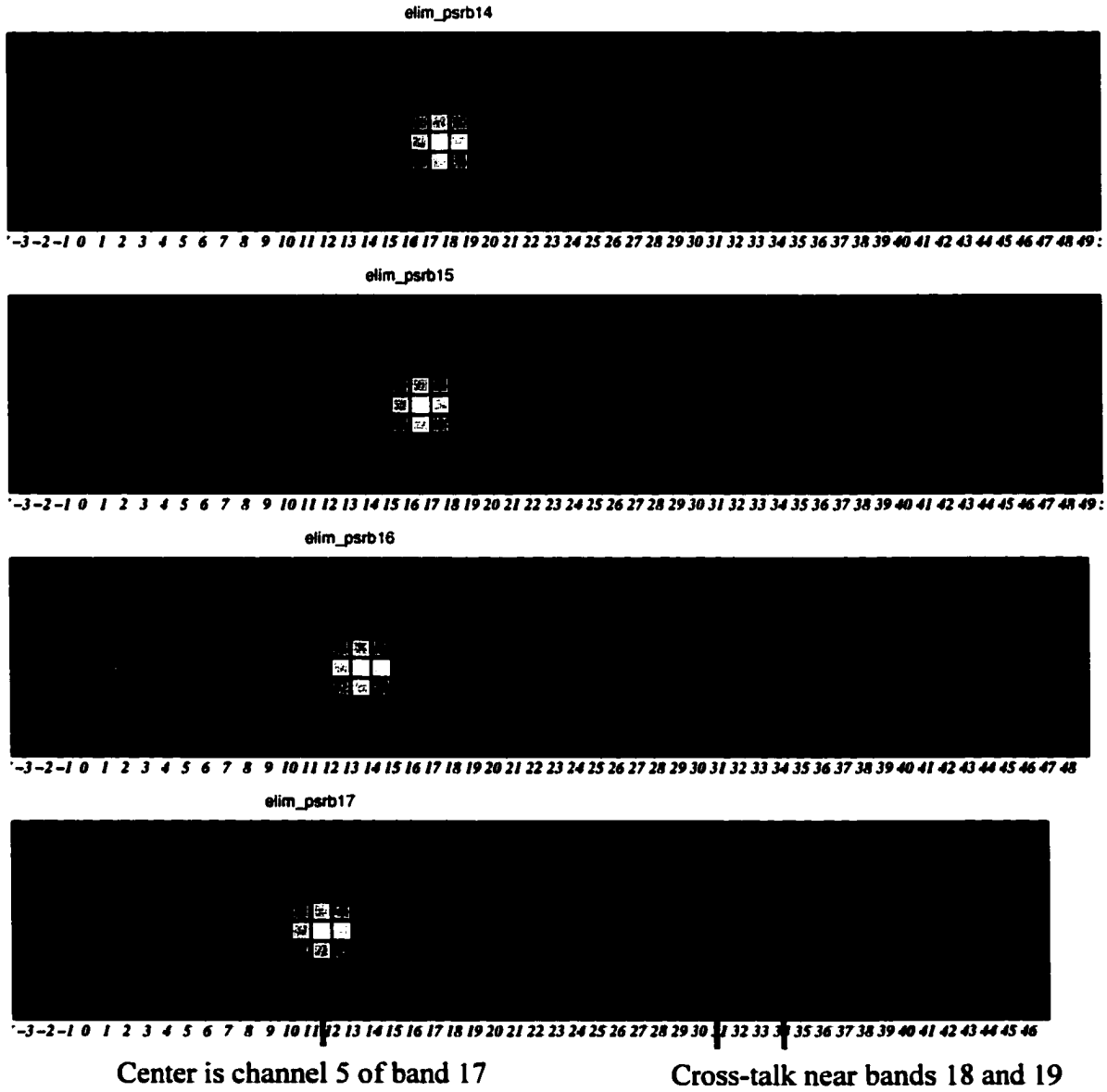

Figure 14. PSR bands 19 (bottom), 18 (middle) and 13 (top).

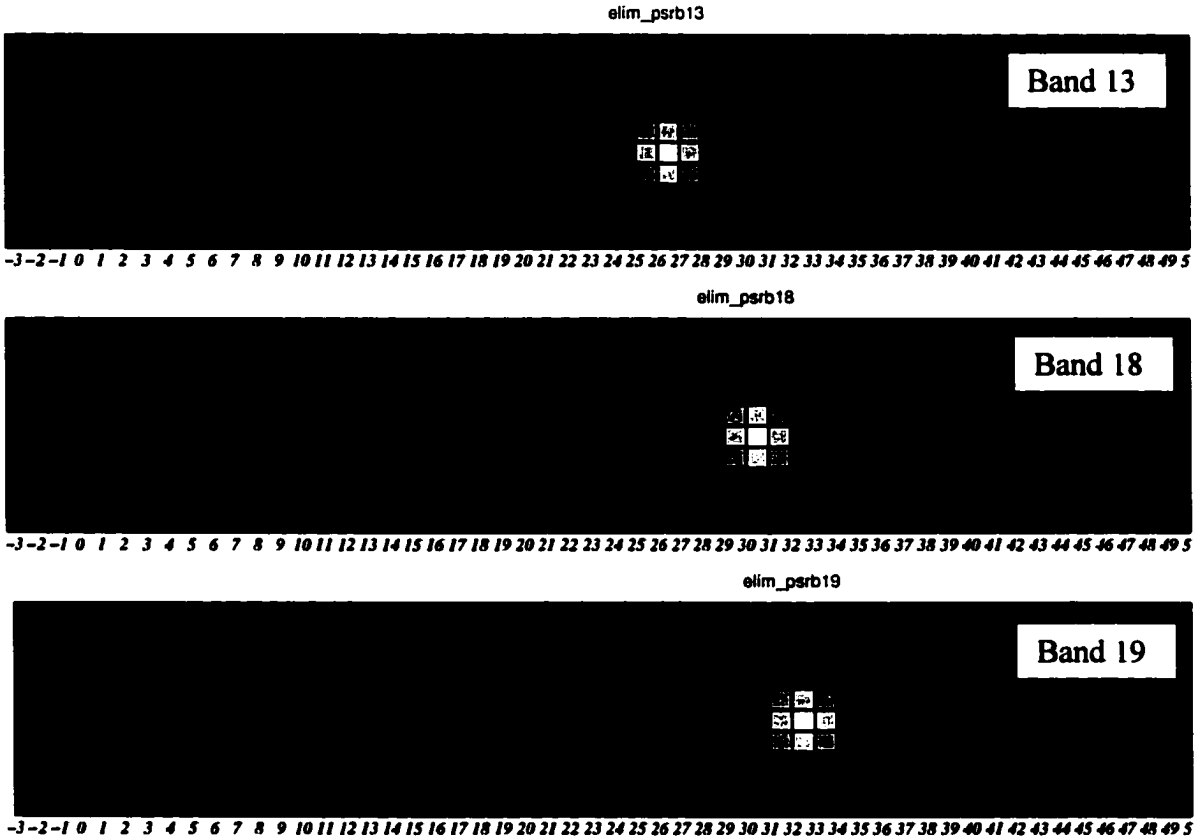

Figure 16. PSR bands 28 (top), 29 (middle), and 30 (bottom).

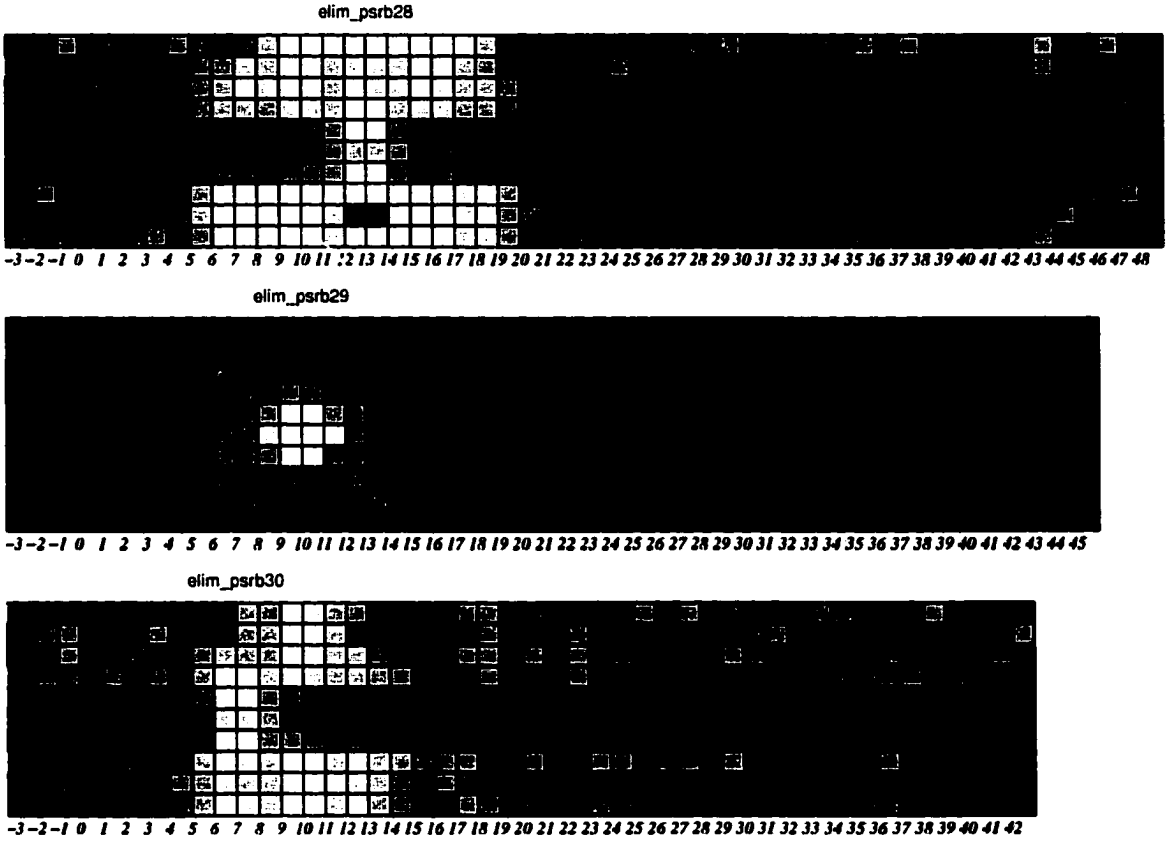

Figure 17. Ensquared energy summation as function of radial distance.

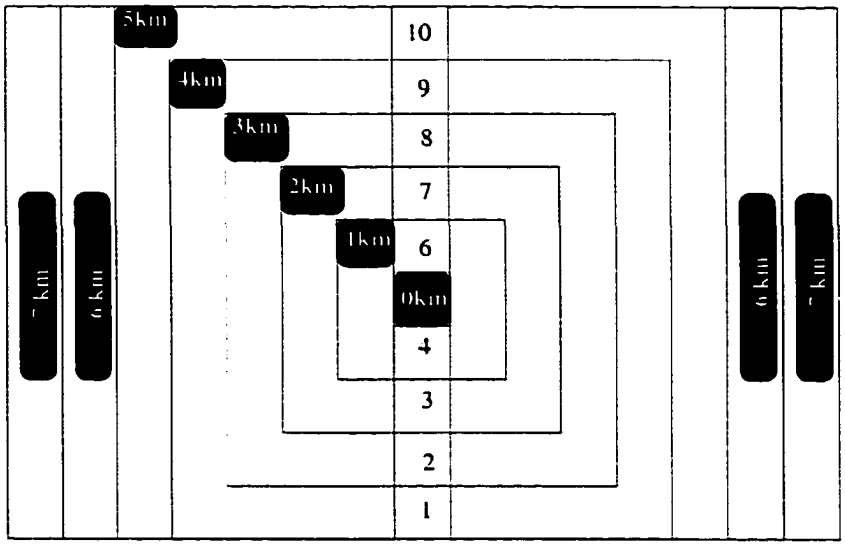

Figure 18. Radial summing for bands 8, 9, 10, 11. Start of track direction summing is identified.

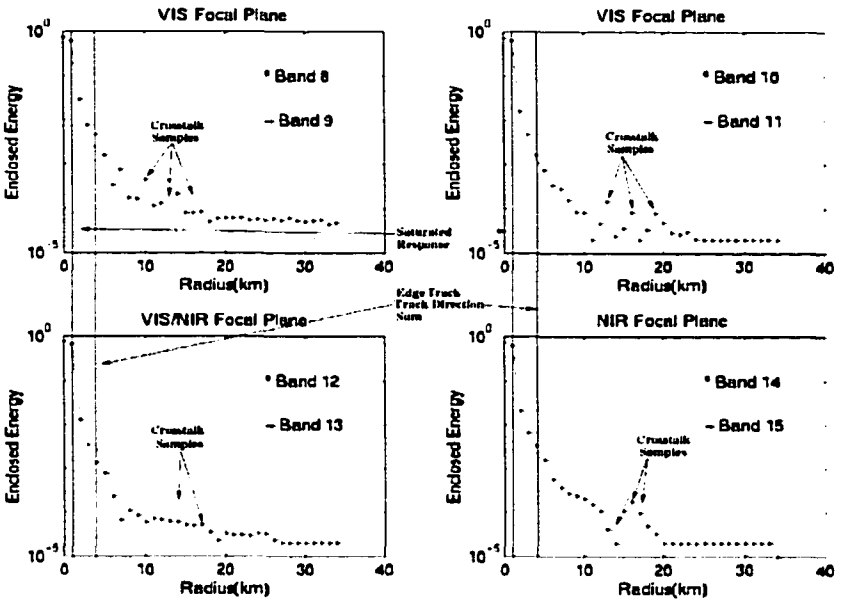

Figure 19. Radial summing for bands 16-24. Band20a is band 20.

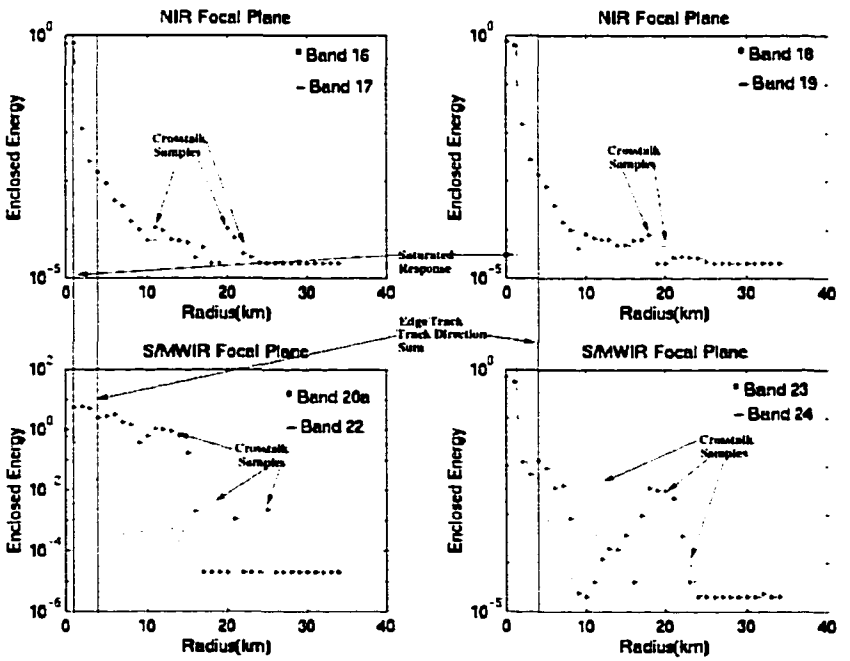

Figure 20. Cross-track (left) and in-track (right) direction MODIS system model, Band 1.

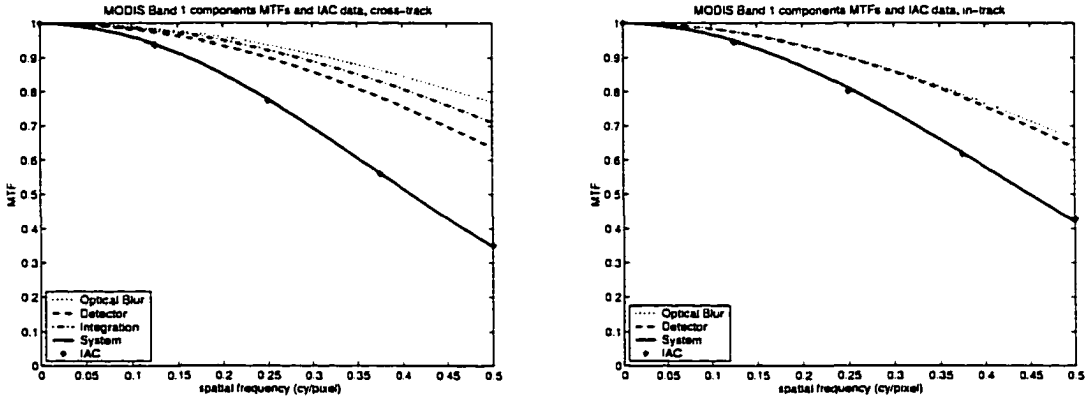

Figure 21. Cross-track (left) and in-track (right) direction MODIS system model, Band 2.

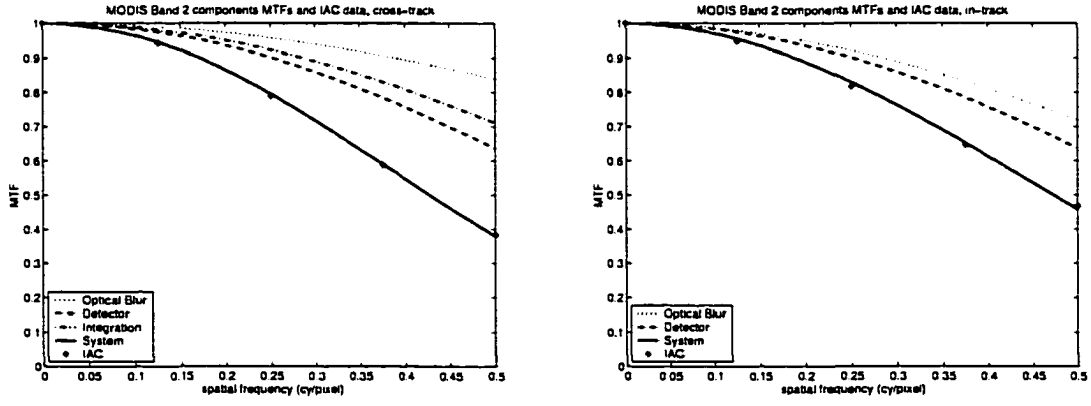

Figure 22. Cross-track (left) and in-track (right) comparison of band 1 and band 2.

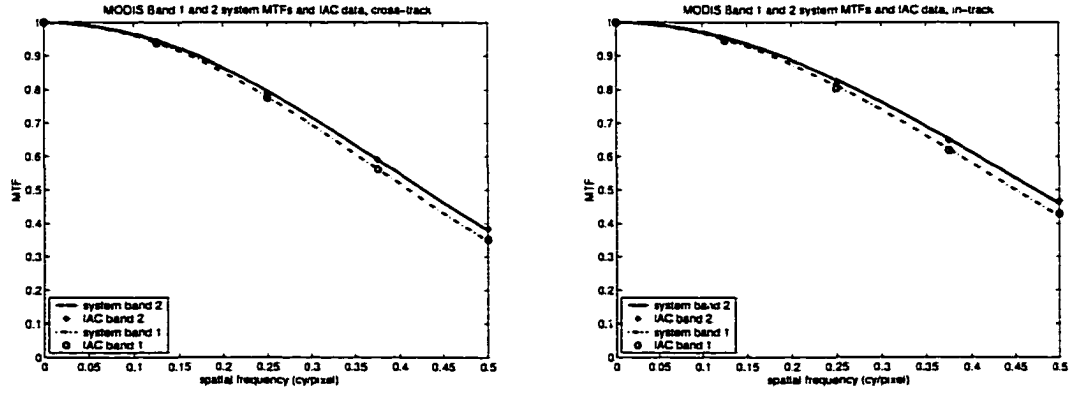

Figure 23 MODIS SR based on model and the geometric SR sampled. The area is normalized to 1.0.

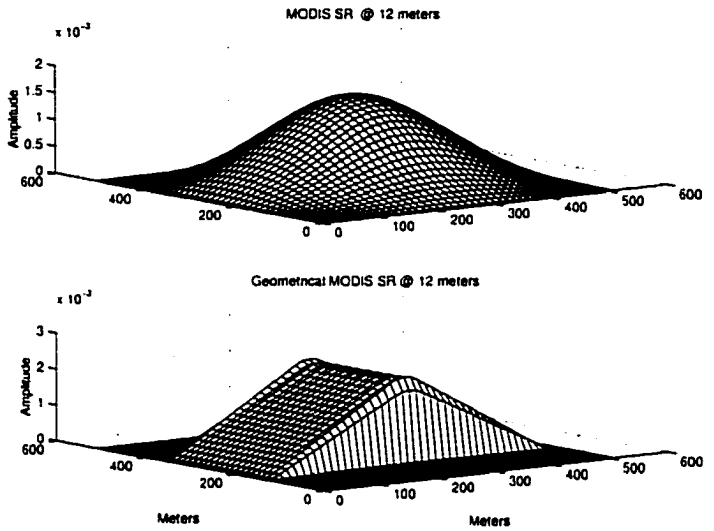

acquisitions in [25, 26]. The spatial mode acquisition uses three lamp settings: 30w, 20w and 10w. Only the 30w acquisition is used for band 1 (Figure 26). The SRCA instrument is scanned by the full MODIS system in every mirror scan, but spatial mode acquisitions are made only every 2 to 3 months.

5.1.1 SRCA MTF analysis

A rectangular aperture, 5km cross-track and 12km in-track (ground-based units), is used in the spatial mode to create an ESF in the cross-track direction (Figure 4). An in-track reticle also exists, but does not provide sufficient samples for adequate MTF analysis. The cross-track reticle creates an over-sampled ESF using an interleaving scheme which samples every 200m. Since the nominal pixel size for band 1 is 250m, a phase difference of 50m results. The five phases created are at 0.2, 0.4, 0.6, 0.8 and 1.0 of a pixel (Figure 26). Thirty six scans of data are averaged at each phase to obtain a profile. The profiles are spatially interleaved to create the ESF, sampled at 50m (Figure 27). The ESF is then processed to obtain the MTF profiles as discussed in section 3.1.

The interleaving process has been applied to five SRCA spatial mode acquisitions, which were obtained over one year (Table 14). The data have been processed to monitor any significant changes in response. The results indicate that the cross-track MTF is less than the pre-launch model MTF and also that it has not experienced any significant degradation since launch through November 22, 2001 (Figure 27) [30].

Table 14. SRCA spatial mode acquistions.

Dates
November 3, 2000
January 8, 2001
July 11, 2001
September 13, 2001
November 22, 2001

5.2 DUAL IMAGE MTF ANALYSIS

Obtaining an MTF from co-registered image pairs is a non-trivial problem. The analysis uses multi-resolution two sensor image pairs for MODIS L1B (section 2.2.3) and ETM+ L1G (section 2.5.3) or ASTER L1B (section 2.5.4) images, which serve as *reference* data. Both ETM+ L1G and ASTER L1B are at-sensor radiance units. The difference between the G "map" and B "path" are based on the geometric configuration of the images. The resolution combinations are based on spectral matching bands (Table 15, Figures 24 and 25). There are two key steps in the process; the geometric and radiometric registration of the reference imagery to the MODIS imagery, and the use of the Fourier transform to estimate the MTF. The image pairs analyzed are listed in Table 16. The geometric and radiometric registration processes for the dual image MTF analysis are described after the temporal monitoring results.

Table 15. Corresponding spectral bands for MODIS, ETM+ and ASTER (GIFOV in parentheses).

MODIS			ETM+ Band	ASTER band
Band	Focal plane	Wavelength (micrometers)		
1 (250m)	NIR	0.62 – 0.67	3 (30m)	2 (15m)
2 (250m)	NIR	0.841 – 0.876	4 (30m)	3 (15m)
4 (500m)	VIS	0.545 – 0.565	2 (30m)	1 (15m)
6 (500m)	SWIR/MWIR	1.628 – 1.652	5 (30m)	4 (30m)
29 (1000m)	LWIR	8.4 – 8.7	-	11 (90m)

Table 16. MODIS, Landsat-7 ETM+, and ASTER geodetic geolocation accuracy. Acquisition angle from Nadir, RMS geolocation error and nominal geolocation error.

Site	Date	MODIS	ETM+		ASTER	
		RMS error (m)	angle from nadir(°)	nominal error (m)	Angle from nadir (°)	nominal error (m)
Mono Lake, CA	9/29/00	200	N/A	N/A	0.45	613[14]
Maricopa, AZ	9/26/00	200	5.2	50	N/A	N/A
Maricopa, AZ	5/24/01	50	5.2	50	N/A	N/A
Gualarajada, MX	3/29/01	50	1.3	50	N[/A	N/A
Islands near Greece	2/05/02	50	N/A	N/A	5.52	613[11]
S.E. Odawaracho, Japan	2/15/02	50	N/A	N/A	5.28	613[11]
Australian Coast	1/01/01	50	N/A	N/A	1.46	613[11]
Tahoe, NV	8/19/01	200	N/A	N/A	1.34	613[11]
Tahoe, NV	4/16/01	200	N/A	N/A	0.65	613[11]
Tahoe, NV	2/27/01	200	N/A	N/A	0.87	613[11]

[14] Based on the magnitude of the in-track and cross-track geolocation requirement.

5.2.1 Image Registration

Before the analyzing the dual image approach, the imagery is converted to at-sensor radiance from scaled integers in the HDF format. The appropriate conversion factors are generally located in the data description, which may be metadata, HDF attributes or published in a web site. Ideally, the image pair should be acquired simultaneously, but that is not always possible. The at-sensor radiance imagery is corrected for differences in the solar elevation angle between acquisition times of MODIS and the higher resolution sensor, Landsat ETM+ or ASTER. The registration process then consists of the following steps:

- Conversion of geolocation grid to a common geo-coordinate reference frame, UTM
- Mapping of geolocation grids between the two sensors
- Radiometric registration between the two sensors
- Registration refinement using image-to-image correlation

Interpretation of the geolocation data involves an understanding of different geocoordinate systems and conversion to a common reference frame. The common reference frame used is the Universal Transverse Mercator (UTM) coordinate system, referred to as the world wide flat grid (Figure 28)

The reference unit is meters on a Cartesian grid. In the UTM system, the Earth is divided into 60 zones, each 6° wide. The latitude coverage is from 80° S. to 84° N.

(Figure 29). The Y UTM coordinate has two references: one is for a point above the equator and one is for a point below the equator. The first reference starts at 0m and increases North from the equator, and the second reference starts at 10,000km and decreases if the point is South of the equator. Similarly, the X UTM coordinate is initialized to 500km using the center of the zone and increases if the point is West of the center and decreases if the point is East of the center of the zone.

5.2.2 Geometric Registration

The coarse registration of ETM+ or ASTER to MODIS is achieved with the UTM geolocation data. The procedure outlined below brings the two sets of data into approximate registration, while maintaining the high resolution of the reference image (ETM+ or ASTER). To describe this process, more detail on the geolocation aspects of MODIS L1B, Landsat-7 ETM+ L1G and ASTER L1B are first presented.

5.2.2.1 MODIS geolocation

As illustrated in the MODIS Advanced Theoretical Basis Document (ATBD), the MODIS data are geolocated for the 1km pixels. If geolocation is desired for the 250m or 500m bands, then the 1km geolocation data must be interpolated [23]. The MODIS geolocation data is shown at the 1km resolution in UTM coordinates for the Maricopa scene from 9/26/2000 (Figure 30). The ETM+ and ASTER geolocation data are matched to this MODIS grid at their respective scales. The geolocation accuracy of the MODIS data varies with image date and has steadily increased since launch because of refinement

in sensor and orbit coordinates. In Table 16, the RMS geolocation error is stated for the MODIS imagery analyzed here.

5.2.2.2 ETM+ geolocation and registration to MODIS

The Landsat ETM+ Maricopa data used in our analysis is level 1G, in either "map" (north-up) (9/26/2000) or "path" configuration (5/24/2001), as discussed in section 2.5.3. Since our geolocation registration process requires a "map" orientation, the 5/24/2001 scene was rotated to match the 9/26/2000 scene using ground control points (Figure 31). The RMS error for the scene rotation in reference to 9/26/2000 is 12m. The geolocation coordinate reference is specified by a $UTM_{x,y}$ upper left corner, and the nominal inter-pixel spacing for bands 3 and 4 is 30m. Using the ETM+ in the "map" orientation simplifies the registration algorithm, because the rotation in the "path" orientation does not need to be accounted for.

ETM+ is registered to the MODIS L1B imagery, both geometrically and radiometrically. This creates a higher resolution version of the MODIS scene, which contains higher spatial frequencies not found in the MODIS image. The MODIS L1B files are calibrated to at-sensor radiance. At this product level the MODIS acquisition geometry is preserved, i.e. the data have not been resampled. The SR has not been altered except for sampling, quantization and a linear correction to convert DNs to radiance.

The MODIS geolocation is interpolated to 250m. The interpolating grid, as explained in the geolocation ATBD [23], is not center oriented, i.e. the center of the 1km pixel does not fall at the center of the 4x4 250m pixel group. The center of the 1km geolocation pixel is offset 375m in-track and 750m cross-track. This offset is taken into

account in the registration algorithm[15]. The interpolated values are then converted from latitude and longitude to $UTM_{x,y}$ coordinates.

The registration process involves two steps. The first is a coarse registration using the geolocation data, and the second is an area cross-correlation to remove any residual offsets due to the geolocation errors. Since the ETM+ and MODIS geolocation are both converted to UTMx,y, the coarse registration process involves the following:

- A MODIS pixel is indexed by (line, sample) and (UTMx, UTMy) coordinates. The (line, sample) are references in image space and the (UTMx, UTMy) coordinates are references in ground units.
- Using the MODIS (UTMx, UTMy) coordinate, the nearest neighbor ETM+ (UTMx, UTMy) pixel is found. The corresponding ETM+ pixel is placed in the position specified by the MODIS (line, sample) coordinate.
- This process is repeated for the complete image extract.

Afterwards, the relative geolocation errors between the sensors are removed using the registration algorithm, section 5.2.2.4. This registration process can take into account and reproduce discontinuities at the MODIS scan boundaries since they are in the imagery and contained in the geolocation (Figure 32). The figure shows the resultant (line, sample) mapping. This map shows where the ETM+ pixels should lie in the MODIS image space. For MTF analysis, the MODIS geolocation and imagery are corrected for the scan boundaries before the registration process.

---

[15] These offsets are specified in reference [19]. They have since been adjusted in reference [24].

After the Landsat image is reconstructed, it is precisely registered to the MODIS L1B image using Area Cross Correlation (ACC). This provides a sub-MODIS pixel cross-track and in-track offset between the two images. The relative residual registration errors after ACC for this analysis are presented (Table 17). The MODIS geolocation is temporally dependent, the RMS geolocation data for earlier datasets being less accurate than that for later datasets (Table 16). After ACC refinement, a window of common coverage is extracted from each image.

The registration process described above does not account for topographic relief distortion in the images. The process is designed to register only selected ETM+ and MODIS bands chosen for spatial characterization. For this purpose, image pairs with little topographic relief, as in the Maricopa agriculture site, are selected, and therefore topographic distortion can be avoided in the registration process. Furthermore, the selected sites are acquired near-nadir thus minimizing off-nadir perspective distortion.

5.2.2.3 ASTER geolocation and registration to MODIS

The ASTER image acquisitions are only for areas specified by principle investigators of the ASTER science team, unlike the "blanket" coverage of MODIS and ETM+ (in the continental US). Acquisitions of suitable high quality MTF targets are therefore less frequent than with ETM+. The advantage of ASTER over ETM+ for MTF measurements is that both ASTER and MODIS are on the Terra platform, and the image acquisitions are within seconds of each other. ASTER and MODIS view the same target through the same atmospheric conditions and sun angle. In fact, the ASTER acquisition

angle for the Mono Lake image is 2.996° off nadir. For MODIS, this angle is negligible in terms of geometric distortion ("pixel growth" off-nadir) of the SR.

The ASTER data used in this analysis are obtained from the Earth Observing System Data Gateway and are considered research quality by the ASTER team as of this writing. The geometric and radiometric accuracy vary with processing date; therefore it is important to note the production date time stamp and the software version used to produce the 1B product. The Mono Lake, California, scene has a production date of November 2000. As with MODIS, ASTER L1B at-sensor radiance is used in the image comparison. The imagery is in a compact format and must be scaled to radiance units. ASTER bands 2 and 3 are the closest matches to MODIS bands 1 and 2, respectively (Figure 25). The geolocation registration process is described for ASTER band 2; the process for ASTER band 3 (with different geolocation parameters from band 2) has not been developed.

The ASTER L1B geolocation data are geocentric referenced and a transformation is necessary to change the reference coordinate system to geodetic to match the MODIS coordinate reference. Since the ASTER field of view is on the order of 60km, a 10x10 geolocation matrix is provided for the scene at a 7470m sample interval [41]. The geolocation coverage is larger than the scene. The ASTER L1B imagery and geolocation is systematically corrected for the orbit which include geolocation scaling and offset parameters that are band dependent. These parameters indicate how the 10x10 matrix references the scene.

The ASTER scene is registered to the MODIS scene in a similar fashion as used for Landsat ETM+. This involves the following procedure: the area of interest is chosen in the MODIS scene, and using the MODIS geolocation to define a rectangle, the corresponding area is extracted from the ASTER scene to the nearest ASTER geolocation boundary of the 10x10 grid (Figure 33). The ASTER geolocation grid is interpolated to 15m and both the grid and the imagery are trimmed to match the MODIS rectangle (Figure 34). The MODIS geolocation grid is also interpolated to 15m to minimize discontinuities in the registration. Placement of the ASTER pixels in the MODIS reference frame is implemented using a distance measurement based on the following equation,

$$(y_1 - y_0)x - (x_1 - x_0)y - (y_1 x_0 - x_1 y_0) = 0 \qquad (15)$$

where y_i, x_i specify a line in ASTER ground units and x, y is the MODIS point used to measure the distance to the line, also in ground units [56]. The nearest neighbor ASTER pixel to the closest MODIS line segment is chosen (Figure 35). The line segment distance measurement is insensitive to the ASTER's path orientation and treats each MODIS x, y geolocation as independent, which also makes it insensitive to the MODIS scan offsets. This algorithm has been refined to vary the search areas based on different criteria, as described below.

5.2.2.4 Geolocation registration algorithm

The registration algorithm is summarized in the following steps:

- Choose initial MODIS geolocation point in the 15m grid in terms of (UTMx, UTMy) and (line, sample) coordinates, corresponding to ground units and image space, respectively.
- Estimate the nearest neighbor ASTER pixel.
- Place the ASTER pixel on the grid indicated by the MODIS (line, sample) in image space.

Since each MODIS pixel corresponds to an approximate 16x16 pixel on ASTER, the search area is very large for the scene cutout. Using a search routine that does not use apriori knowledge of the previous result requires 2048^4 search operations for an image that is 2048x2048 pixels. To speed up the search, it is assumed that the next geolocation pixel should not be too far from the previous one. The steps for the refined search algorithm are,

1. Choose the initial MODIS (UTMx, UTMy) geolocation datum.
2. Search the complete ASTER geolocation data for the nearest (UTMx, UTMy) geolocation point (Figure 35).
3. On the next MODIS (UTMx, UTMy) geolocation datum, limit the search area to two MODIS pixels, which is approximately a 480x480m geolocation area, but only uses at most 64 operations per search. This search starts with the previous ASTER (UTMx, UTMy) result.
4. If the distance between the MODIS and the ASTER geolocation result is less than 15m, the result is acceptable; otherwise go to 2, i.e. do a full search.
5. Return to 3 until the complete MODIS geolocation data is processed.

This process brings ASTER into approximate registration. The next step is the removal of relative geolocation errors between the sensors.

5.2.3 Area cross correlation

The relative errors are removed by finding the highest correlation coefficient between the two images. To reiterate, we have two images, the lower resolution MODIS image at 250m and the higher resolution ASTER image at 15m or ETM+ at 30m. The two images cover approximately the same area since they are derived using the MODIS geolocation information. The procedure starts by convolving the MODIS geometric response, section 4.5, with the Higher Resolution Image (HRI), ASTER or ETM+, and downsampling at different phases to get the 250m resolution image for comparison. The MODIS geometric SR is either sampled at 15m or 30m, which is sensor dependent and normalized as indicated in equation 16.

$$\sum\sum SR(x,y) = 1 \tag{16}$$

Circular convolution is used because it helps minimize the edge effects due to the Gibbs phenomena, which add undesired noise along the DC spectra in the in-track and cross-track directions. The circular convolution is implemented with the discrete Fourier transform as shown in equation 17.

$$SR(x,y) \otimes HRI(x,y) = \Im^{-1}[\Im(SR(v,u)) \cdot \Im(HRI(v,u))] \tag{17}$$

The cross correlation is a two step process. The first step is to compute a coarse shift to get HRI and MODIS within a pixel of registration. The second step refines the registration to a sub-MODIS pixel. For ETM+, the sub-pixel scale is 30m and for ASTER it is 15m. The complete procedure consists of the following steps,

1. Convolve the HRI with the MODIS geometric response at the respective scale.
2. Trim the MODIS image.
3. Compute the coarse shift step for MODIS (250m shifts).
4. Shift and downsample the HRI image to 250m.
    a. Match the radiometry using a normalization stretch [10, 57]. The normalization stretch consists of making HRI's μ_{HRI} and σ_{HRI} equal to MODIS's μ_{modis} and σ_{modis}.

$$DN_{newHRI} = (DN_{HRI} - \mu_{HRI})\frac{\sigma_{\text{modis}}}{\sigma_{HRI}} + \mu_{\text{modis}} \tag{18}$$

where DN_{newHRI} are the new radiance values, DN_{HRI} are the original HRI radiance units.

    b. Compute the correlation coefficient between HRI and MODIS.

$$c_{newHRI,\text{modis}} = \frac{1}{N-1}\sum_{p=1}^{N}(DN_{p,newHRI} - \mu_{newHRI})(DN_{p,\text{modis}} - \mu_{\text{modis}}) \tag{19}$$

$$\rho = \frac{c_{newHRI,\text{modis}}}{\sqrt{c_{newHRI,newHRI} \cdot c_{\text{modis,modis}}}} \tag{20}$$

where ρ is the correlation coefficient computed for each shift, p indexes

over N pixels in the image, and $C_{x,y}$ is the cross correlation.

5. Estimate the maximum ρ using the sub-MODIS pixel offsets after the coarse registration. Step 4 is repeated using a sub-MODIS pixel step-size.

At the end of the procedure, the best correlation and registration offsets have been obtained. The offsets are applied to the original HRI scene. Tables 17 and 18 list relative geolocation errors found between the HRI (ASTER or ETM+) and MODIS. The MODIS imagery and geolocation are corrected for the scan shifts before ACC registration by an automatic scan removal algorithm. The scan shifts are shown in Figure 36. Example final, registered ETM+, ASTER and MODIS images are shown in Figures 37-40.

Table 17. Relative registration error for ETM + and MODIS.

Site	Date	MODIS B1 and ETM+ B3		MODIS B2 and ETM+ B4	
		in-track (m)	cross-track (m)	in-track (m)	cross-track (m)
Maricopa, AZ	9/26/00	-30	90	-30	60
	5/24/01	30	90	0	60

Table 18. Relative geolocation error for ASTER[16] and MODIS

Site	Date	Relative geolocation error	
		MODIS B1 and ASTER B2	
		in-track (m)	cross-track (m)
Mono Lake, CA	9/29/00	1095	630

[16] The relative error is large, probably because these ASTER data were acquired early in the validation phase.

5.2.4 Radiometric registration

The MODIS and the HRI, once converted to at-sensor radiance, should be registered radiometrically. However, relative errors in the calibration processes of the different sensors leave residual radiometric differences. These are removed to insure proper normalization of the derived MTF via the normalization stretch, which normalizes the two images so that the subsequently derived MTF has the correct DC frequency value of one [10, 57].

5.2.5 MTF estimation procedure

Since the ETM+ and ASTER sensors have GIFOVs that are several times smaller than the MODIS GIFOV, their imagery serves as a reference to calibrate the spatial frequency content of a given scene [40, 41]. The spatial frequency bandwidth of either ETM+ or ASTER is several times higher than the MODIS SR; the details of the reference sensor's SR are assumed negligible relative to MODIS. The estimation procedure used to find the in-track and cross-track MTF for each band is described in the following steps.

- Fourier transform the reference image (ETM+ or ASTER) and the MODIS image
- Trim the spatial frequency spectrum of the reference image to the same bandwidth as the MODIS spectrum
- Calculate the MTF as the ratio of the amplitude and the Phase Transfer Function (PTF) as the difference in phase of the two image spectra. The square of the MTF is calculated at this point for better noise reduction by the subsequent median filtering.

- Apply a 3x3 median filter to the square of the MTF. This removes "spike" noise in the MTF resulting from low amplitude scene frequency components.
- Calculate the inverse Fourier transform of the smoothed MTF and the PTF. This is an initial estimate of the MODIS SR.
- Multiply the MODIS SR by a Hanning window, of size 4x4[17], to reduce noise [58].
- Fourier transform the windowed SR to obtain a smoothed MODIS MTF estimate.
- Average the MTF azimuthally over $\pm 5^{\circ}$ in the in-track and cross-track directions.

This process is applied to the imagery for MODIS bands 1, 2, 6 and 29. The final cross-track and in-track MTF profiles attained are shown in Figures 41 and 42 and discussed in section 5.2.7.

5.2.6 Validation of the MTF estimation procedure

The MTF estimation described above has been optimized for this particular application using three cases (Table 19). The goal is to determine if the MTF estimation procedure is robust under the three conditions. The first case is ideal, i.e. continuous simulation with no aliasing. The second case is semi-ideal, i.e. simulation with aliasing, and the third case is real, i.e. using real data. The reference image is ASTER at 15m for all three cases, referred to as the "true scene" (Figure 43). The MODIS geometrical response, Figure 23, is convolved with this true scene to create Case I, using the island in Mono Lake, which has been registered as described in section 5.2.2.3. This image is

[17] This window size was chosen based on the study in section 5.2.6.

down sampled to 250m to create Case II. The real registered MODIS image is used for Case III.

In Case I, the data do not have registration, radiometric or spectral errors and have been adequately sampled according to the Nyquist criteria (Figure 43). The procedure is tested to see whether a reliable MTF estimate is obtained, given that it is known that the correct MTF is the Fourier transform of the MODIS geometric response.

Table 19. MTF estimation optimization criteria.

Cases	Condition	Notes
I. Ideal	Adequate sampling no radiometric errors no registration errors no spectral mis-matches no atmospheric differences	16 x oversampling exists
II. Semi-ideal	Inadequate sampling (aliasing exists) no radiometric errors no registration errors no spectral mis-matches no atmospheric differences	Undersampling exists Sampling is ½ the Nyquist rate
III. Real data	Inadequate sampling (aliasing exists) radiometric errors registration errors spectral mis-matches atmospheric differences	Acquisition between ASTER and MODIS is on order of several seconds.

In Case II, the data have been inadequately sampled, but no registration, radiometric or spectral errors exist. The only difference between Case I and II is inadequate sampling. The same procedure is applied to find the aliased MTF estimate, given that the correct

answer has been obtained in Case I. In Case III, registration, radiometric, spectral bandwidths, calibration, acquisition system and atmospheric differences exist. The resultant MTF is compared to the Case II result.

The MODIS geometric response consists of a sinc (in-track) and a $sinc^2$ (cross-track) in the frequency domain. For Case I, the validation procedure indicates that the estimation distorts the high frequency response past the 1^{st} null in both the in-track and cross-track direction, but the overall shape of the main lobe is retained. Cross-track, the main lobe increases slightly, and in-track, it is slightly smaller (Figure 44). In Case II, the frequency limit is only to 0.5 cy/pix as opposed to 8.0 cy/pix for Case I. Therefore, only half of the major lobe is estimated. The cross-track results follow the general trend of the ideal $sinc^2$ response, but they are lower. The in-track results are much lower than the sinc, which indicate that this algorithm is not as robust in this direction. The Case III results have the same type of response as Case II simulation. The estimated MTF in Case III should not be the same as in Case II, because the SR applied is slightly different. In Case II, the geometric SR excludes the optical component. In Case III, the SR is the MODIS SR being applied to the scene as observed by MODIS, on-orbit. The MTFs from Case II and III are similar.

All images were normalized to the MODIS image mean prior to processing. During validation, the MTF estimation procedure was modified by changing the Hanning window size, median filter size and processing order, as described in section 5.2.5 (Figure 44). The final processing order, described in section 5.2.5, uses a 4x4 Hanning window and a 3x3 median filter for Cases II and III. The Hanning window size is chosen

to encompass the SR for the 250m bands, which is 4 pixels * 250m. The main lobe of the SR, which includes the optical component, is on the order of 600m wide. The median filter size is based on empirical trials. From this point on, the procedure is held fixed for subsequent on-orbit processing using the MODIS - ETM+ and MODIS – ASTER pairs.

5.2.7 Dual Image On-orbit Results

The results of the on-orbit two image MTF analysis are dependent on the ability to accurately register the two images spatially and radiometrically. Relative geolocation errors between these different coordinate grids can lead to mis-registration errors (section 5.2.2). There are two types of relevant geolocation errors. The first is absolute geolocation error. This error is sensor dependent and indicates how far a geolocation pixel is from the actual point on the Earth. This error is reported for each MODIS granule and, as indicated by the RMS errors in Table 16, has improved since the Terra launch. The second type of error is the relative geolocation error between MODIS and the other sensors. This relative error is the offset between two geolocated images in the in-track and cross-track directions, as found by ACC (Tables 17 and 18, not all datasets are shown). The data products from these dates are still considered research quality, and improvement is expected as processing system improves.

Radiometric registration is considerably eased because the image acquisitions are nearly coincident. ETM+ leads MODIS by 30 minutes and ASTER is with MODIS on the Terra platform. Therefore, differences in the atmosphere are minimized.[18] An obvious radiometric requirement is to match the spectral bands of the two sensors as closely as

[18] High altitude aircraft contrails remain a problem, even for such a short time interval.

possible. ETM+ bands 3 and 4 were chosen for their spectral match to MODIS bands 1 and 2. ASTER band 2 also matches MODIS band 1. These pairs provide an MTF estimate for the NIR FP. ASTER bands 4 and 11 match MODIS bands 6 (S/MWIR) and 29 (LWIR), respectively (Table 8). Based on the scene features and band response, different areas were chosen for MTF analysis. A scene for the 250m bands may not have adequate high contrast features for the 500m or 1000m bands; the spectral response is also different per band and may cause the same scene to provide different MTF results in different bands.

Once the images have been geometrically and radiometrically registered, they are processed using Fourier analysis to obtain the MODIS MTF estimates. In Figure 41, the cross-track estimate for MODIS band 1 matches closely the system model for most of the data. The processed data are islands near Greece, a lake near Guadalajara, Mexico, a waterfront area southeast of Odawaracho, Japan, and the Maricopa agricultural center near Phoenix, AZ. The Maricopa scenes were acquired on 5/24/2001and 9/26/2000 (Figures 37 and 38, respectively). The islands near Greece were acquired on February 5, 2002 (not shown) and the waterfront area southeast of Odawaracho, Japan was acquired on February 15,2002 (Figure 39). The MTF estimate using the Australian Coast was lower than the other cross-track results. In band 2, the cross-track MTF for Maricopa 5/24/2001 and 9/26/2000 is closer than the in-track measurements to the system model. For bands 1 and 2, the in-track measurements are somewhat inconsistent to the model. The Guadalajara and Australia scenes are the ones that are closest to the model, while Maricopa 9/26/2000 and 5/24/2001 are lower than the system model, and Greece and

Japan are higher. The band 2, in-track MTF for Maricopa 5/24/2001 is also less than the system MTF, but 9/26/2000 does agree with the system model. This may be because the 9/26/2000 scene has more high contrast field boundaries and higher frequency content.

The MTF analysis for the S/MWIR FP band 6 agrees with the MTF model in-track and cross-track directions (Figure 42). The data used in the analysis are Tahoe, NV, Mono Lake and Japan. The Japan extract is within the same ASTER scene. Several Tahoe images were acquired on 8/19/2000, 2/27/2000 and 4/16/2000. The lake edge is chosen in each of the scenes. The same area was not chosen on each date due to the seasonal variation within the scene.

The LWIR FP MTF results are reliable in the cross-track direction, but not in the in-track direction. The spectral matching bands are MODIS band 29 and ASTER band 11. The data used for this comparison are Tahoe (8/19/2000), Tahoe (4/16/2001) (cross-track), Mono Lake, and Japan. In the cross-track direction, the MTF estimate below 0.25 cy/pix is close to the system model, and above 0.25 cy/pix, Japan and Tahoe 4/16/01 are closer to the system model. The other two dates, Tahoe 8/19/2000 and Mono Lake are below the MTF model. In the in-track direction, Mono Lake and Japan MTF estimates follow the model response.

Overall, the on-orbit dual image cross-track MTF measurements are comparable to the cross-track system model. Some of the in-track measurements are comparable to the system model, while others are not. Some of the errors may be due to aliasing, mis-registration and calibration errors. Error due to aliasing was observed during the MTF validation phase and may indicate that either the MTF estimation procedure is not as

reliable in-track. Since there is no type of pre-filtering in the in-track direction, the MTF response is more prone to be aliasing (Figure 44).

5.2.8 Pixel interleaving

In an attempt to improve the in-track on-orbit MTF measurements, pixel interleaving was investigated to improve the sampling rate. Pixel interleaving may be interpreted as subpixel phasing. One interleaving technique has been shown to improve results in closely-controlled experiments using least squares to estimate sub-pixel locations [59]. This technique uses several images at sub-pixel offsets to create an oversampled image with improved resolution. In another interleaving technique, a model of the Lake Ponchartrain Bridge in New Orleans is used to obtain an MTF estimate for Landsat 7 ETM+. The bridge is almost in-track in reference to the ETM+ orbit. Phased profiles are taken from the bridge at different locations and interleaved to increase the sample rate [17].

In an effort to improve the sampling rate, two approaches are presented. The first approach is based on [17], but instead of the bridge, a model of a line target convolved with the MODIS SR sampled at 15m (Figure 23) is used to simulate the MODIS acquisition of All-American Canal, located west of Yuma, AZ. Two All-American Canal images were acquired on 4/12/2000 (Figure 5) and 6/29/2000 (not shown). The canal approximates a line target, in reference to MODIS at 250m resolution, with the provisions mentioned in section 3.2. The canal is straight for 6.6km at 19.68°, in reference to the MODIS scan, and 62m wide [30]. The two dates are used to obtain candidate phase profiles.

The radiometric properties of the images were matched using the normalization stretch, section 5.2.4, in which 4/12/2000 served as the reference for 6/29/2000 and convolved model. The candidate profiles from the convolved model were extracted every 50m and correlated with each row, using both dates, to find the highest correlation per phase (Figure 45). The highest correlated profiles were interleaved, according to the phase, to create the oversampled 1-D profile of the canal. In this approach, only three independent profiles, out of the five candidates, were found; the resultant sampling rate was 83.33m per sample instead of 50m per sample. A difficulty with this approach is that the canal profile candidates depend on the angle between the canal and MODIS scan [2]. The phased canal result at 83.33m per sample and the model are shown in Figure 46.

The cross-track MTF estimate, using equation 4 (Chapter 3) in which $image_{MODIS}$ is the interleaved result and $image_{REFERENCE}$ is the model convolved with the MODIS SR, has a magnitude of nearly 1.0 (Figure 47). This means that the numerator and dominator cancel, which show that the SR model used is adequate for this type of analysis. Even with this result, targets with a higher grazing angle, i.e. closer to the in-track or cross-track direction, and of sufficient quality as described in section 3.2 are needed for a more reliable MTF estimate.

In the second approach, the geolocated data, using multi-date imagery, are used to determine the phasing for a 2-D analysis. An oversampled grid is created, and the imagery is used to fill the grid using nearest neighbor selection from multiple dates. Ideally, this approach requires four images at a minimum to improve the sample rate by a factor of two. An example is the 250m grid being resampled to 125m (Figure 48). Four

holes open at this resolution as indicated by the crosses, one between each pixel (circles at 250m) and one in the center in between the four corners. In Figure 49, an extract of the MODIS geolocation is shown (circles), and the dots and crosses represent two candidate dates. As seen in the figure, the resultant geolocation values do not always fall near the 125m pixel hole, therefore several inverse-mapping functions may be used to fill the holes. For this example, nearest neighbor is used.

Five multi-date images of the lava field near Sevillita, New Mexico, for MODIS band 1, are used and chosen for the spectral neutrality, and temporal stability in the field. The Sevillita dates are 5/09/2000, 6/10/2000, 6/26/2000, 7/28/2000 and 9/14/2000 (Figure 50). Clouds pose a challenging a problem for this type of analysis. The radiometry appears to vary slightly from date to date. This may be due to changes in the MODIS calibration, since the data were acquired early during the MODIS validation stage.

This multi-date approach removal of the scan shifts is necessary for both the imagery and geolocation, and the relative geolocation error between the images must be removed. The assumptions made are that the pixel-to-pixel geolocation error is negligible at 125m, and the sensor viewing angle is approximately the same for the scenes. A correction for the solar elevation angle is required for each scene. In this example, no correction is made for temporal changes in atmospheric conditions.

The date 5/09/2000 is used as the reference since it is the most cloud free scene. This date's geolocation grid is resampled to 125m, and the nearest neighbor geolocated pixels from the multi-date images are used to fill in the grid (Figure 48). In Figure 49, an

extract of the geolocation is shown for 5/09/2000 (circles), and the dots and crosses represent two of the five dates. As seen in the figure, not all the geolocation elements fall at corresponding pixel locations to be filled in. Therefore, this process requires more scenes to create the oversampled image, or interpolation can be used to fill the "holes" as long as they are a small fraction of the image.

Once the process has been completed, the oversampled scene is created (Figure 51). This scene may then be used in the two-image approach with ASTER or ETM+ for analysis, or in a target-based approach to get the MTF. Aliasing in the MODIS data are considerably reduced by the interleaving process, which should improve the MTF estimates.

Figure 24. Corresponding spectral bands of ASTER, MODIS and Landsat ETM+. Not all are used in the analysis presented here.

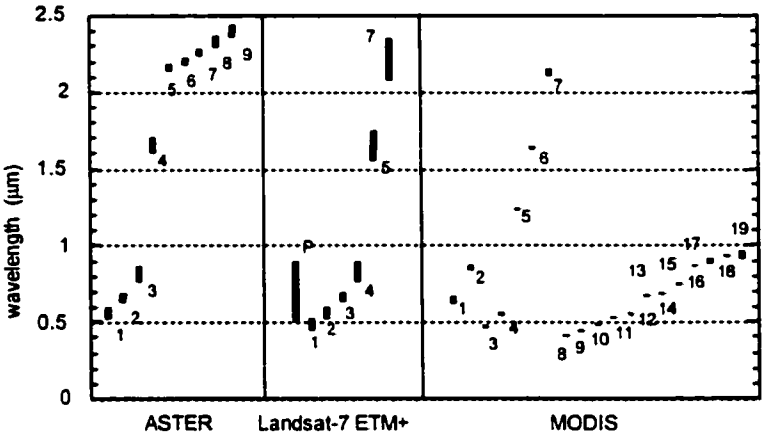

Figure 25. Relative spectral responsivity for MODIS band 1 (left) and band 2 (right) for the corresponding ASTER and ETM+ bands.

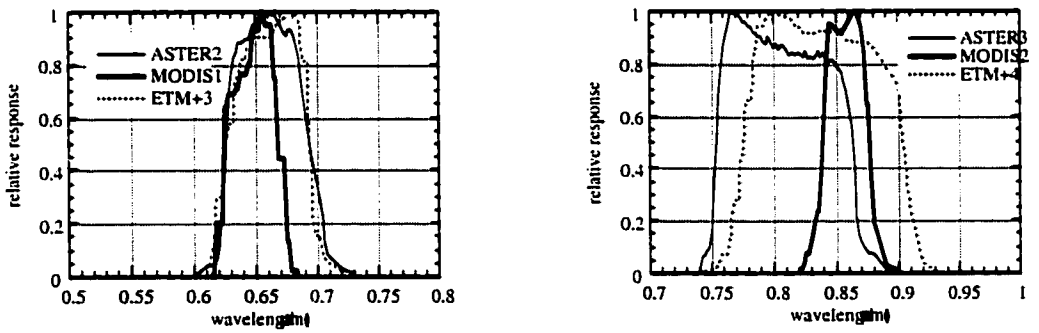

Figure 26. SRCA spatial, 30w, mode datum with 4 of 5 phases shown (November 3, 2000)

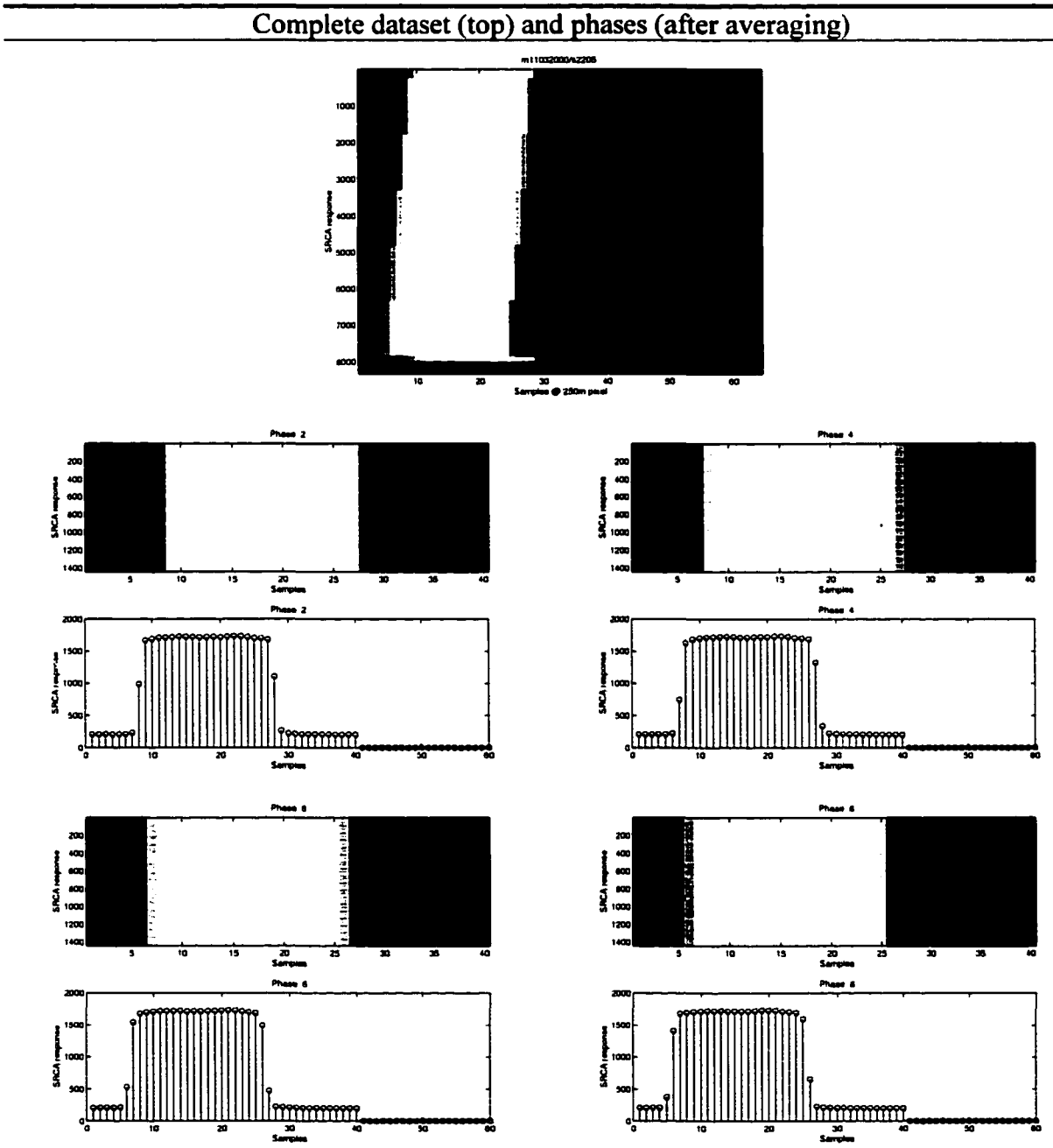

Figure 27. Combined phases to produce ESF, different line types used (left) and complete (right). The SRCA cross-track MTF results for 5 dates indicate that the results are temporally very stable (below).

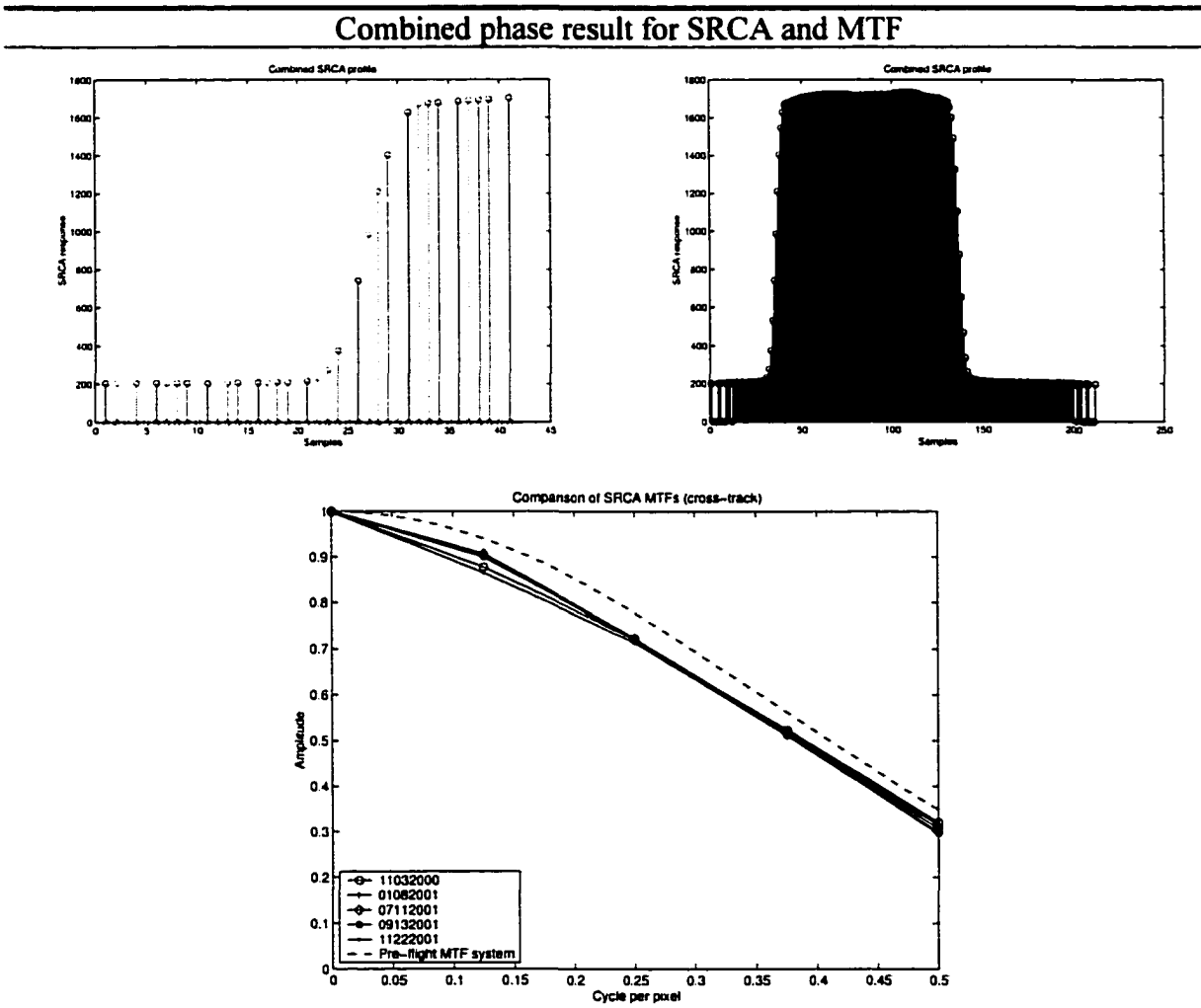

Figure 28. UTM world reference system (Courtesy of Peter H. Dana[19]).

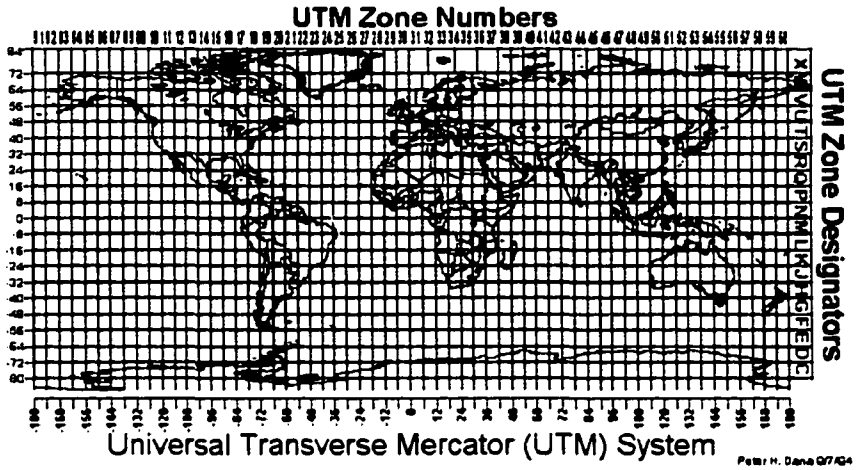

Figure 29. UTM construction.

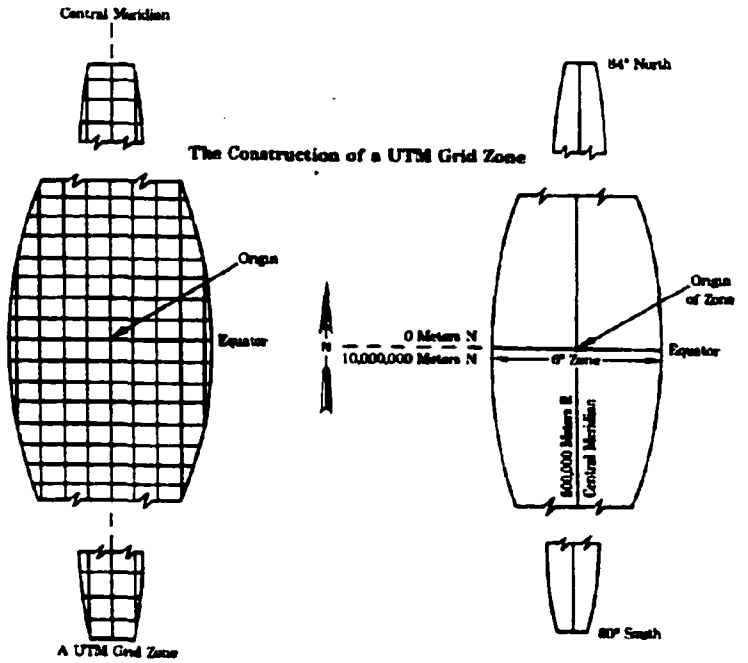

[19] The Geographer's Craft Project, Department of Geography, The University of Colorado at Boulder.

Figure 30. MODIS L1B geolocation for Maricopa 9/26/2001 at 1km geolocation resolution. The geolocation grid is interpolated to 250m.

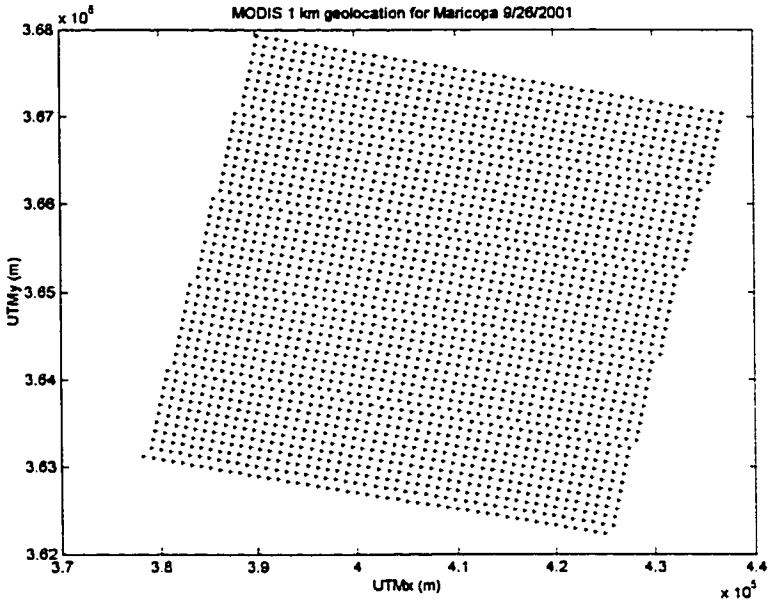

Figure 31. Landsat ETM+ band 3 scene for Maricopa 5/24/2001, path 37 row 37 level 1G without the north up configuration and ground control points labeled (left) and scene with a north-up orientation (right). This rotated image matches the reference (not shown) 9/26/2000.

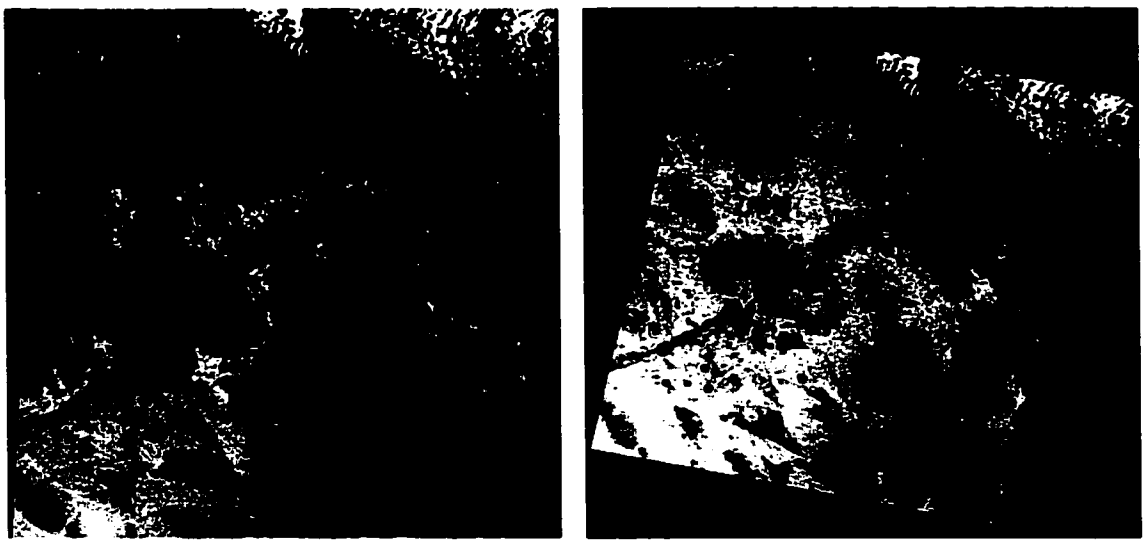

Figure 32. Mapping of the ETM+ (line, sample) geolocation geometry to MODIS image space. Note the scan offsets are reproduced.

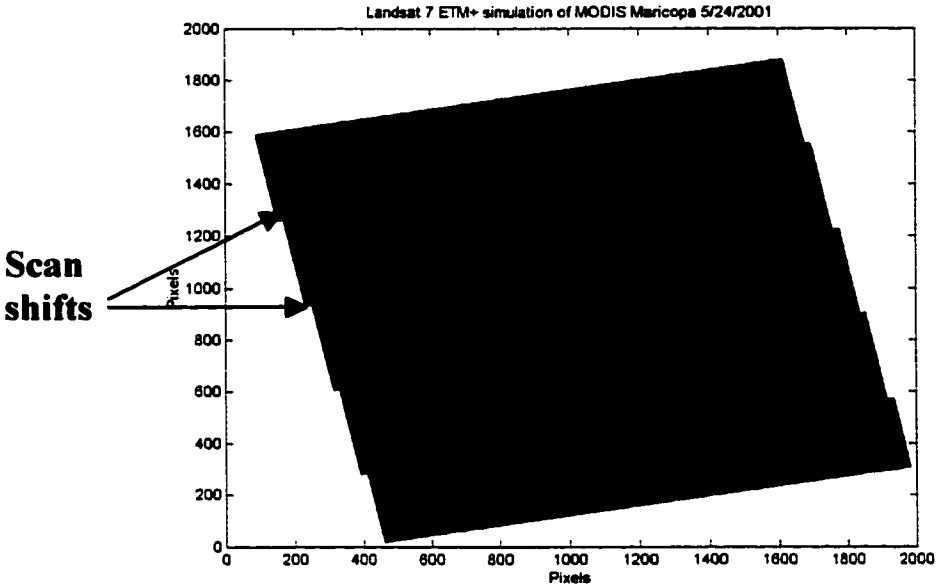

Figure 33. ASTER geolocation grid after being converted to UTMx,y (indicated by +) and the MODIS 250 m geolocation values indicated by the dots. The ASTER trimming is cut at the nearest geolocation points.

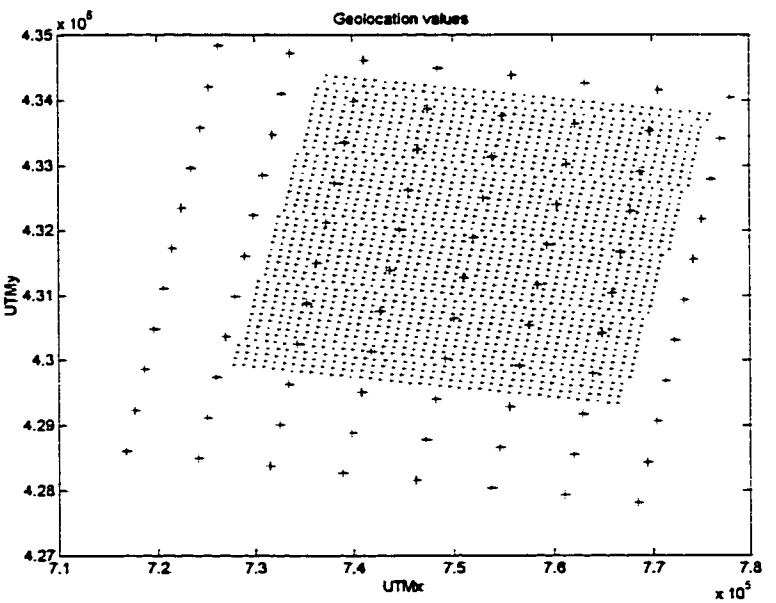

Figure 34. ASTER geolocation grid interpolated to 15m (solid dark area) and truncated to match the MODIS geolocation rectangle (+, white).

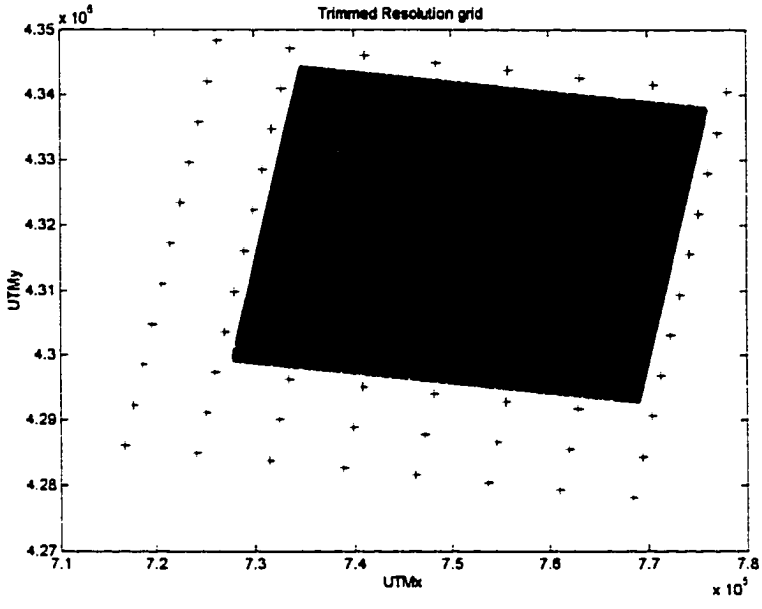

Figure 35. Distance measurement between MODIS and ASTER geolocation to figure out the nearest line sample coordinate.

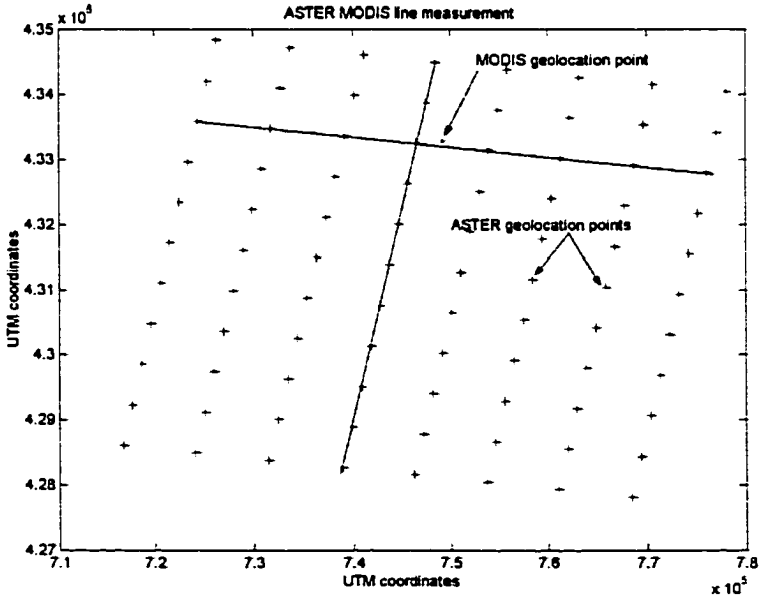

Figure 36. MODIS L1B band 1 (left) and simulated co-registered ETM+ band 3 (right). The arrow shows scan-to-scan offset reproduction.

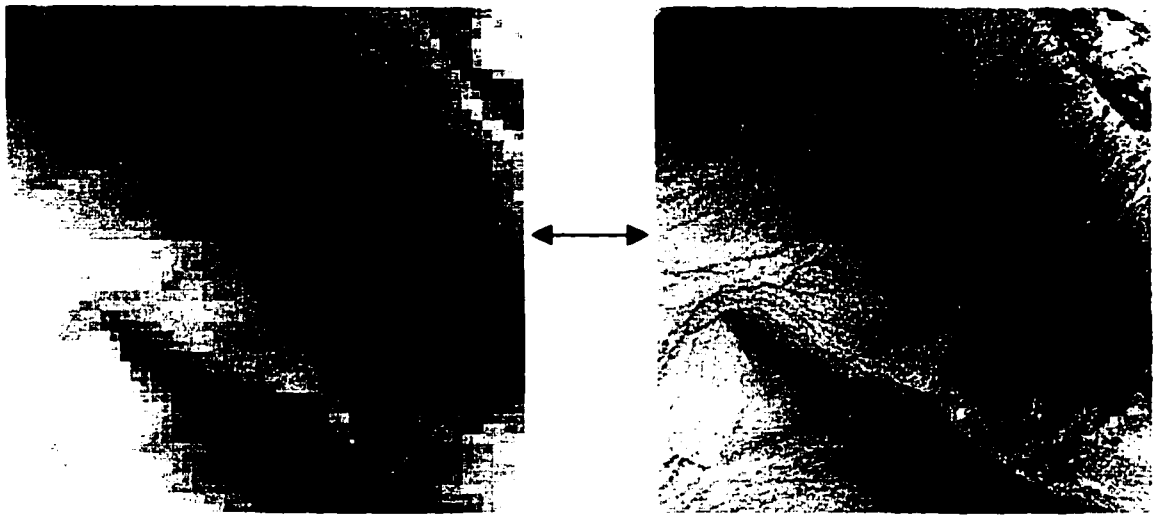

Figure 37. Registered ETM+ band 3 scene (left) and MODIS band 1 (right), Maricopa, AZ, acquired Sept. 26, 2000. The variation in field structure is different in reference to Figure 38.

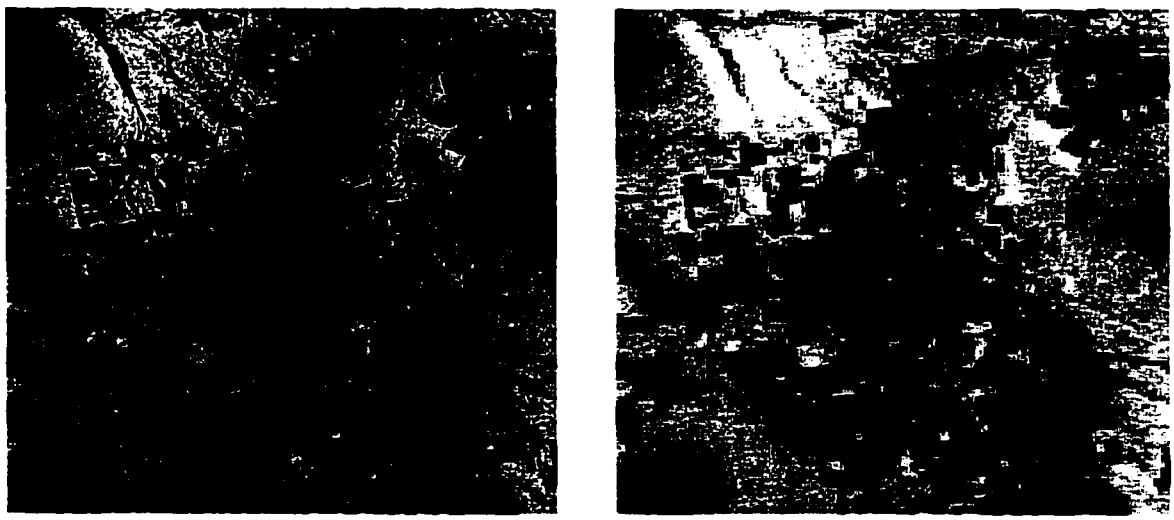

Figure 38. Registered ETM+ band 3 scene (left) and MODIS band 1 (right), Maricopa, AZ, acquired May 24, 2001.

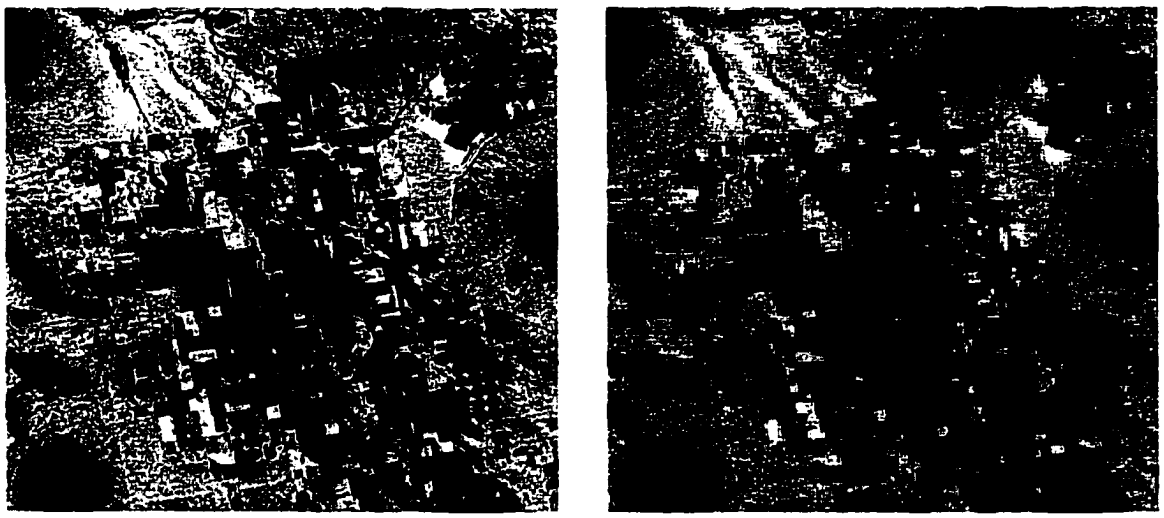

Figure 39. Registered ASTER band 2 scene (left) and MODIS band 1 (right), Odawaracho, Japan, acquired February 15, 2002.

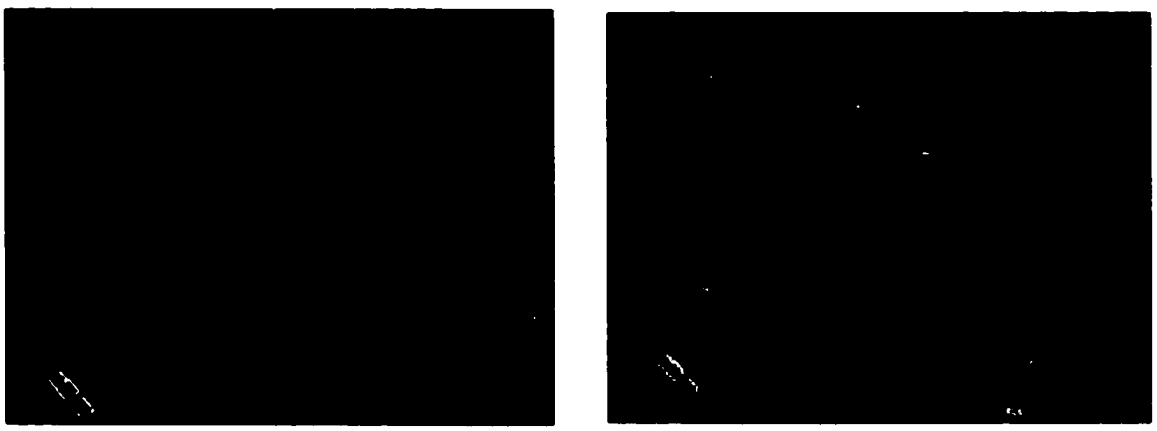

Figure 40. Registered Mono Lake with the island extract used for MTF analysis. ASTER band 1 (left) and MODIS band 2 (right), acquired September 29, 2000.

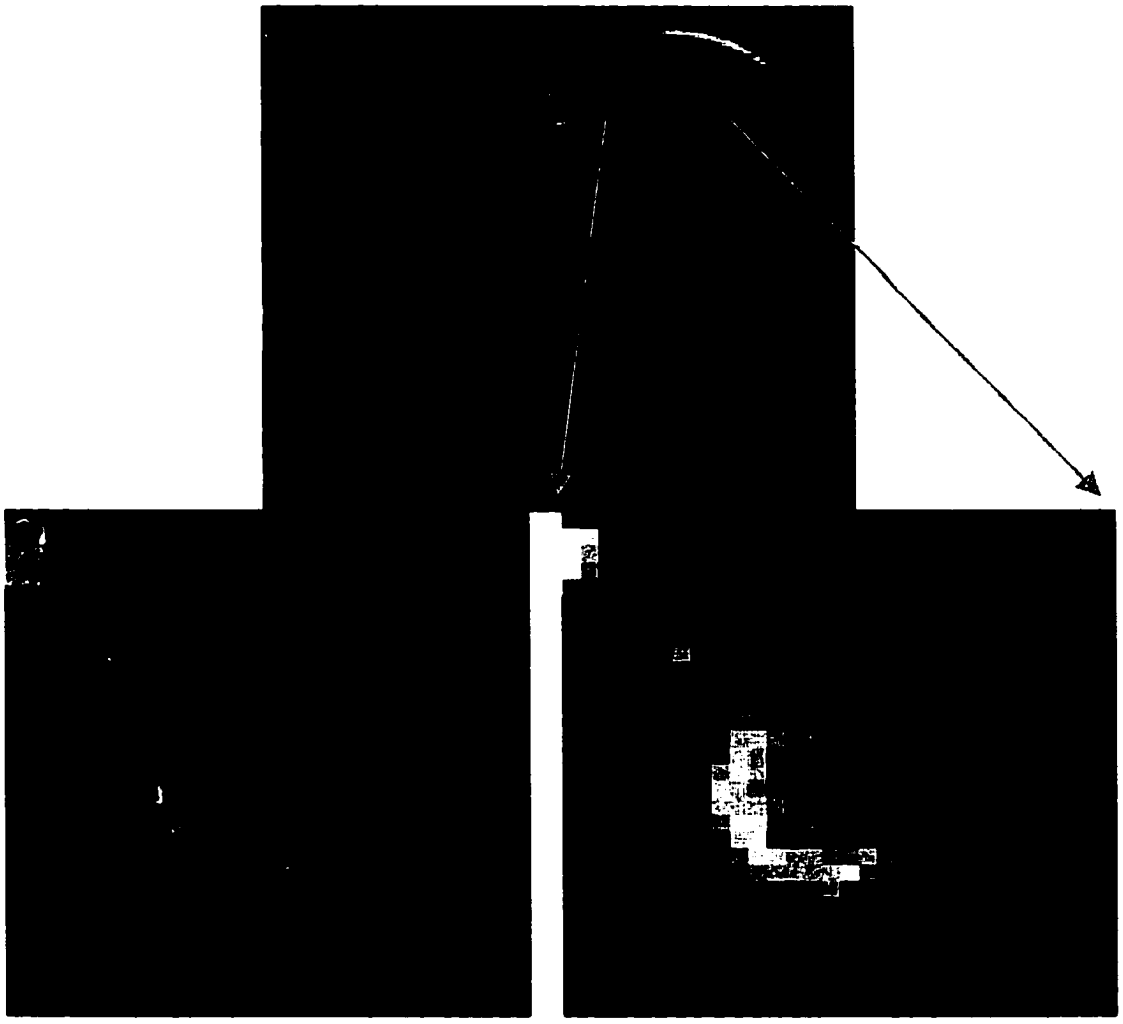

Figure 41. MTF results for bands 1 and 2 (NIR FP).

Band	In-track	Cross-track
1	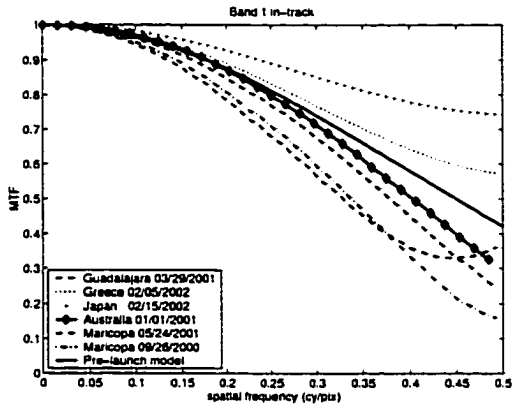	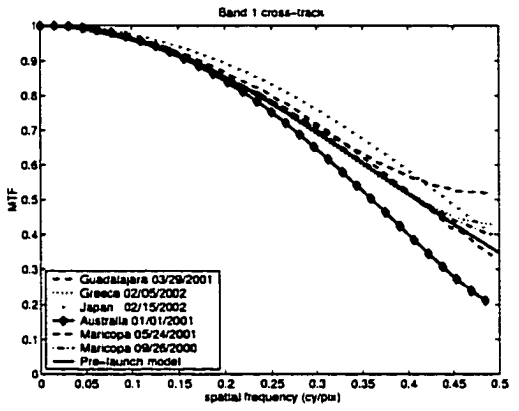
2	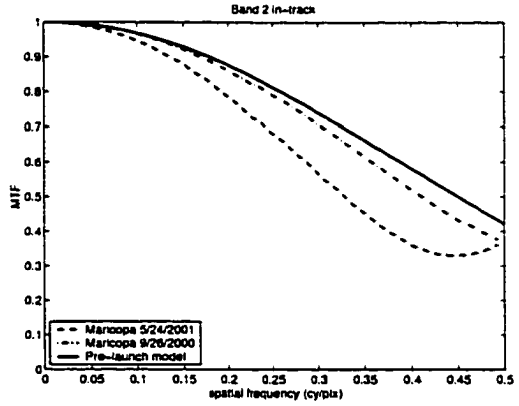	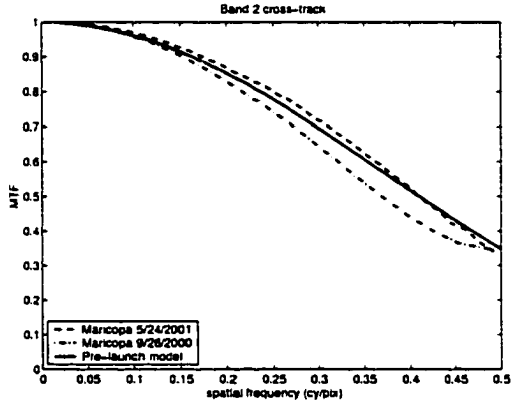

Figure 42. MTF results for bands 6 (S/MWIR FP) and 29 (LWIR FP).

Band	In-track	Cross-track
6	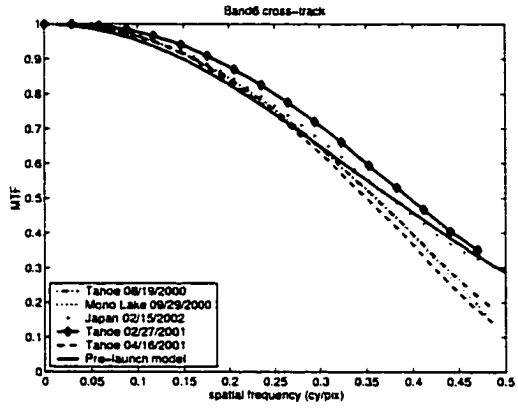	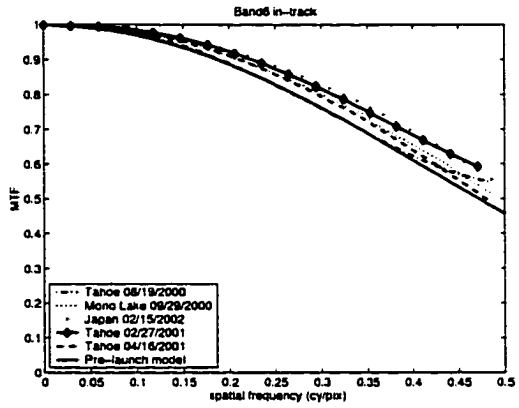
29	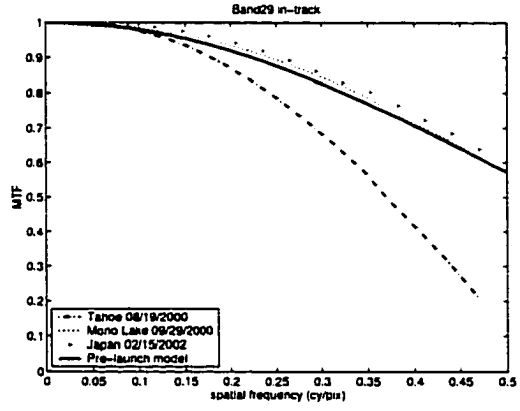	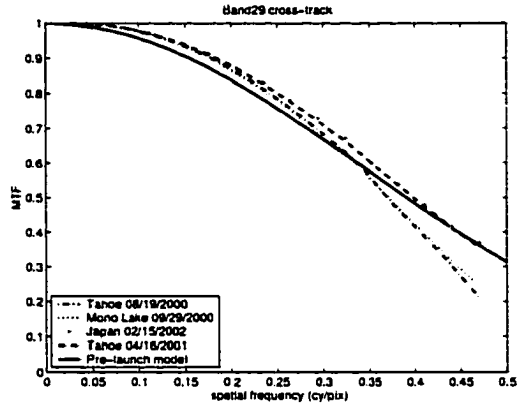

Figure 43. Candidate scenes for validation.

Cases:	Image Description (m):	Candidate image
Reference Image	Registered ASTER @15	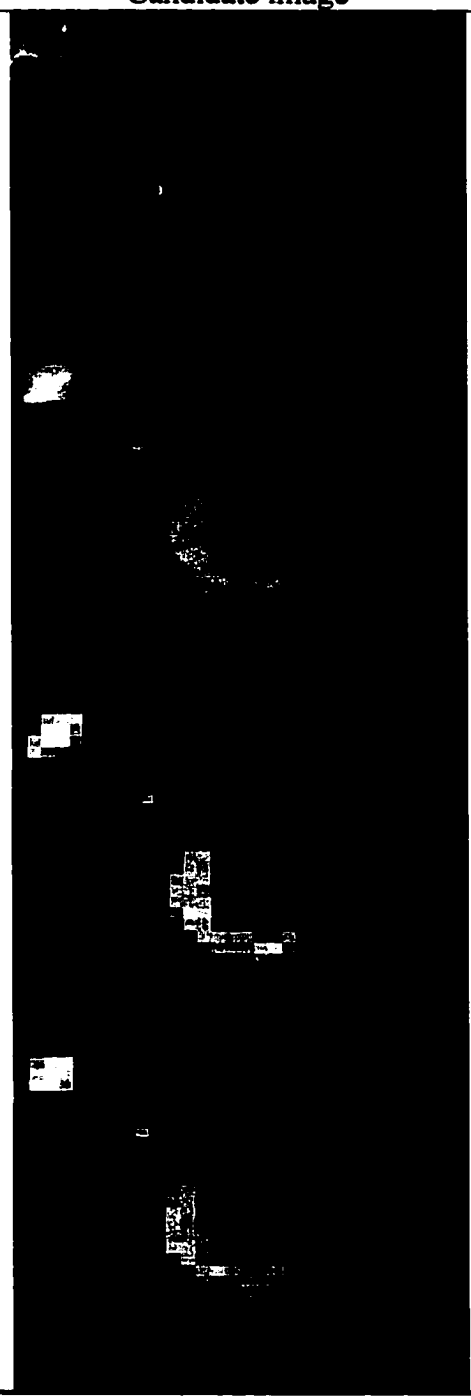
Ideal	Simulated MODIS @15	
Semi-ideal	Simulated MODIS @250	
Real	Real MODIS	

Figure 44. MTF validation result.

Cases:	In-track result	Cross-track result
Ideal	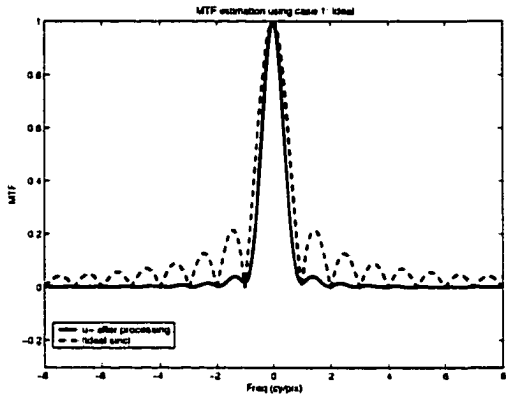	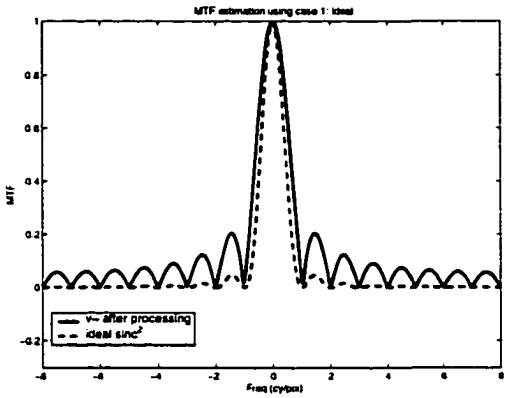
Semi-ideal	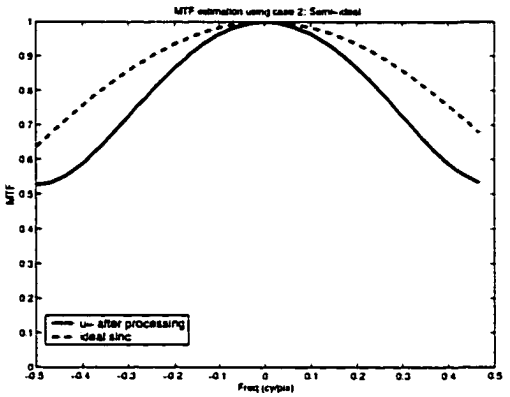	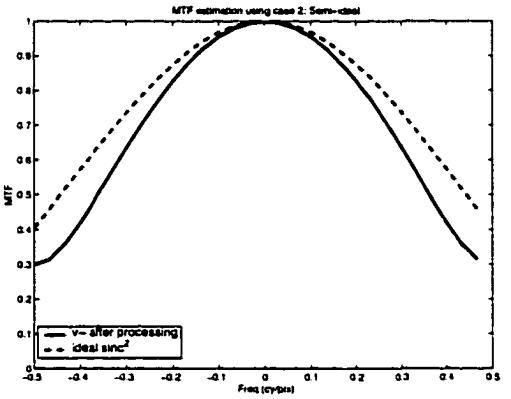
Real	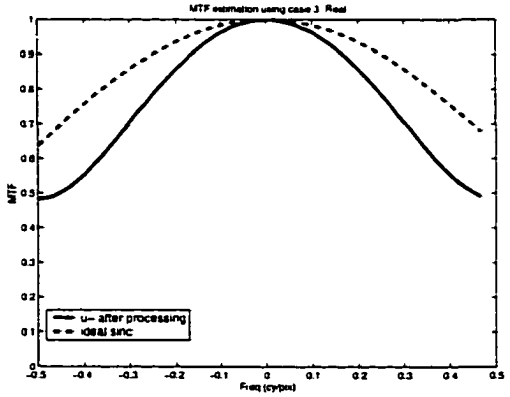	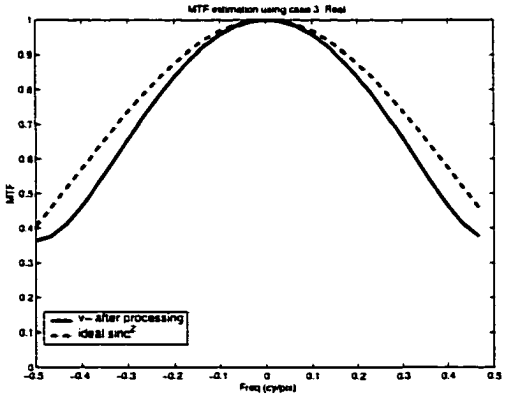

Figure 45. Candidate phases for All American Canal. Result of convolution MODIS SR with canal model

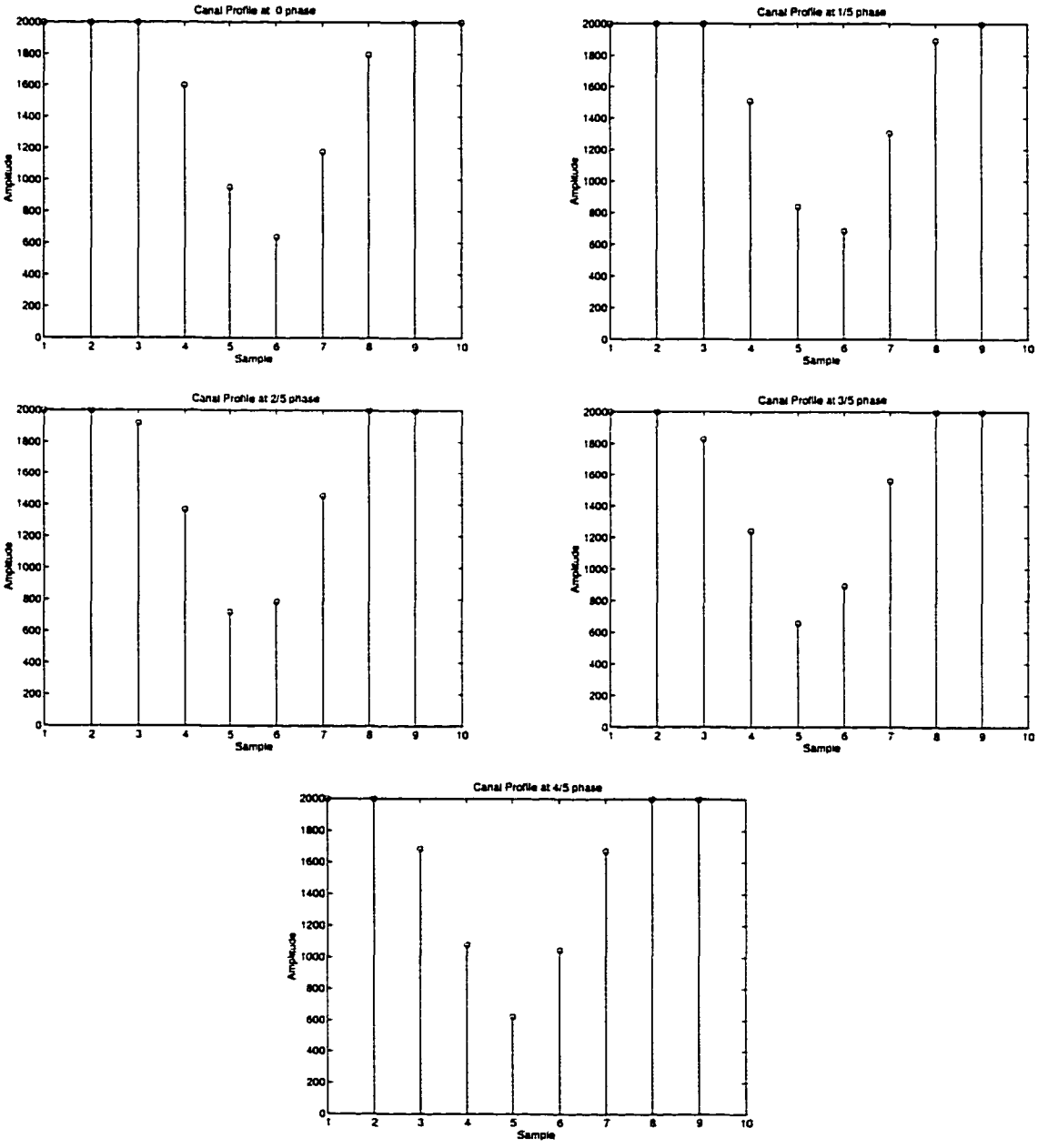

Figure 46.The model and resultant interleaved response obtained for the All-American Canal.

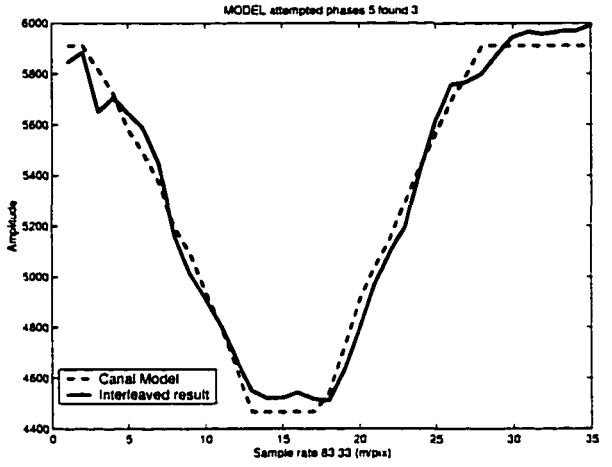

Figure 47. Estimated MTF result using the interleaved result and the model. The result shows that the MTF model matches the interleaved result.

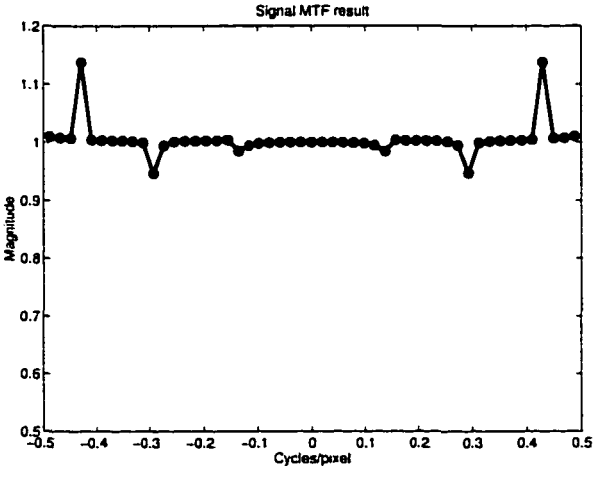

Figure 48. Interleave geolocation example. Circles indicate the 250m pixel distance, and crosses are the areas to be filled in.

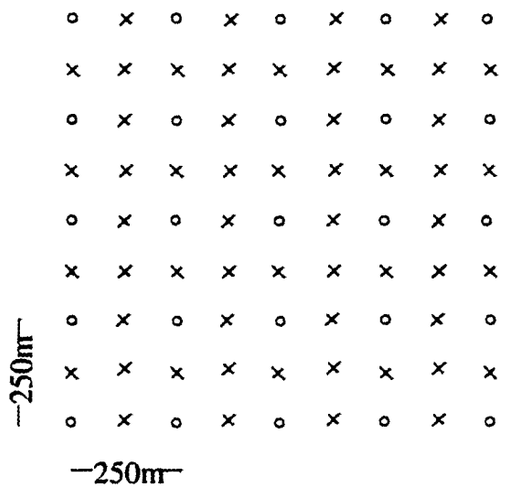

Figure 49. Geolocation example using three dates. The reference is indicated by the circles, and the crosses and dots are candidate geolocation entries for interleaving.

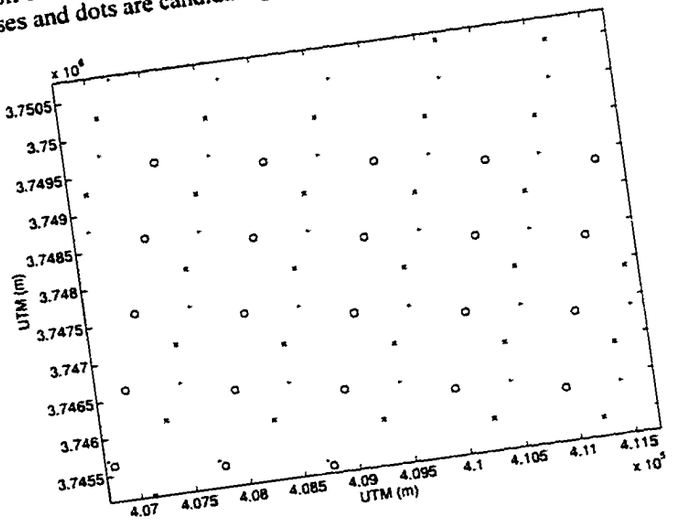

Figure 50 Candidate scenes of the lava field near Sevillita, New Mexico[20].

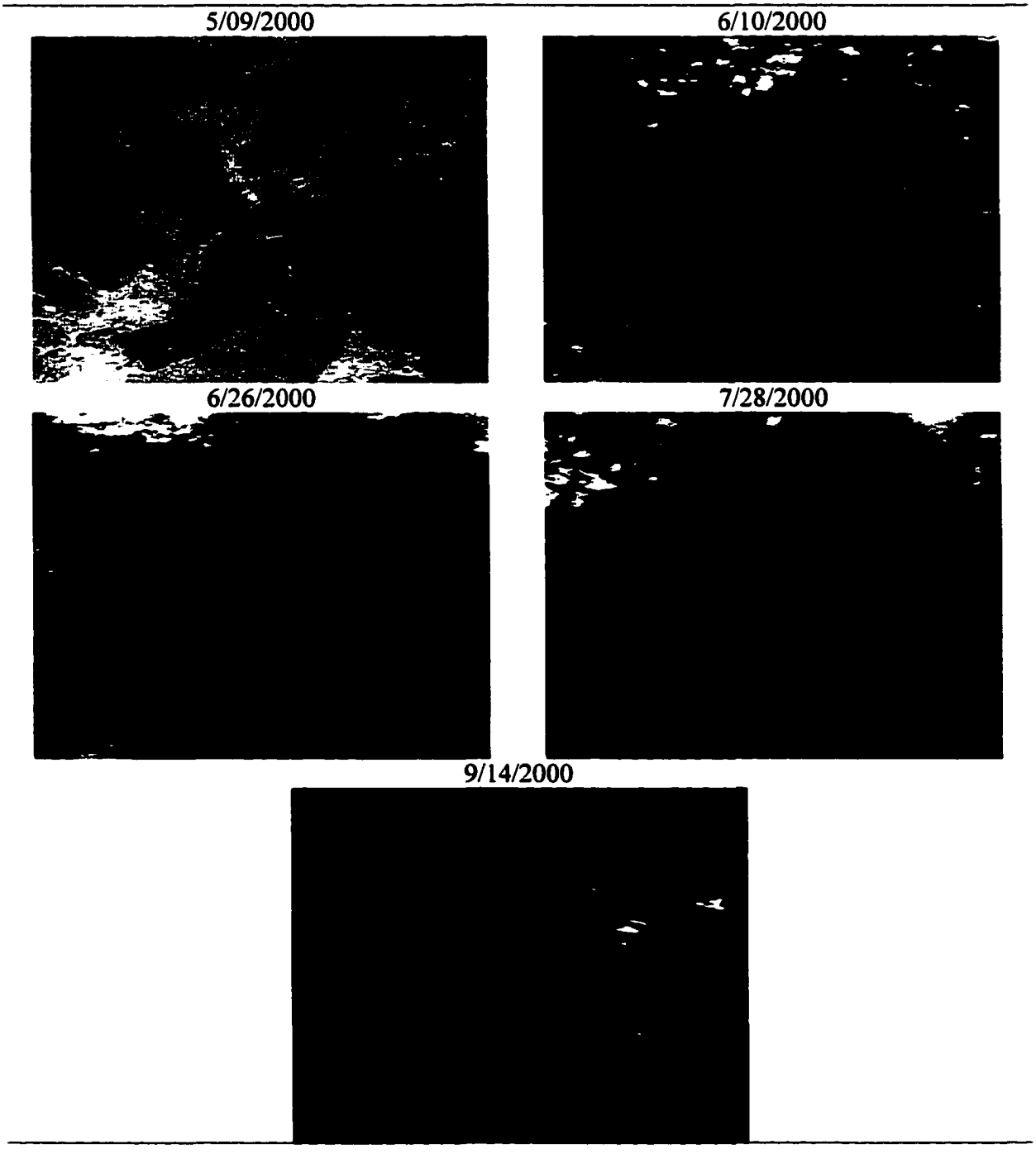

[20] Same contrast enhancement applied to all images. Radiometrically should be similar.

Figure 51. Interleaved result using the lava field near Sevillita, New Mexico.

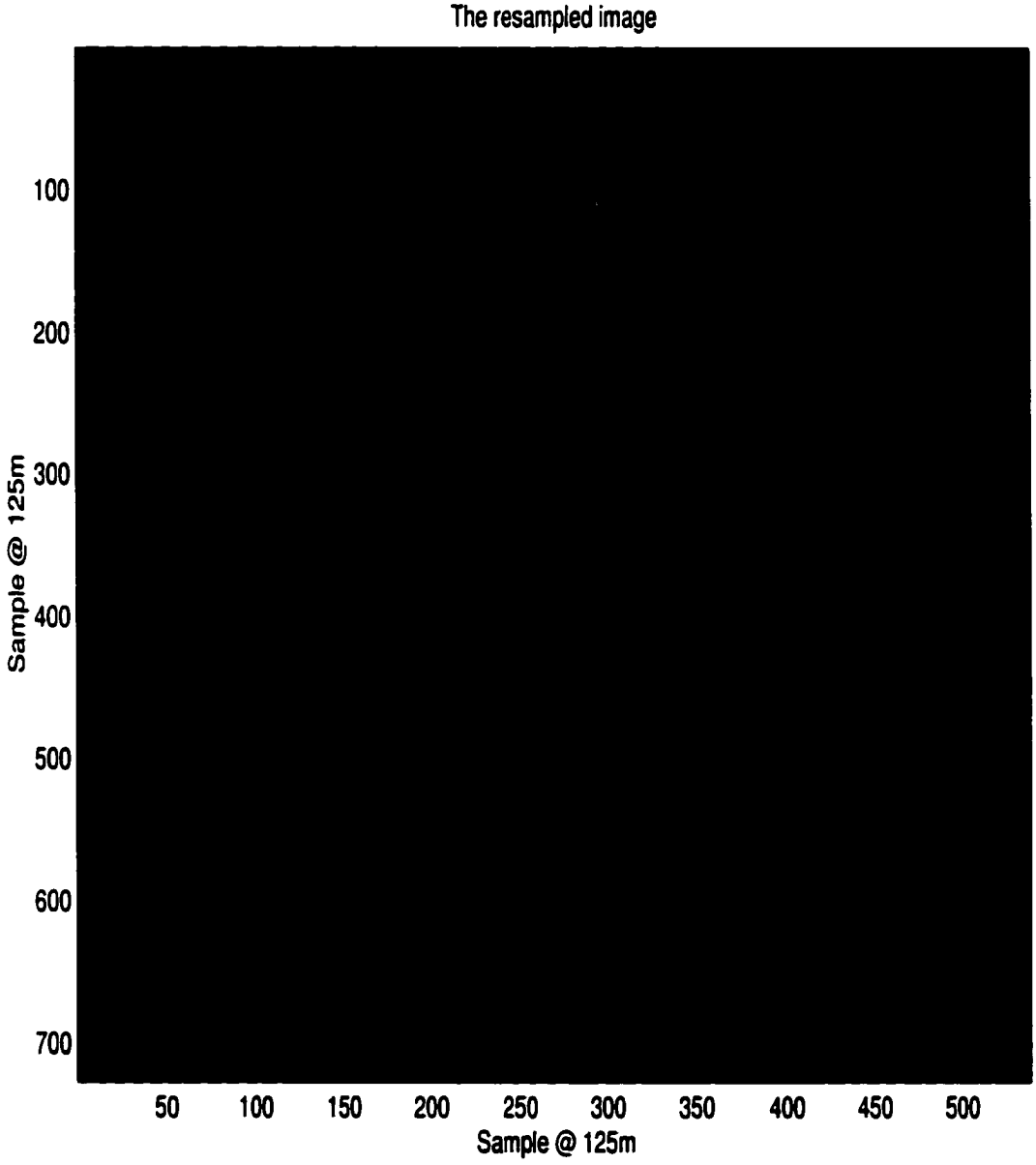

6 SPATIAL RESPONSE EFFECT

The major MODIS scientific disciplines ocean, land and atmosphere are all affected by the SR. The affected land discipline science products include, for example, Vegetation Indices (VI). The study Earth's vegetation using VIs requires "...a precise radiometric measure of spatial and temporal patterns ..." [25]. The SR is a limiting factor in obtaining accurate measurements near boundaries, since averaging takes place over several pixels. In MODIS, clouds or water bodies several kilometers away may influence the measured VIs. A correction for the MTF's non-ideal components in MODIS leads to improved results especially near boundaries, which may include land, water and clouds.

This chapter is separated into two topics. The first demonstrates the effect of the SR on VI science products, Normalized Difference Vegetation Index (NDVI) and Enhanced Vegetation Index (EVI) via simulations. The second topic demonstrates the qualitative and quantitative improvement in NDVI using MTFc [60]. The MTFc corrects the SR in the cross-track and in-track directions using an ideal response as a reference.

6.1 VEGETATION INDICES

The VIs are a major product of the MODIS Land Science Team (LST) and useful for global monitoring in spatial and temporal studies. "[The indices] are designed to enhance the vegetation signal from the measured spectral responses" [61]. These products provide complete global coverage on a 16 day and monthly cycle at 250m, 1km and 25km resolution [25]. Improvement in NDVI is used as the basis for the MTF correction filter and the results are compared to ETM+ NDVI, as a reference.

6.1.1 Normalized Difference Vegetation Index (NDVI)

The NDVI is used to determine the amount of vegetation in a scene using two spectral bands, the Near Infrared (NIR) and the red [10]. The range is typically between 0.0 and 1.0, and the formula is

$$\frac{\rho_{Nir} - \rho_{Red}}{\rho_{Nir} + \rho_{Red}} \tag{21}$$

where ρ is the surface reflectance for the respective bands. An NDVI value equal to 0.0 implies that there is no vegetation. It is not uncommon for the NDVI to be slightly below 0.0 for desert scenes. An NDVI equal to 1.0 implies that the area has significant vegetation cover.

6.1.2 Enhanced Vegetation Index (EVI)

The EVI, equation 22, is a variant of the NDVI which includes the blue spectrum [62]. The EVI has been shown to be more robust than the NDVI. Low values of EVI mean that the targets are spectrally flat, and EVI close to 1.0 also implies significant vegetation cover.

$$\frac{G(\rho_{NIR} - \rho_{Red})}{\rho_{NIR} + C1\rho_{Red} + C2\rho_{Blue} + L} \tag{22}$$

The values of G=2.5, C1=6.0, C2=7.5, L=1.0 are the same as the ones used in references [62] and [63].

6.2 ADJACENCY EFFECT ON SCIENCE PRODUCTS

The effect is demonstrated using an error analysis in NDVI and EVI. The background and target mixing, using the SR, is modified using the FFR values. The FFR is attributed to the area beyond the 2^{o} IFOV [32]. A contribution of 0.0 FFR implies that the signal is noise free, i.e. contains no adjacency effect.

6.2.1 Linear mixing model and analysis

The upper limits for the FFR were found to be $\nabla\omega_{red}$=30%, $\nabla\omega_{NIR}$=29% and $\nabla\omega_{blue}$=8%, section 4.4. The $\nabla\omega$ percentages are based on the following equation,

$$\begin{aligned} \nabla\omega_b &= \frac{FFR_b}{Total_b}, where \\ Total_b &= FFR_b + Saturated\ \mathrm{Re}sponse_b \end{aligned} \tag{23}$$

where $\nabla\omega_b$ is the maximum weighting factor per band and FFR_b is the FFR per band. Figure 52 shows the region from 0.0 to 2.0km as the Saturated Response (left of the vertical line), and the area beyond this line is the FFR contribution. This simulation neglects the atmosphere and other calibration uncertainties associated with MODIS to isolate the changes in NDVI and EVI [62, 64]. The mixing model for the adjacency effect is based on the following,

$$\rho_{total,b} = \rho_{target,b}(1-\nabla\omega_b K) + \rho_{background,b}\nabla\omega_b K \tag{24}$$

where $\rho_{total,b}$ is the total reflectance observed at the Nadir pixel of interest for band b, and the term $\rho_{target,b}$ is the reflectance within the saturated response for band b. This term is multiplied by the weighting function, $(1-\nabla\omega_b K)$. As mentioned above, $\nabla\omega_b$ is the total weight for the band based on the FFR. K is a quantization factor, ranging from 0.0-1.0, which weights $\nabla\omega_b$. K=1.0 means that the contribution for the red, blue and NIR are at the maximum$\nabla\omega_b$ and referred to as 100% FFR in Figures 53 and 54. Similarly, for a value of K= 0.25 the contributions for the spectra would be at 25% of the maximum $\nabla\omega_b$. The $\rho_{total,b}$ is used in the NDVI and EVI equation via the reflectance terms for the NIR and red bands,

$$NDVI = \frac{(\rho_{total,NIR} - \rho_{total,red})}{(\rho_{total,NIR} + \rho_{total,red})} \tag{25}$$

The EVI equation is the following,

$$EVI = \frac{G(\rho_{total,NIR} - \rho_{total,red})}{(\rho_{total,NIR} + C_1\rho_{total,red} - C_2\rho_{total,blue} + L)} \tag{26}$$

where the terms $\rho_{total,NIR}$, $\rho_{total,red}$ and $\rho_{total,blue}$ are the total simulated reflectance for the respective band.

The changes in spectral variation due to the adjacency effect are demonstrated using two scenerios. One is a 2km uniform vegetated target surrounded by a soil background, and the other is a 2km uniform soil target surrounded by a vegetated background. The targets are simulated using an experimental dataset, growing cotton (*Gossypium hirsutum* L. var. Dpl-70) at 95%, 60%, 40%, 20% and 0% soil cover with the

Leaf Area Index (LAI) ranging from 0.0-3.3. These data were acquired using a Barnes Modular Multiband Radiometer (MMR) [62, 65]. The relation between the MODIS bands and the MMR bands are listed in Table 20.

Table 20. Comparison of MODIS and MMR Bands (Adapted from [62])

	MODIS band	Bandpass (μm)	MMR band	Bandpass (μm)
Blue	3	0.459-0.476	1	0.45-0.52
Red	1	0.620-0.670	3	0.63-0.69
NIR	2	0.841-0.876	4	0.76-0.90
Middle-IR	7	2.105-2.155	7	2.08-2.30

Values for K=1.0, 0.75, 0.5, 0.25 and 0.0 are used in equation 24 to observe the influence on ρ. K controls the amount of simulated adjacency effect. A drop in ρ is shown when the vegetation target is surrounded by soil (Figure 53). The change in ρ is more pronounced in the NIR region as it is on the order of 0.13 for 100% FFR adjacency effect.

The soil target is surrounded by 95% cotton (Figure 53). As the value of K increases, the soil signature starts resembling a vegetation signature. The NIR spectrum dominates the signature. There is a 10% increase in ρ_{NIR} using the max values in FFR. The change in the NDVI product is shown in Figure 53 using the difference,

$$\Delta = NDVI_{pure} - NDVI_{mixed} \tag{27}$$

where $NDVI_{pure}$ is the signal without any adjacency effects, the ideal case, and $NDVI_{mixed}$ is the signal mixed with the FFR background. In the case of vegetation

surrounded by soil, the NDVI is underestimated (Figure 54). At NDVI= 0.3, $\Delta_{max} = 0.06$. At 75% FFR, the NDVI = 0.7 and $\Delta = -0.11$. If the target is surrounded by vegetation, the NDVI is overestimated (Figure 54). An NDVI of 0.3 and K= 0.25 causes an overestimate of $\Delta = 0.07$. The error due to the FFR is calculated similarly for the EVI.

$$\Delta = EVI_{pure} - EVI_{mixed} \tag{28}$$

where EVI_{pure} is signal without any adjacency effects and EVI_{mixed} includes the FFR response. Using the same approach as before, vegetation surrounded by soil, the EVI is also underestimated (Figure 55). The errors increase significantly if the FFR of the blue band is on the same order as the NIR and red bands. For an EVI = 0.6, and K= 0.5, the EVI is underestimated by 0.1. When $\Delta < -0.05$ for the case of K= 0.25, the EVI suppresses the FFR effects better than the EVI = 0.6 case.

6.2.2 Adjacency effect conclusions

The simulations in this section demonstrate that the FFR affects the accuracy of science products. The errors are computed using laboratory PSR data without atmospheric propagation effects. It is concluded that the NDVI and EVI are underestimated in situations where vegetation is surrounded by soil. The errors in NDVI and EVI are shown in Figures 54 and 55. Both the NDVI and EVI are overestimated in situations where the MODIS is looking at soil surrounded by vegetated areas. The simulations demonstrate that accurate characterization of the FFR response via the MODIS SR is important.

6.3 MTF SIMPLIFIED MODEL

In the previous section, simulations on the NDVI and EVI show that the MODIS SR affects the accuracy on science products. Correction for the MODIS SR, via the MTF, is important in science applications especially where "...precise radiometric measurements of spatial and temporal patterns..." are warranted [25]. In these cases a calibration of the SR is necessary. Without a correction for the SR, the adjacency effect is more pronounced. Reference [66] has shown a reduction in the adjacency effect when the SR is accounted for. The improvement is most noticeable near boundaries of high contrast. The correction filter is applied to several datasets, a scene from Mono Lake September 29, 2000, a scene from the Maricopa Agricultural Center (MAC) fields September 26, 2000 and a scene from Rail Road Valley June 14, 2001.

6.3.1 Correction for the MTF model

The correction filter was developed using the MTF model, section 4.5. The correction filter developed for $MTF_{system}(u,v)$ is based on the following equation,

$$MTF_{Correction}(u,v) = \frac{MTF_{ideal}(u,v)}{MTF_{system}(u,v)} \ni u,v : [0,0.5) \tag{29}$$

MTF_{ideal} is the ideal MTF response using a partial restoration and consists of the detector component only (Figure 56); this is the fundamental component. In an ideal case, no motion or optical blurring should exist in the cross-track or in-track directions. The $MTF_{Correction}$ term is the system transfer function with the valid frequency range [0, 0.5) cycle per pixel. This range is used in the derivation since the 1st null exists at 1 cycle per

pixel in the ideal case. The null will cause the transfer function to be unstable. The cross-track and in-track transfer functions are shown for bands 1 and 2, based on equation 29 (Figure 57).

Like most orbital passive sensors, MODIS is an undersampled system and any frequencies greater than 0.5 cycle per pixel are subject to aliasing [58]. If MODIS data were sampled at least the Nyquist rate, the frequency spectrum would be separated, but since it is not, the frequency spectrum is aliased (Figure 58). This technique only corrects the MTF frequency response to bring it near the ideal case and does not attempt to deconvolve the aliasing.

The theoretically corrected and uncorrected cross-track (left) and in-track (right) modeled SR using the frequency range [0,1) cycle per pixel is shown (Figure 59). Using the FWHM measure, the uncorrected cross-track response is 284m. The *theoretically* corrected FWHM is 218m. If MODIS data met the Nyquist sampling criteria, there would have been a theoretical 22.15% reduction of the FWHM. Similarly, in the in-track direction the uncorrected FWHM value is 256m. The theoretically corrected PSR FWHM is 218m. This is a theoretical 12.5% reduction of the FWHM. A summary is in Table 21.

6.3.2 MTF correction for MODIS bands 1 and 2

With the cross-track and in-track MTF correction filters derived, application and evaluation of the filters is the next step. Radiometric corrections are only type of manipulation applied to the MODIS 1B product [23, 67, 68]. The Mono Lake scene acquired on September 29, 2000 and the Maricopa scene, from the MODLAND

validation core site, acquired on September 26, 2000 are used as examples (Figures 60 and 61).

Table 21. Theoretically estimated FWHM parameters for band 1.

Parameter	SR at FWHM (m)	Error[21] (m)
cross-track uncorrected	281	± 7.53
cross-track MTF corrected	218	± 7.53
in-track uncorrected	256	± 7.53
in-track MTF corrected	218	± 7.53

Application of the correction filter is summarized in Table 22. The scan shift correction is necessary because artificial frequencies, due to the discountinuities, will be created if the filter is applied without removal of them first. Application of the correction filter in this example uses 128 points in the cross-track and in-track. After extracting the 128x128 point image, the magnitude of the spectra is multiplied by the $MTF_{Correction}$ filter and the inverse 2-D FFT is performed [58]. At this point the scan shifts may be reintroduced. The corrected image is sharper than the uncorrected (Figure 60). The improvements are most noticeable near high contrast features such as upper portion of the lake and the island. In a more complex scene, the MAC fields, the improvement is slight and best seen on the field boundaries (Figure 61).

[21] The SR sampled at 15.6m. The error is ±½ a pixel.

Table 22. Procedure for MTF correction application.

Procedure for MTF correction
Extract MODIS level 1B region near center of scan ≥ 128x128 pixels
Correct for the scan shifts
Apply a 2-D FFT to the image
Multiply by the 2-D correction filter
Apply an inverse 2-D FFT to result
Re-introduce the scan shifts (if needed)

6.4 MTF IMPROVEMENT PERTAINING TO SCIENCE PRODUCT, NDVI

The visual improvement is more noticeable in an NDVI image. In addition to the qualitative analysis a quantitative analysis is demonstrated [69]. The procedure uses ETM+ as the reference with the understanding that differences exist between the sensors, calibration, IFOV and quantization scales. In addition, the ETM+ IFOV is 30m, which is 8.33x smaller than nominal MODIS IFOV.

MODIS and ETM+ images are scaled to at-sensor radiance units and registered as described in section 5.2.2. The ETM+ registered image, the true scene, is used in the NDVI analysis. The MODIS image has the MTF correction applied to it. The chosen scene is Rail Road Valley. Reference [70] provided in-situ measurements to convert the at-sensor radiances to ρ in which a first order approximation was used for MODIS bands 1 and 2 and ETM+ bands 3 and 4. Three NDVI images were created one for ETM+, one for MODIS without MTF correction (MTFn) and one for MODIS with MTF correction (MTFc) (Figures 70 and 71).

The analysis consists of estimating the Root Mean Squared Error (RMSE) for MTFc and MTFn using ETM+ as the reference. No averaging is implemented for ETM+ NDVI (Figure 64). The RMSE computed for transect 1 with MTFc is .0687 vs .0987 with noMTFc, and the RMSE computed for all transects is 0.1802 for MTFc vs 0.2406 for noMTFc.

Figure 52. The FFR is shown for the red, NIR and blue bands. The two target scenario is shown.

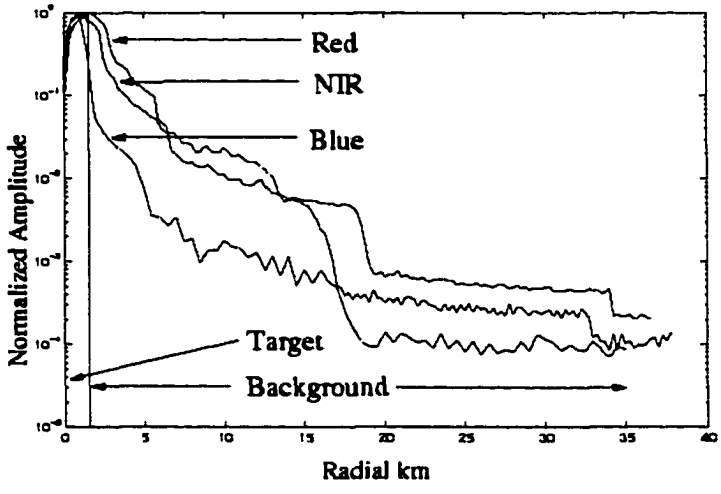

Figure 53. The spectral response for different percentages of K*FFR. 95% cotton with a soil background target (left). Soil with 95% cotton background (right).

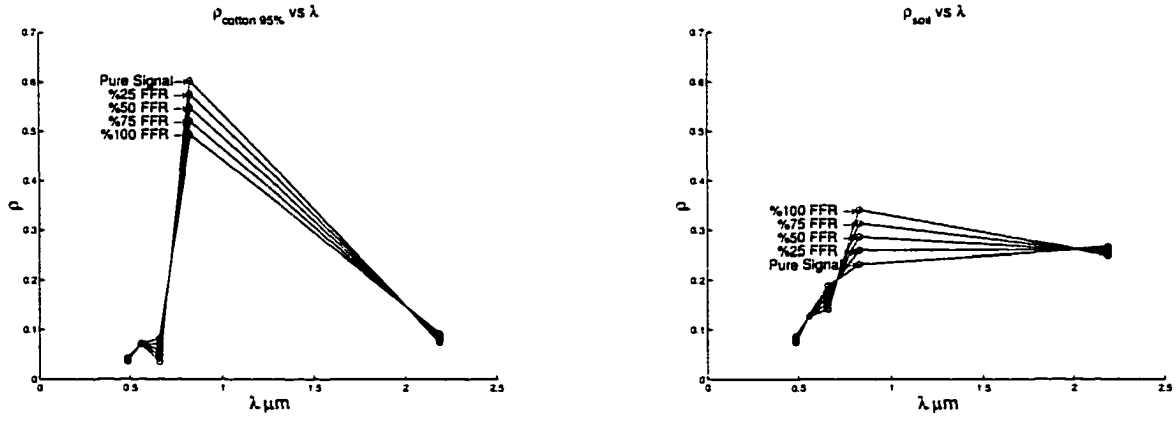

Figure 54. Δ vs NDVI with background soil target (left). Δ vs NDVI with a background of 95% cotton (right). Scales are different in both figures.

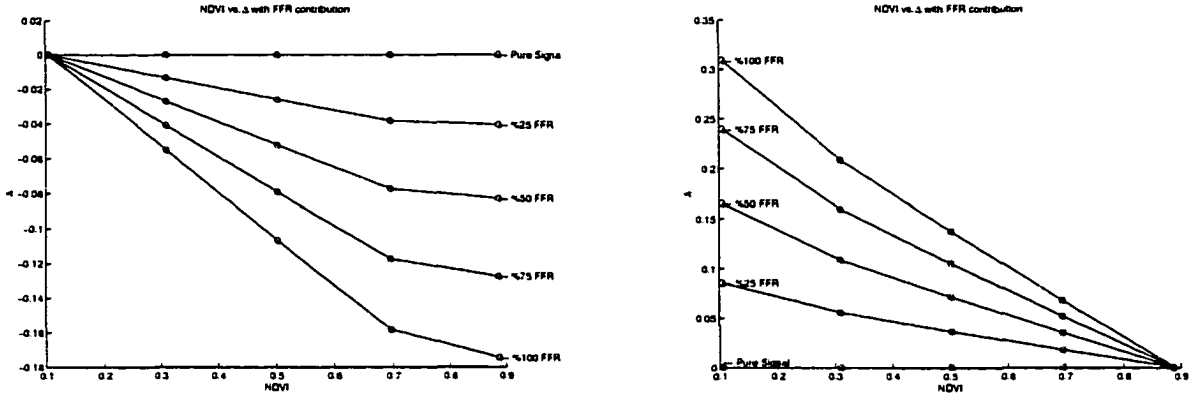

Figure 55. Δ vs EVI with background soil target (left). Δ vs EVI with a background of 95% cotton (right). Scales are different in both figures.

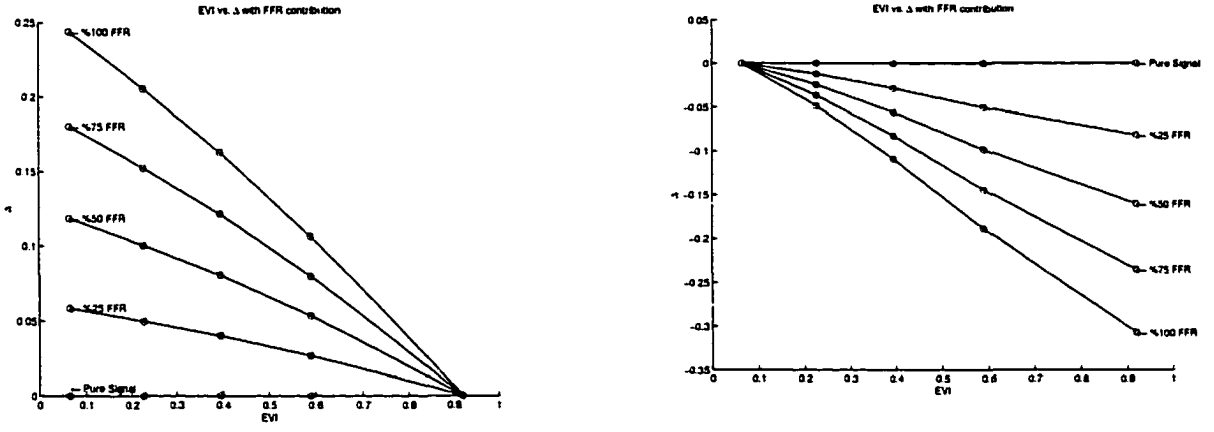

Figure 56. In-track and cross-track system MTFs and ideal response for bands 1 (left) and 2 (right).

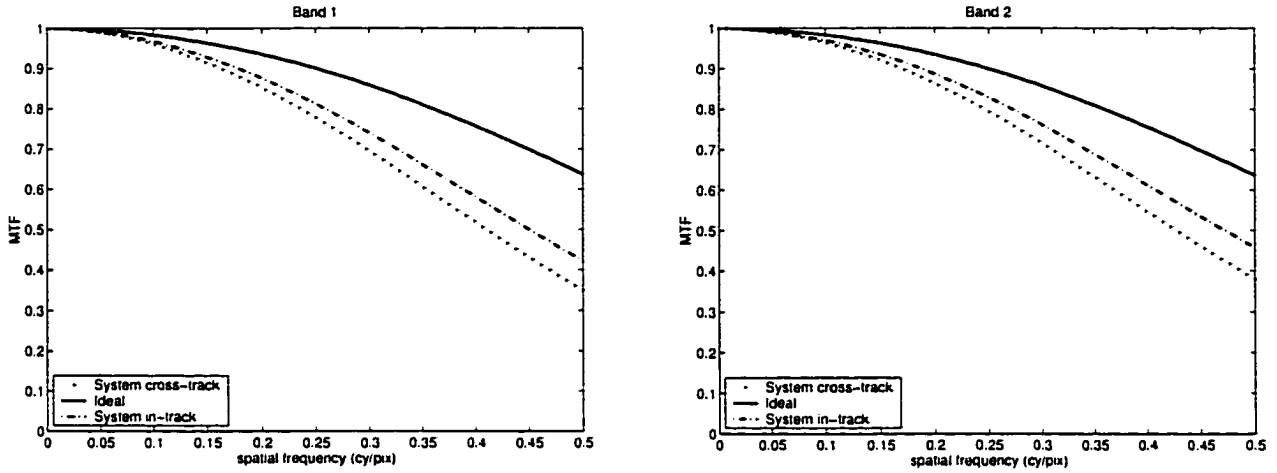

Figure 57. In-track and cross-track correction MTFs for bands 1 (left) and 2 (right).

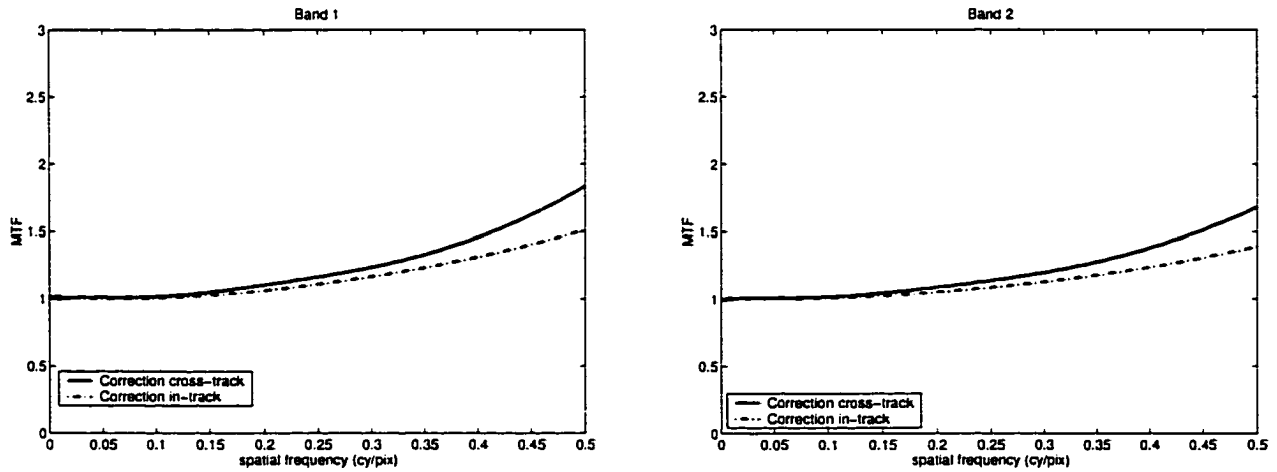

Figure 58. Frequency spectrum at Nyquist (ideal case left), and frequency spectrum for undersampled system (aliasing case, right)

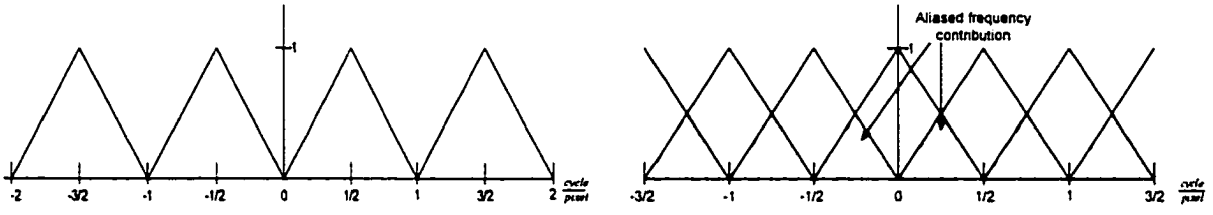

Figure 59. Cross-track (left) and in-track (right) SR with and without correction for band 1. The area of the SR is normalized to 1 for each curve.

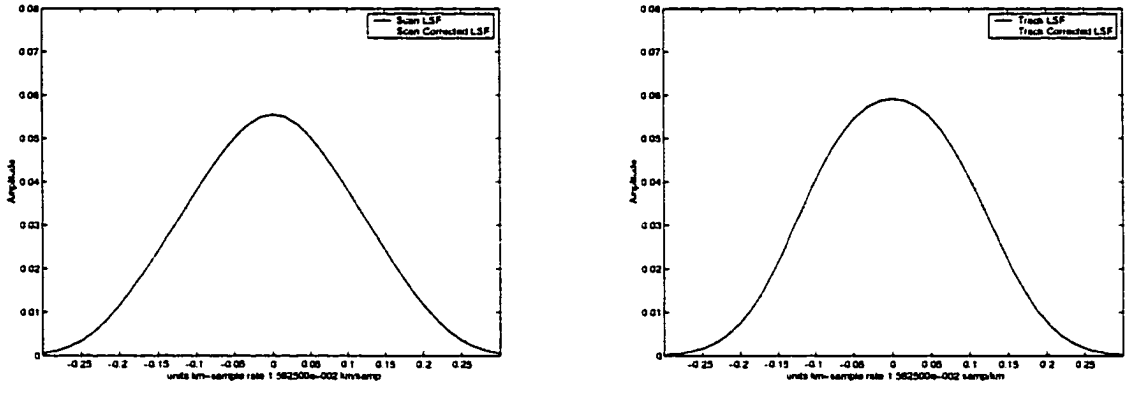

Figure 60. MODIS uncorrected for scan shift (left) and the MTF corrected result (right). The MTF correction is slight and appears to focus the image. The correction is most noticeable near boundaries and high contrast edges.

Figure 61. MODIS level 1B image of MAC fields (left) and the MTF corrected MAC fields (right). The improvement is seen in the field edges.

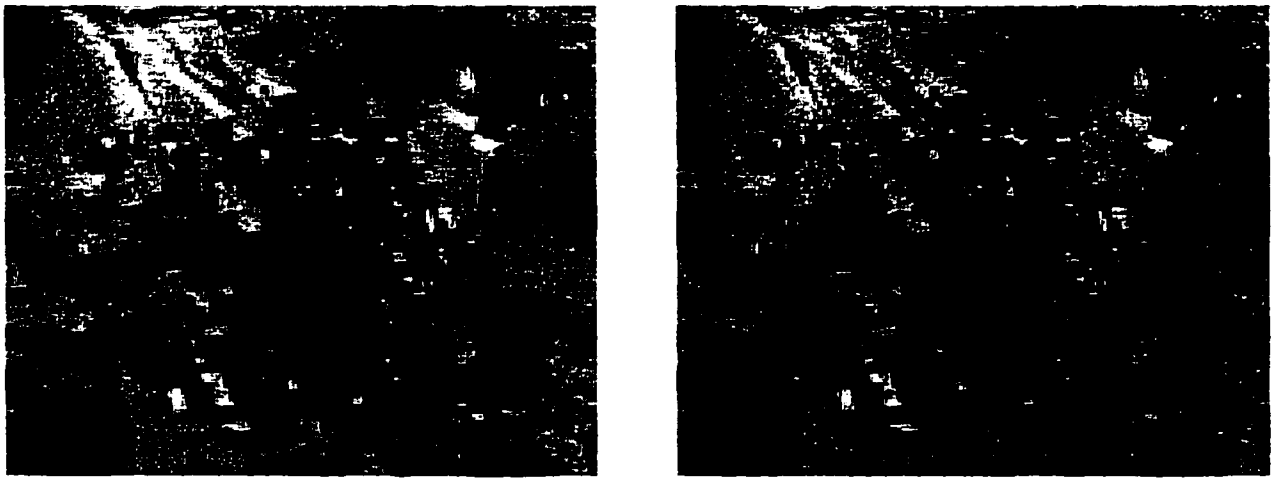

Figure 62. ETM+ NDVI registered image of Rail Road Valley with transects.

Figure 63. MODIS NDVI image for Rail Road Valley. Top is uncorrected image and bottom is MTFcorrected image. White squares show visual improvement.

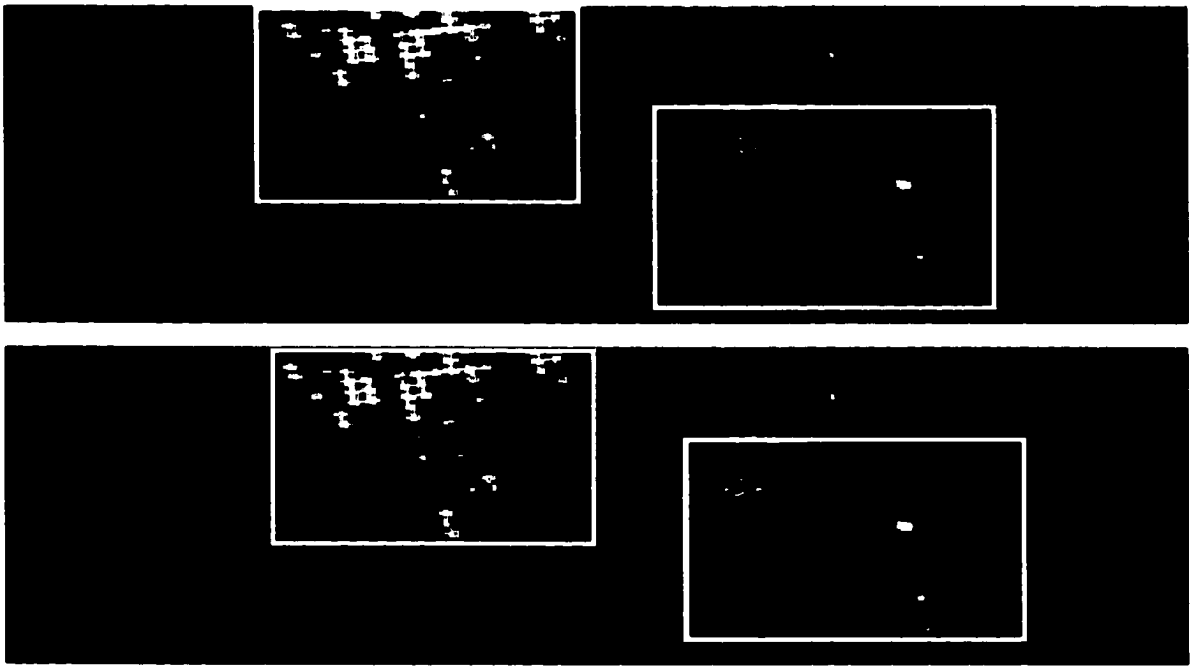

CONCLUSION

Reliable characterization of the MODIS MTF requires using as many sources of information as possible. In this research, a model, pre-launch measurements, and measurements from on-orbit imagery are used to develop a consistent characterization of the MTF. The pre-launch measurements, which are a review of the channel registration and cross-talk are discussed in the first part of Chapter 4. The second part of that chapter develops the MTF system model.

Chapter 5 introduces a technique for estimating the on-orbit MTF using a two-image method which includes an innovative approach for registering two images and using the geolocation data associated with a given scene. The advantage of this technique is that the process is automated and ground control points are not needed. The disadvantage of the technique is that it heavily depends on the accuracy of the geolocation. The geolocation for ETM+, ASTER and MODIS are converted to a common reference. As part of the registration process, radiometric registration is also performed.

Data obtained over a course of a year, from the on-board SRCA, show that the MODIS MTF is stable. The other on-orbit MTF estimation technique uses Fourier analysis of image pairs. The robustness of the algorithm was validated using three cases: an ideal, a semi- ideal and a realistic case. The algorithm was optimized to get the best result before using it with real data. The validation approach is general enough to use for validating other MTF estimation algorithms.

The cross-track MODIS MTF indicate that on-orbit performance is comparable to pre-launch performance. Some of the in-track MTF on-orbit are comparable to pre-

launch, but not to the degree of the cross-track measurements. A concern using the on-orbit MTF measurements is the scene dependence in the MTF estimate. The candidate scenes are chosen on the basis that they should have plenty of high contrast features, otherwise there are not enough frequency components to estimate the MTF.

Finally, the impact of the MODIS SR on science products is shown in Chapter 6. A simulation study demonstrates that the SR influences the measurements. The measurements are biased by the MODIS SR, especially in cases where the SNR from Earth scenes is low, therefore a correction for the SR is desired. The second part of the chapter derives an MTF based correction filter for MODIS. The sampling rate limits the effectiveness of the correction.

Improvements may be made in several areas to improve the results and extend the MTF estimates. Some of the areas are image registration, SR estimation, temporal monitoring and MTF estimates for other bands. In terms of image registration, a possible improvement could be to use wavelets instead of the AAC technique in the registration process. The approach would still take advantage of the geocoding for the coarse registration, the sub-pixel registration would switch to a multi-resolution wavelet algorithm. Studies have shown robustness using wavelets for sub-pixel accuracy and a higher efficiency over conventional methods [71, 72].

The current dual-image MTF estimation procedure works well in the cross-track direction, but the results are not as reliable in the in-track direction. A plausible explanation is that aliasing is more severe in-track; so an improved MTF algorithm would improve the results in the in-track direction. The temporal pixel interleaving technique,

introduced in section 5.2.8, may address improvement in the sampling rate, but atmospheric correction would be required for each date and temporally stable scenes are required, such as the lava field in Sevillita, New Mexico.

In addition, the data from the SRCA can be used to monitor any temporal changes occurring over the life of the instrument, given that it has been shown to be fairly stable over the coarse of a year.

Obtaining MTF estimates for the other bands or, at a minimum, for the VIS FP, would improve characterization of MODIS. Inter-sensor MODIS comparison could be implemented using matching bands on the similar FPs (Table 23).

In terms of the final evaluation criteria for the effectiveness of the MTF correction, the MODIS Science Teams should decide whether the correction filter is warranted for their product. If an MTF correction filter is desired application of the filter will lead to an image restoration study for each particular product, which is open to a variety of implementation techniques for the restoration filter, such as a Wiener filter or wavelets. The approach could also include noise suppression techniques to improve results such for the MODIS Ocean Science Team whose valid signal is only 10% for the complete signal detected for the water-leaving radiance product.

Table 23. Corresponding spectral bands for MODIS (GIFOV in parentheses).

MODIS band A	MODIS band B
1 (250m)	13 (1000m)
2 (250m)	16 (1000m)
4 (500m)	12 (1000m)

APPENDICES

A. SRCA ACQUISITION SCHEME

The MCST minutes highlighting the SRCA spatial mode time of acquisition.

Mission Operations Days: 2001/006 to 2001/012
January 5, 2001 20:00:00 GMT to January 12, 2001 20:00:00 GMT

Terra Spacecraft and MODIS Instrument Status:
Terra (AM-1) is in Normal Mode
MODIS is in B-side Science Mode

Blackbody	A Off; B On	Nominal
Calibration Electronics	A Off; B On	Nominal
Control Processor	A Off; B On	Nominal
Door: Nadir	Unlatched, open	Nominal
Space View	Unlatched, open	Nominal
Solar Diffuser	Unlatched, closed	Nominal
FDDI Formatter	A Off; B On	Nominal
FDDI Port	A On; B Off	Nominal
FIFO Memory	1 & 2 Off; 3 & 4 On	Nominal
Format Processor	A Off; B On	Nominal
Power Supply: 1	Off	Nominal
Power Supply: 2	On	Nominal
PV FPAs: VIS	A Off; B On	Nominal
NIR	A Off; B On	Nominal
SMIR	A Off; B On	Nominal
LWIR	A Off; B On	Nominal
PC FPA: LWIR	A Off; B On	Nominal
Radiative Cooler:		
Outgas Heaters	All Off	Nominal
LWIR FPA Heater	On	Nominal
SMIR FPA Heater	Off	Nominal

This Week's Completed MODIS Activities:

Friday, January 5, 2001

005/21:53:22-21:55:53 ATC OA27: PV ECAL (Centered around orbit 5600 Maximum Latitude)
005/23:31:15-23:35:45 ATC OA28: PC ECAL (Centered around orbit 5601 Maximum Latitude)

Saturday, January 6, 2001

None

Monday, January 8, 2001

008/12:27:08-12:38:36 ATC OA15: SD/SDSM Open
008/13:27:01-14:00:34 ATC OA19: SRCA Full Radiometric (Data collect centered in S/C Night)
008/14:06:01-14:17:29 ATC OA16: SD/SDSM Screened
008/21:28:48-22:26:19 ATC OA23: SRCA Full Spatial (Data collect centered in S/C Night)

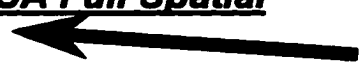

Tuesday, January 9, 2001

009/13:59:43-14:51:22 ATC OA22: SRCA Full Spectral (Part 1) (Data collect centered in S/C Night)
009/15:55:10-16:29:55 ATC OA22: SRCA Full Spectral (Part 2) (Data collect centered in S/C Night)
009/17:17:25-18:08:41 ATC OA22: SRCA Full Spectral (Part 3) (Data collect centered in S/C Night)
009/19:12:37-19:50:35 ATC OA22: SRCA Full Spectral (Part 4) (Data collect centered in S/C Night)

Friday, January 12, 2001

None

This Week's Scheduled MODIS Activities Not Completed:

None

B. FREE HDF SOFTWARE AND COMMERCIAL TOOLS

There are several free and commercial viewers that allow users to access or view HDF files. Some of the commercial applications are MATLAB and ENVI. MATLAB is difficult to use with the HDF libraries because MATLAB expects the user to understand the HDF accessing scheme. This means that the user is expected to follow the steps described in Table 4. Setting up the interface accessing scheme is not a trivial task. Other products are not cost effective, but are easier to use. The software has certain limitations, and the user is bounded by the limitations. One such problem with ENVI is accessing attribute information attached to an SDS. It is often difficult to obtain the appropriate conversion factors to convert scaled units to geophysical parameters. The free HDF related software includes viewers, libraries, and HDF validating software. Some of the viewing software includes H5View (http://hdfeos.gsfc.nasa.gov/hdfeos/index.cfm) , HDFview (http://hdf.ncsa.uiuc.edu/hdf-java-html/hdfview), and Webwinds (http://linkwinds.jpl.nasa.gov). The some of the free HDF libraries have been ported to the major platforms. The libraries consist of different toolkits. To compile the HDF-EOS library, one needs to also compile the regular HDF libraries, SCFTK libraries, and PGSTK toolkit. For someone developing HDF files, useful validating tools exist to ensure the integrity of the HDF file (http://ivanova.gsfc.nasa.gov/hdfeos). Some of the tools are metadump, heosls, ascii dump, bindump, metacheck. These programs check and output the metadata structure, and the HDF EOS structure.

REFERENCES

1. Schowengerdt, R. A., and P. N. Slater. "Determination of Inflight MTF of Orbital Earth Resources Sensors". *Proc. ICO IX Congress on Space Optics*. p. 693-703. October 1972.

2. Schowengerdt, R. A., R. W. Basedow, and J. E. Colwell. "Measurement of the HYDICE System MTF from Flight Imagery". *Hyperspectral Remote Sensing and Applications*. p. 127-136. Denver, CO. SPIE: 1996.

3. Park, S. K., R. A. Schowengerdt, and M. A. Kaczynski, "*Modulation-transfer-function analysis for sampled image systems* ". *J.* Applied Optics, 1984. **23**(15): p. 2572-2582.

4. Rauchmiller, R. F. Jr., and R. A. Schowengerdt, "*Measurement of the Landsat Thematic Mapper MTF Using an Array of Point Sources* ". *J.* Optical Engineering, 1988. **27**(4): p. 334-343.

5. Markham, B. L., "*The Landsat Sensors' Spatial Responses* ". *J.* IEEE Transactions on Geoscience and Remote Sensing, 1985. **GE-23**(6): p. 864-875.

6. Wood, L., R. A. Schowengerdt, and D. Meyer. "Restoration for Sampled Imaging Systems". *Proc. SPIE, Applications of Digital Processing IX*. p. 333-340. August 1986.

7. Meyer, D., and R. A. Schowengerdt. "Resampling kernel design for image restoration". *Proceedings of the American Society Photogrammetry Remote Sensing Annual Convention*. p. 293-304. March 1990.

8. Schowengerdt, R. A., R. L. Antos, and P. N. Slater. "Measurement of the Earth Resources Technology Satellite (ERTS-1) Multi-spectral Scanner OTF from Operational Imagery". *SPIE, Image Assessment and Specification*. p. 247-257. May 1974.

9. Schowengerdt, R. A. "A Method for Determining the Operational Imaging Performance of Orbital Earth Resources Sensors". *Proc. of the Annual Am. Soc. of Photogrammetry Convention*. p. 25-62. February 1976.

10. Schowengerdt, R. A., *Remote Sensing, models and methods for image processing, 2nd ed.* 2 ed. 1997, San Diego, California: Academic Press.

11. Reinersman, P. N. and K. L. Carder, "*Monte Carlo simulation of the atmospheric point-spread function with an application to correction for the adjacency effect. " J.* Applied Optics, 1995. **34**(21): p. 4453-4471.

12. Reinersman, P. N., K. L. Carder and F. R. Chen, "*Satellite-Sensor Calibration Verification With the Cloud-Shadow Method ". J.* Applied Optics, 1998. **37**(24): p. 5541-5549.

13. Liang S., Fang H. and Chen M., "*Atmospheric correction of Landsat ETM+ land surface imagery. Part I. Methods ". J.* IEEE Transactions on Geoscience and Remote Sensing, 2001. **39**(11): p. 2490-2498.

14. Slater, P. N., *Remote Sensing Optics and Optical Systems*, ed. David S. Simonett. 1980, Reading, Massachusetts: Addison-Wesley. 560.

15. Schowengerdt, R. A., C. Archwamety, and B. C. Wrigley, "*Landsat Thematic Mapper Image-Derived MTF ". J.* Photogrammetric Engineering and Remote Sensing, 1985. **51**(9): p. 1395-1406.

16. Schowengerdt, R. A., C. Archwamety, and B. C. Wrigley. "Operational MTF for Landsat Thematic Mapper". *SPIE, Image Quality: An Overview*. p. 110-118. April 1985.

17. Storey, J. C. "Landsat 7 on-orbit Modulation Transfer Function Estimation". *Sensors, Systems, and Next-Generation Satellites V*. p. 50-61. Toulouse, France. SPIE: September 2001.

18. Leger, D., J. Duffaut, and F. Robinet. "MTF measurement using spotlight". *Geoscience and Remote Sensing Symposium, 1994. IGARSS '94*. p. 2010 - 2012. Pasadena, CA, USA. 8-12 August 1994 1994.

19. Viallefont-Robinet, F., and P. Henry. "VEGETATION MTF in-flight measurement using HRVIR". *Proceedings of SPIE - The International Society for Optical Engineering, v4135, 2000, Earth Observing Systems V*. p. 314-323. San Diego, USA. SPIE: August 2-4 2000 2000.

20. Liao, L., P. Jarecke, D. Gleichauf, and T. Hedman. "Performance characterization of the hyperion imaging spectrometer instrument". *Proceedings of SPIE - The International Society for Optical Engineering,*. p. 264-275. San Diego, USA. Society of Photo-Optical Instrumentation Engineers, Bellingham, WA, USA: August 2- 4 2000 2000.

21. Biggar, S., K. J. Thome, J. M. Holmes, M. A. Kuester, and R. A. Schowengerdt. "In-flight radiometric and spatial calibration of EO-1 optical sensors". *Geoscience*

and Remote Sensing Symposium, 2001. IGARSS '01. p. 305-307. Sidney Australia. 9-13 July 2001 2001.

22. Nelson, N.R., and P. S. Barry. "Measurement of hyperion MTF from on-orbit scenes". *Geoscience and Remote Sensing Symposium, 2001. IGARSS '01.* p. 2967-2969. Sidney, Australia. IEEE: 9-13 July 2001 2001.

23. Nishihama, M., R. Wolfe, D. Solomon, et al., *MODIS Level 1A Earth Location: Algorithm Theoretical Basis Document Version 3.0.* 1997, NASA/Goddard Space Flight Center: Greenbelt, MD.

24. Rojas, F., R. A. Schowengerdt, and S. Biggar. "Modulation Transfer Analysis of the Moderate Resolution Imaging Spectroradiometer (MODIS)". *SPIE, Earth Remote Observing Sensors VI.* p. 222-230. San Diego, Ca. August 1-3 2001.

25. Gao, X., and A. R. Huete. "Validation of MODIS land surface reflectance and vegetation indices with multi-scale high spatial resolution data". *Geoscience and Remote Sensing Symposium, 2000 Proceedings. IGARSS 2000.* p. 533-535. Hawaii. July 24 , 2000 2000.

26. Howard, G. R., and K. J. Voss, *MODIS Normalized Water-leaving Radiance Advanced Theoretical Basis Document (MOD-18) version 4.* 1999, Department of Physics, University of Miami: Goddard. p. 100.

27. webmaster, MODARCH, *MODIS Technical Specifications and Data Products.* 2000, Goddard Space Flight Center.

28. Wolfe, R. E., M. Nishihama, A. J. Fleig, J. A. Kuyper, et al., "*Achieving Sub-Pixel Geolocation Accuracy in Support of the MODIS Land Science ". J.* Remote Sensing Environment, 2002. **In publication.**

29. Braga, A., R. A. Schowengerdt, F. Rojas, and S. Biggar. "Calibration of the MODIS PFM SRCA for on-orbit, cross-track MTF measurement". *Earth Observing Systems V Aug 2-Aug 4 2000 v4135 2000 San Diego, USA.* p. 71-79. San Diego, Ca., USA. SPIE Society of Photo-Optical Instrumentation Engineers: 2000.

30. Braga, A. *Modulation Transfer Function Derivation for Spatial Calibration of NASA's Moderate Resolution Imaging SpectroRadiometer (MODIS). MS Thesis. Electrical and Computer Engineering.* p. 108. Tucson. University of Arizona: 2000.

31. Venzon, J., and J. Pierce, *In-flight calibrators performance characterization (ALPC17).* 1997, Santa Barbara Research Center: Goleta, CA. p. 25.

32. Barnes, W. L., T. S. Pagano, and V. V. Solomonson, "*Prelaunch Characteristics of the Moderate Resolution Imaging Spectroradiometer (MODIS) on EOS-AM1 ". J.* IEEE Transactions on Geoscience and Remote Sensing, 1998. **36**(4): p. 1088-1100.

33. Therrien, N. J., *Proto-Flight Optical Bench Assembly Data Results.* 1996, Santa Barbara Research Center.

34. Franco, A.J., *(OBA) Spatial Verifications (AOI-14).* 1996, Santa Barbara Research Center.

35. Therrien, N.J., and S. Broberg, *Proto-Flight Spatial Performance (PC02). Test Analysis Report.* 1997, Santa Barbara Research Center.

36. Aho, A. E., and C. B. Crauney, *Sytem Spatial Performance, Test Procedure for (ALPC-02)*, in *unpublished*, 152787, Editor. 1996.

37. Zukowski, T., *MODIS PFM Point Spead Response Data.* 1997, MCST MODIS-PFM Reflective Bands Workshop.

38. Applications, National Center for Supercomputing, *HDF User's Guide, V4.1r4.* 2000, Board of Trustees University of Illinois.

39. Wynne, D., *HDF-EOS Interface Based on HDF5, Volume 1: Overview and Examples, Technical Paper.* 2001, Darryl Arrington.

40. USGS, EROS Data Center, *USGS, EROS Data Center.* 2000.

41. Center, Earth Remote Sensing Data Analysis, *ASTER User's Guide (Ver. 3.1) Part I and II.* 2001.

42. Schowengerdt, R. A. "Measurement of the Sensor Spatial Response for Remote Sensing Systems". *Proceedings of SPIE - The International Society for Optical Engineering.* p. 65-71. Orlando, Florida. SPIE: April 19-20 2001.

43. Rauchmiller, R. F., and R. A. Schowengerdt. "Measurement of the Landsat Thematic Mapper MTF using a 2 - Dimensional Target Array". *Proc. SPIE, Applications of Digital Processing IX.* p. 105-114. August 1986.

44. Rojas, F., R. A. Schowengerdt, and S. Biggar, "*Early Results on the Characterization of the Terra MODIS Spatial Response ". J.* Remote Sensing Environment, 2002: **83**(1): p. 554-565 .

45. Rojas, F., R. A. Schowengerdt, A. Braga, and S. Biggar. "Spatial Analysis of the MODIS PFM Channel Alignment and Far-Field Response using Pre-Resistor fix data". *SPIE 45th annual meeting*. p. 60-70. San Diego, Ca. SPIE Society of Photo-Optical Instrumentation Engineers: July 31 - Aug 4 2000.

46. Kintner, E. C., "*Calculating the encircled energy in the point spread function* ". *J.* Optica Acta, 1977. **24**(10): p. 1075-1076.

47. Baliga, J. V., and B. D. Cohn, "*Simplified method for calculating encircled energy* ". *J.* SPIE Simulation and Modeling of Optical Systems, 1988. **892**: p. 152-156.

48. Mahajan, V. N., "*Included Power for Obscured circular pupils* ". *J.* Applied Optics, 1978. **17**(6): p. 964-968.

49. Therrien, N.J., and S. Broberg, *Proto-Flight Aft Optics Assembly (2nd Build Data Results)*. 1996, Santa Barbara Research Center.

50. Welch, B. C., *Practical Programming in Tcl and Tk*. 3rd ed, ed. Joan L. McNamara. 2000, Upper Saddle River, New Jersey: Prentice-Hall Inc.

51. Shamordola, K., *F1 PV Channels Band-to-Band Crosstalk*. 1997, Santa Barbara Research Center.

52. Pagano, T.S., *Modulation Transfer Function Model And Predictions for MODIS-N*. 1991, Santa Barbara Research Center.

53. Gaskill, J. D., *Linear Systems, Fourier Transforms, and Optics*. Wiley Series in Pure and Applied Optics, ed. Stanley S. Ballard. 1978, New York: John Wiley & Sons.

54. Adimi, F., *Calibration Parameters: Other Product Codes*. 1998, MODIS Characterization Science Team (MCST).

55. Press, W. H., W. T. Vetterling, S. A. Teukolusky, and B. P. Flannery, *Numerical Recipes in C. The Art of Scientific Computing*. 2nd ed. 1992, Cambridge, New York: Press Syndicate of the University of Cambridge. 965.

56. Foley, D. F., A. van Dam, S. K. Fiener, and J. F. Hughes, *Computer Graphics Principles and Practice 2nd edition*. 1992: Addison-Wesley Publishing Company, Inc.

57. Richards, J. A., and Xiuping J., *Remote Sensing Digital Image Analysis - An Introduction*. 3rd ed. 1999: Springer-Verlag.

58. Oppenheim, A. V. , and R. W. Schafer, *Discrete-Time Signal Processing*. Prentice Hall Signal Processing Series, ed. Alan V. Oppenheim. 1989, Englewood Cliffs, New Jersey: Prentice-Hall International.

59. Fryer, J. and K. McIntosh, "*Enhancement of Image Resolution in Digital Photogrammetry* ". *J.* Photogrammetric Engineering and Remote Sensing, 2001. **67**(6): p. 741-749.

60. Frans, E. P., and R. A. Schowengerdt. "Spatial-Spectral Unmixing Using the Sensor PSF5". *SPIE, Imaging Spectrometry III.* p. 241-249. San Diego. July 1997.

61. Huete, A. R., C. Justice, and W. van Leeuwen, *MODIS Vegetation Index (MOD 13) Algorithm Theoretical Basis Document Version 3.* 1999, University of Arizona: Tucson, Arizona. p. 129.

62. Muira, T., A. R. Huete, and H. Yoshioka, "*Evaluation of Sensor Calibration Uncertainties on Vegetation Indices for MODIS* ". *J.* IEEE Transactions on Geoscience and Remote Sensing, 2000. **38**(2).

63. Huete, A. R., H. Q. Liu, K. Batchily, and W. van Leeuwen, "*A Comparison of Vegetation Indices over a Global set of TM images for EOS-MODIS* ". *J.* Remote Sensing Environment, 1997. **59**: p. 440-451.

64. Guenther, B., G. D. Godden, X. Xiong, E. Knight, et al., "*Prelaunch Algorithm and Data Format for the Level 1 Calibration Products for the EOS-AM1 Moderate Resolution Imaging SpectroRadiometer (MODIS)* ". *J.* IEEE Transactions on Geoscience and Remote Sensing, 1998. **36**(4): p. 1142-1151.

65. Huete, A. R., R. D. Jackson, and D. F. Post, "*Spectral Response of a Plant Canopy with Different Soil Backgrounds* ". *J.* Remote Sensing Environment, 1985. **17**: p. 37-53.

66. Hsien-Huang, W. P., and R. A. Schowengerdt, "*Improved Fraction Image Estimation using Image Restoration* ". *J.* IEEE Transactions on Geoscience and Remote Sensing, 1993. **31**(4): p. 771-778.

67. (MCST), MODIS Characterization Support Team, *MODIS Level 1B Product User's Guide, For Level 1B Version 2.3.x Release 2.* 2000, Goddard Space Flight Center: Greenbelt, Maryland.

68. (MCST), MODIS Characterization Support Team, *MODIS Level 1B Products Data Dictionary (Applicable to L1B code version 3.0.0, file specifications version 3.0.0).* 2001, Goddard Space Flight Center: Greenbelt, Maryland.

69. Rojas, F., R. A. Schowengerdt, and S. Biggar. "Error Analysis of the Adjacency Effect on the Vegetation Indices for the Moderate Resolution Imaging Spectradiometer using Laboratory Data". *SPIE Conference on Earth Observing Systems VII.* p. Seattle, Wa. July 7-11 2000.

70. Thome, K. J. Railroad Valley NV 14 June 2001: Atmospheric parameters for MODIS and ETM+. Personal Communication. 2002. Tucson, Arizona

71. Charlermwat, P. and T. El-Ghazawi. "Multi-resolution Image Registratione using Genetics". *International Conference on Image Processing, 1999. ICIP 99.* p. 452-456. Kobe, Japan. October 1999.

72. Le Moigne, J., N.S. Netanyahu, J.G.Masek, J.G. Mount, and S. N. Goward. "Robust matching of wavelet features for sub-pixel registration of Landsat data". *International Geoscience and Remote Sensing Symposium, 2001. IGARSS '01.* p. 706 - 708. Sydney, NSW, Australia. July 2001.